EXTRATROPICAL STORM-GENERATED SWELLS INDUCED VULNERABILITY EFFECTS ON THE TROPICAL ISLANDS OF HAWAIʻI

A DISSERTATION SUBMITTED TO THE GRADUATE DIVISION OF THE UNIVERSITY OF HAWAIʻI AT MĀNOA IN PARTIAL FULFILLMENT OF THE REQUIREMENTS FOR THE DEGREE OF

DOCTOR OF PHILOSOPHY

IN

OCEAN AND RESOURCES ENGINEERING

AUGUST 2018

By

Yaprak Onat

Dissertation Committee:

Oceana P. Francis, Chairperson

Bruce Howe

Zhenhua Huang

Eva-Marie Nosal

Karl Kim

© Copyright 2018

By

Yaprak Onat

To my mother Binnur Akay for her unconditional love and support.

Acknowledgements

"For everything in the world, for civilization, for life, for prosperity, our true mentor is science."

These words belong to the founder of the Republic of Turkey, Ataturk, and a great leader who brought not only democracy and egalitarianism to the nation, but he also created a culture that held up knowledge and science as an essential pillar of a modern and just country. I am grateful for this vision that gave science and education an important role in my life. The passion that I had for scientific literacy and ocean sciences led me to the other side of the world and made me fall in love with Hawai'i, my second home.

Certain people important to me have guided my career during the dissertation. I would like to express my deepest appreciation to my committee chair Oceana Francis, who gave me opportunities and motivation for my improvement, and my committee members and ORE faculty Eva-Marie Nosal, Zhenhua Huang, Bruce Howe, Karl Kim, John Wiltshire, Gerard Nihous and Kwok Fai Cheung for their intellectual contribution and guidance through my academic career. I am grateful for the generous help that Ning Li, Alex Gibbs and Linqiang Yang offered with the simulation processing, Michelle Marchant for assisting me with GIS, and Chip Fletcher, Alex Gibbs, Victor N. de Jonge, Jeff Hanson, Robert Frantantonio, Tiffany Anderson and Troy Heitmann for their scientific insight. I would like to thank May Izumi for editing the dissertation. Many thanks to Ron Merrill and David Schanzenbach for their help with high-performance computing systems, Natalie Nagai, Janis Kusatsu and Jean Zheng for helping me with my administrative work, Mitchell Pinkerton and Jonathan Imai for assisting me in the University of Hawai'i Coastal Hydraulics Engineering Resilience (CHER) Lab, and Daniela Bottjer-Wilson and Michelle Teng for guiding me with teaching. I also would like to also thank ORE and CEE for my teaching assistantship, the Denise B. Evans Fellowship, the UH Graduate Division and International Student Office for academic merit scholarships, the Graduate Student Office for conference travel awards, the U.S. Army Corps of Engineers, Hawaii Department of Transportation and BinYapi Engineering for funding opportunities.

Many thanks to my colleagues Linyan Li, Ian Hardy, Andrew Schwartz, Courtney Lynn, Cagil Kirezci, and mentors Dora Farkas, Aysen Ergin and Ahmet Cevdet Yalciner who supported me, and my friends Dallas Nagata and Ed White, Dustin Gaessner, Charlie Field, Patrick Anderson, Wes and

Fran Cummins, and Jacob Himoto who always place a smile on my face and showed kindness and care.

Special thanks to my close friends Ezgi Koker and Can Gokgol, Gulseda and Onur Gungor, Betsy Seiffert and Vu Nguyen, Jerica Nolte, Ayse Karanci, Elahe Tajfar, Eda Lisiak, Ahu Hettema, Lelemia Irvine, Meltem Kaso, Nina Ribbat, Rachael Hager, Yasemin Karabudak and William Busby, and Ally and Mario Mendykowski, who were there for me and shared many special moments.

The Hawaiian culture also inspired me through my dissertation journey. The dissertation process instilled in me the value of ʻike loa – the importance of knowledge, and that, when we have confidence in our understanding, we will not lose our way in life. I also dedicate this dissertation to Hawaiʻi, as I want to pay back its kindness by using my newfound knowledge and skills to mālama, or care, for the land and our community. I would like to finish my gratitude with mahalo to my family. I am grateful for the love and support of Claudia, John and Sarah Justeson, as they always stand by me. This journey would not have been possible without the support of my mother Binnur Akay and husband Peter Justeson. My mother is the first person that I aspired to, a woman who shows incredible strength and intelligence and always guided my way as my foremost mentor. My husband was always there to provide comfort and love. I'm lucky to call him my teammate and thankful for his understanding, supportive and kind nature. They always believed in me, showed great patience and sacrifice and became the source of encouragement to achieve my goal and complete my dissertation work. I'm grateful for all their support.

Abstract

The poleward shift of strong extratropical storms due to global warming's effect on baroclinicity raises the question of how the storm intensification affects the susceptibility of distant remote islands under high wave energy environments. This study aims to identify the effective linkages between the intensification of extratropical storms and the corresponding swells in order to reduce the uncertainty in prioritizing vulnerable coastal systems in Hawai'i. The minimum mean sea level pressure and geopotential height, and maximum vorticity are used as a criteria to define strong cyclonic activity from an atmospheric reanalysis dataset to hindcast swell states of the North Pacific from 2007-2017. The de-seasonalized trend of the northwest swells and the spatial distribution of the wave exposure are visualized in an index-based coastal vulnerability GIS model to classify coastal exposure. The correlation between strong extratropical cyclones and swells show an increase in the frequency of swells, which accounted for a quarter of the total swells reaching the Hawaiian Islands over the record period. The significant wave height and peak period of the associated swells at the northwest of O'ahu displays a significant upward trend of up to 0.51 m and 1.72 s in open ocean respectively, while keeping a rather stable direction range of 325-330º during the record period. These swells contribute to the already alarming 34% of the medium to high vulnerability of the coastlines of the Hawaiian Islands. Understanding the dominant factors affecting shoreline vulnerability and the impact of strong extratropical storm-generated swells related to their susceptibility allows the formulation of better strategies to more effectively mitigate the potential risk for Pacific Island communities. The value of this work lies in both identifying the swell trends and customizing the proposed framework to determine crucial elements that increase the susceptibility of critically exposed shoreline segments. This work provides a guide for policymakers to promote public awareness and support deliberation, planning, and design of adaptation strategies.

Table of Contents

List of Tables

List of Figures

List of Abbreviations

CDIP: Coastal Data Information Program

CFSR: Climate Forecast System Reanalysis

CVI: Coastal vulnerability index

EI: Coastal exposure index

ErI: Coastal erosion index

EX: Extratropical

GIS: Geographic information system

GPH: Geopotential height

IPCC AR5: Fifth assessment report of Intergovernmental Panel on Climate Change

MEI: Multivariate El Niño Southern Oscillation index

MSLP: Mean sea level pressure

NP: North Pacific

PDO: Pacific Decadal Oscillation index

SLR: Sea level rise

WW3: WAVEWATCHIII wave model

CHAPTER 1. Introduction

In recent years, the Hawaiian Islands have seen major impact from storm surge caused by long-period surface gravity waves generated by extratropical storms. One of many examples of the effect of storm surge can be seen on Hawai'i's coastal infrastructure, which has been affected by sea level rise and storm surge. During February 2016, for example, swells reached heights of up to 20 m along the Kamehameha Highway, North Shore, O'ahu, causing a shut down because of inundation (D'angelo, 2016; Now, 2016). Due to unlimited fetch, tropical islands such as Hawai'i are often faced with high-energy swells. Swells travel long distances (Barber and Ursell, 1948; Munk et al., 1963; Snodgrass et al., 1966) with little attenuation (Ardhuin et al., 2009) and are able to carry most of their energy to coastlines relatively unimpeded. The weekly and annual variations in direction, maximum wave height, frequency, and duration of the swells (Caldwell, 2005) have a tremendous impact on the north and west shores of the Hawaiian Islands. Therefore, defining the ocean state and knowing the degree to which a coastline is vulnerable to swells and changes are crucial to reducing infrastructure damage and causalities.

The wave state and swell occurrences in the Hawai'i region are studied using observations (Caldwell, 2005), buoy measurements (Vitousek and Fletcher, 2008), and hindcast modeling (Hemer et al., 2011; Li et al., 2016). Despite the low precision in observations, Caldwell (2005) shows that the primary direction of winter swells is west to northwest (273-295° in oceanographic convention) and mostly affected by island shadowing. The extremal probability model applied to offshore buoys and wave hindcast data shows an annual significant wave height of 7.7 m, and the highest 10% and 1% of waves approaching O'ahu are 9.8 and 12.9 m, respectively (Vitousek and Fletcher, 2008). The 100-year wave height of the northwesterly swells has increased in recent years (Hemer et al., 2011). The wave state and climate pattern studies using high-resolution wind reanalysis data and hindcast models demonstrate that northwest and north swells approaching the Hawaiian Islands during winter are from extratropical (EX) storms, generated near the Kuril and Aleutian Islands (Li et al., 2016; Stopa et al., 2013a). Even though modeling applications are advanced enough to capture wave distributions interisland and at headlands, northwest swells are still overestimated in sheltered areas (Li et al., 2016). These studies reaffirm that the annual highest events affecting the Hawaiian Islands are from winter swells and that swell generation and propagation need to be examined in order to fully interpret the impact of swells on the islands.

The evolution of waves is based on the action balance equation in third generation wave modeling applications (Komen et al., 1994). The energy density of radiated waves propagates over frequency and direction in time and space. Action density is the energy density over frequency, which is conserved during wave propagation. Numerical models calculate the change of energy in a coordinate grid cell by summing the net import energy and local generation of energy (Komen et al., 1994). The source/sink terms are the summation of growth by the wind, triad quadruplet wave-wave interactions, wave decay due to whitecapping, bottom friction, and depth-induced wave breaking. Swells traveling nearshore are mostly affected by refraction. Propagating as a group of waves with the same period and direction allows swells to disperse starting from the lower period and conserve a regular periodic pattern in fully developed seas. Thus, swells conserve most of their energy and are assumed to be unaffected by wind waves and coexisting wave systems (Alves, 2006). However, studies reveal that on a small scale, swells contribute to ocean mixing (Ardhuin and Jenkins, 2006; Babanin, 2006) and modify air-sea interactions because some of their momentum is lost into the atmosphere (Grachev and Fairall, 2001). The dissipation of energy is more evident in steeper swells, reaching up to 65% over a distance of 2800 km (Ardhuin et al., 2009). Current wave models are unable to accurately represent swell dissipation in real-world situations, which results in underestimating swell heights (Ardhuin et al., 2009; Rascle et al., 2008). Nonetheless, wave modeling approaches are needed to determine the swell budget of an area. Swells contribute to global wave climate (Alves, 2006; Semedo et al., 2011; Young et al., 2011) by traveling from their origin at higher latitudes and reaching the Hawaiian Islands with high wave energy reaching up to 60 kW/m (Stopa et al., 2013b).

There is an increasing trend in wave height climatology of the North Pacific (NP) at mid-latitudes (above 30°N) from October through April (Arinaga and Cheung, 2012) and at high latitudes in the Pacific-Arctic (above 66°N) (Francis et al., 2011). Researchers observe wave heights and long periods of swells using visual ship observations (Gulev and Grigorieva, 2006), buoy measurements along the west coast of the United States (Allan and Komar, 2000; Bromirski et al., 2005), and satellite data analysis (Young et al., 2011). Buoy analysis shows that the northeastern side of the Pacific between 30-45°N is experiencing an increase in wave height (Menéndez et al., 2008). This increase has a rate of 1cm/year between 1948-2008 from the hindcast reanalysis database and 2-3 cm/year between 1985-2007 from buoy data (Mendez et al., 2010). The wind speeds and wave heights also display seasonal variability around 40°N in the Pacific with variability of up to 50 and

60%, respectively (Stopa et al., 2013a). Because the seasonal climatic pattern analysis supports the claim that EX storms are the primary driver for variability (Stopa et al., 2013a), EX storm generated annual wave climate trends and their impacts are likely associated with each other.

Swells generated along the EX storm tracks are observed to have a high correlation with high wind speeds, intensity, duration, and fetch of the wind due to the energy exchange between air and ocean (Alves, 2006; Francis and Atkinson, 2012a, 2012b; Parise and Farina, 2014; Young et al., 2011). Thus, the substantial impact of cyclones on ocean wave disturbances indicates change in EX cyclone intensity, frequency, lifespan, and trajectory trends.

The variability of EX cyclone tracking, intensification, and generation have been studied by many researchers (Eichler and Higgins, 2006; Geng and Sugi, 2001; Gulev et al., 2001; Hodges et al., 2003; Mesquita et al., 2010; Sinclair and Revell, 2000; Wang et al., 2013, 2006). Changes in the EX cyclone trends were noticed after the 1970s. A poleward broadening of the Pacific jet during winter caused a northward shift in storm tracks (Berry et al., 2011; Chang and Fu, 2002; Chang and Yau, 2016; Geng and Sugi, 2001; Graham and Diaz, 2001; Gulev et al., 2001; Harnik and Chang, 2004; Lambert, 1996; Ulbrich et al., 2009; Wang et al., 2006). Graham and Diaz, (2001) evaluated winds from December through March over the last 50 years using NCEP-NCAR reanalysis data and concluded that there is a increase in surface winds between 25°–40°N and in the Gulf of Alaska. This rise in surface winds is related to an increase in upper-tropospheric winds and vertical wind shear, causing cyclone intensification in the northern Pacific (NP) Ocean climatology. This intensification is not surprising considering the correlation between the rise in sea surface temperatures in the western tropical Pacific and resulting changes in the organized tropical convection (Graham and Diaz, 2001). Cyclone frequency increases 0.21 per year, minimum central pressure decreases 4-5 hPa, relative vorticity increases 10-15%, and the frequency of deep pressure lows increases 50% between 1948-2000 (Graham and Diaz, 2001). Moreover, the explosive cyclones lead to strong and frequent events at mid- to high latitudes due to this northward shift in cyclone activity (Bengtsson et al., 2006; Fischer-Bruns et al., 2005; Lambert and Fyfe, 2006; Löptien et al., 2008; Seiler and Zwiers, 2016; Ulbrich et al., 2009; Yin, 2005). Another prediction drawn about the cyclone activity in the northern hemisphere is a decline south of 35-40°N and an increase north of 40°N by the 21st century (Graham et al., 2013).

1. The motivation of the Dissertation

The effect of amplified global warming, enhanced greenhouse gases and sulfate aerosols on the sea ice in high latitudes during winter generates pole-to-equator high temperature differences. This, in turn, effects the vertical wind shear associated with the equatorward meridional temperature gradient (Geng and Sugi 2003). The changes in the temperature gradient and vertical wind shear results in changes in the baroclinicity and EX storm characteristics. The consensus reached in the fifth assessment report of the Intergovernmental Panel on Climate Change (IPCC AR5) is that EX cyclones will not show a significant decrease in the future and the NP storm track shift to the north will continue (Christensen et al., 2013). Even though the baroclinic change effects are observed through altimeter measurements of wind speed and wave height measurements (Young et al., 2011), EX cyclone trends and their relation to climate change require more modeling approaches to define the impact of the Aleutian low deepening of the mean sea level pressure. Currently, there is no reasearch being done on the intensity of the NP EX storms that impact swells in the Hawaiian Islands. The changes related to the wind-wave climate needs to be defined in order to estimate the vulnerabilities of coastal regions to climate stressors (Hemer et al., 2010). The degree of vulnerability is a complex phenomenon that demands a multidisciplinary perspective. Defining vulnerability requires extensive, objective research, although there is a degree of subjectivity. The vulnerability from high-energy swells due to EX storms in NP has also not been quantified in terms of coastal vulnerability indices.

EX cyclone statistics have uncertainties due to the use of different cyclone detection and tracking algorithms (Neu et al., 2013). The differences come from the interaction of the background flows in capturing cyclones in synoptic scale and ignoring small-scale events. In addition to this, there is uncertainty over swell generation during the EX cyclones and isolating storms in wind fields is challenging (Alves, 2006). Limiting the boundaries of wave systems through segmentation breaks nonlinear wave-wave interaction and swell evolution (Alves, 2006) if the regions defined by the boundaries chosen are very small. Therefore, the effects of swells on an area cannot be considered by looking at individual storms to form the basis for modeling a region. The characteristics of the swells reaching Hawai‘i are either lacking in the time domain, which Alves (2006) demonstrated in two years of swell propagation, or given in a multi-modal wind state (Li et al., 2016), in which swells and wind waves are combined. Therefore, the literature has a gap when it comes to examining the

EX storm generated swell impacts on coastal vulnerability and its variation over the years. The trend of EX storm generated swells on remote coastal zones has not been identified.

2. Purpose of the Dissertation

The first goal of this research is to link the intensification of EX storms with presumed changes in generated swell characteristics on distant shorelines. This study focuses on the strong cyclonic generation locations rather than individual storms. Thus, the statistics of significant cyclones are less dependent on a chosen cyclone tracking algorithm and more on the frequency of the occurrence of the generation on a specific coordinate location. Moreover, the algorithm includes microscale events as well as synoptic events. The significant increase in the frequency and intensification observed in the EX storms shift the focus of wave modeling to the last decade. The features of EX storms as an atmospheric driver for generating swells that reach the Hawaiian Islands are investigated by wave hindcasting the ocean response for the period 2007-2017.

The second goal of this research is to establish the trend of these remotely generated swells. The wave state of swells originating from EX storms is investigated by comparing buoy analysis with the hindcast model (WAVEWATCH III) to understand the characteristics of these swells over the last ten years.

The third goal of this research is to reduce the uncertainty in the prioritization of vulnerable coastal systems. The research focuses on the vulnerability created by strong EX storms on the Hawaiian Islands. A coastal vulnerability index (CVI) is used to quantify the vulnerability in which, among other coastal exposures, includes wave exposure vulnerability due to swells and shows what the wave exposure contribution is to the total coastal exposure. A CVI is an exposure measure of the coastlines relative to each other and taking into account the contributing vulnerability components. The CVI provides an initial stage towards building a dynamically complex susceptibility map in a high-energy swell environment.

2.1 Research Questions

The proposed research contributes towards our understanding of swells on remote islands and quantifies remote island vulnerability in the open ocean. The hypothesis addressed here states "The change in the swell trend of the Hawaiian Islands can be explained by buoy analysis and wave

modeling of strong EX cyclones throughout the decades." This study considers three research questions for the 2007-2017 record period.

- What is the relationship between the strong EX cyclones and swell characteristics around the Hawaiian Islands?
- What is the trend of strong EX-generated swells affecting the coasts of the Hawaiian Islands?
- What is the impact of the swells generated by the EX storms on the vulnerability of the Hawaiian Islands?

This study includes identifying the strong EX cyclones, characterizing atmospheric criteria of the cyclones for generating swells that can reach the Hawaiian Islands, the characteristics of these swells, and wave climatology of the swells during 2007-2017. This research seeks to examine the yearly trend of the swells due to EX storms, and discover how much these swells contribute towards the vulnerability of the coasts of the Hawaiian Islands. A CVI map identifies and defines the vulnerable areas of the islands. The model used to map CVI reflects a general overview of the surveyed area and depends on the quality and quantity of the data available. It also enables overlapping CVI variables and visualizes their overlaying spatial distribution, which gives a clearer understanding of immediate action points.

2.2 Approach

The study identifies the strong cyclones in the NP by setting up constraints in the algorithm that looks at geopotential height, mean sea level pressure (MSLP), and vorticity of storms. A poor estimation of hurricanes results in the underestimation of wave events. A comparison of nine reanalysis datasets reveals that the datasets show differences in trends and interannual variability in the mean intensity of deep cyclones (Wang et al., 2016). For this study the National Centers for Environmental Prediction (NCEP) Climate Forecast System Reanalysis (CFSR), which has many more cyclones of moderate intensity than the others (Wang et al., 2016), is used. The CFSR is considered a conservative choice but it gives a better representation of the upper percentile wind data relating to extreme event observations (Stopa and Cheung, 2014). The study identifies the coordinates of the eye of EX storm and correlates the associated swells by backtracking hindcast results. The NP boundary is closed at the Arctic Circle, although the effect of EX storms on wave

heights north of the Aleutian Islands is assumed to be less of a contributing factor to the NP wave climate than the waves south of the Aleutian Islands. However, the NP boundary is selected to reduce underestimating events.

The third-generation spectral wave model WAVEWATCHIII (WW3) is used for wave hindcasting. Advances in the swell propagation theory allow for increased precision in modeling. The nested domain is used to better represent the coastlines and provide computationally less time-consuming applications. The results are validated using buoy measurements.

3. Structure of the Dissertation

This dissertation is composed of three publications that form the basis for Chapter 2, 3, 4 and the Appendices. Chapter 2 addresses the swell trends caused by strong EX cyclones by answering first and second research questions. Chapter 2 extensively focuses on the EX detection algorithm, wave hindcast modeling. The validation of the defined detection algorithm and hindcast results with buoys are also presented in the same chapter. Chapter 3 demonstrates the coastal vulnerability of the islands using CVI map formation to emphasize wave exposure, sea level rise (SLR), and surge potential. Finally, Chapter 4 uses the swell events as sole wave exposure contributer on the coastal vulnerability model and examines the significance of boreal winter swells on coastal shores emerges through vulnerability maps. Chapters 3 and 4 address the third research question. Each of the chapters 2, 3, and 4 includes a review of the literature, description of methodologies, conclusions drawn from the results, and implications for ocean and coastal research.

Chapter 5 provides concluding remarks on the dissertation and recommendations for future work. Appendices include the coastal vulnerability map generated for the Hawaiian Islands using a multi-modal sea state and the local scale application of the map used for preparing vulnerability assessments and proposing adaptation methods. Tables and figures are placed after each related chapter.

CHAPTER 2. Evaluation of the strong extratropical-storm generated swells on the tropical islands of Hawai‘i

The material presented here is a version of an article titled "Evaluation of the strong extratropical storm generated swells on the tropical islands of Hawai'i" by Yaprak Onat and Oceana Francis that will be submitted for publication in Ocean Modeling.

Global warming and the increase in greenhouse gas concentration reflect the changes in the meridional temperature gradient and vertical wind shear change. The resulting change in baroclinicity is observed in the storm intensification and raises a question on the effect of the environment on swells in the NP. The work identifies the effective linkages between EX cyclone trends and associated swells that affect the Hawaiian Islands. The strong cyclonic generation coordinates identified by the location of the eye of the storm are chosen from 2007-2017 atmospheric reanalysis dataset and are used to hindcast swells in the NP. The deseasonalized trend shows that poleward and westward movement and increment in the frequency of EX storms causes a significant rise in swell generation and intensity. The strong swells cause almost one quarter of the swell systems reaching Hawai'i with significant wave height and peak period reach up to 0.51 m and 1.72 s in the open ocean. However, the peak direction does not show a significant trend and most occurrences are observed in the ranges between 325–330º.

1. Introduction

Extratropical (EX) storms are known for generating severe weather conditions in the mid-latitudes. These storms transfer heat, moisture, and momentum in the atmospheric layers (Wang et al., 2016) and cause oceanic wave disturbances. The swells generated by EX storms travel while conserving most of their energy and develop high wave energy environments. The contribution of the swells with respect to island vulnerability can be understood by analyzing the trend and links between EX storms and generated swells.

The strong EX cyclones are born from the baroclinic instability due to the mean zonal circulation potential energy conversion into the transient eddies when the kinetic energy peaks (Chang et al., 2002). The baroclinic instability moves towards the equator and boosts the number of EX cyclones, especially during winter in the NP (Chang et al., 2002). The cyclone growth has high

variability in winter months (November-February) and peaks in December and January, however, strong hurricane-force wind fields are generated mostly in February (Jelenak et al., 2009). The cyclone tracks follow an east-northeast direction (~50° from the north) and their wind speed varies anywhere between 13 m/s (Jelenak et al., 2009) and 18 m/s (Businger et al., 2015). In addition to their seasonal dynamic shift, EX cyclones demonstrate variability in their meridional and zonal extant in the NP. The intensified cyclone growth rates are recorded in the western portion of the NP (Iwao et al., 2012). The boreal cyclone belt at the Aleutian lows (Lambert, 1996) around 40°N latitude (Simmonds and Keay, 2002) produces strong storms. The total count and mean intensity of the cyclones increase at the mid-latitudes (30–60° N) and otherwise decrease at the high-latitudes (60–90° N) during winter (Wang et al., 2013). In addition to their seasonal and place-bound fluctuating growth rates, the EX cyclones have demonstrated variability over the years.

Even though Chen and Kuo (1994) linked a definite increase in explosive cyclones to mean temperature changes during 1951–1970 in the northwest Pacific, Lambert (1996) and Paciorek et al. (2002) do not indicate a significant trend on the total number of EX cyclones before the 1970s. A noticeable increase in the trend of EX cyclones becomes pronounced after the 1970s. Many researchers noted a northward shift in the storm tracks due to a poleward broadening of the Pacific jet during winter (Berry et al., 2011; Chang and Fu, 2002; Chang and Yau, 2016; Geng and Sugi, 2001; Graham and Diaz, 2001; Gulev et al., 2001; Harnik and Chang, 2004; Lambert, 1996; Ulbrich et al., 2009; Wang et al., 2006). The 2.2º latitude shift on the average northward movement of the explosive cyclones leads to strong and frequent events at the high latitudes, leaving a significant decrease in the concentration of cyclone events below 45ºN (Bengtsson et al., 2006; Fischer-Bruns et al., 2005; Lambert and Fyfe, 2006; Löptien et al., 2008; Seiler and Zwiers, 2016; Ulbrich et al., 2009; Yin, 2005). The number of strong EX cyclones have increased by 48% over 1948-2000 with 50% deeper central pressure lows, 4-5 hPa decrease in central pressure, and a 10-15% increase in vorticity (Graham and Diaz, 2001). The decrease in the total count and mean intensity of mid-latitude cyclones varies in the eastern and western NP, which shows an increase in storm intensity but a decrease in storm frequency due to strong meridional gradients in cyclonic activity (McCabe et al., 2001; Vose et al., 2014). The decrease in the storm numbers are in the weak-to-medium strength variety during December–January–February by 7% and June–July–August by 3% (Geng and Sugi, 2003). Geng and Sugi (2003) emphasize a significant increase in the frequency of intense storms during June–July–August by 20% in the northern hemisphere along the east and west coasts of the

NP. Thus, the frequency of strong storms has increased even though the total number of storms per year has decreased. As a result, any future decrease in the number of EX cyclones will be small and stronger storms are likely to become more frequent with a fewer total number of storms due to the north poleward shift (Christensen et al., 2013).

The intensification of the winter NP cyclones are thought to be linked with stratospheric ozone depletion in polar latitudes (Bengtsson et al., 2009; Vose et al., 2014), enhancement of greenhouse gas emission concentrations into the troposphere (Geng and Sugi, 2003; Graham and Diaz, 2001), and strengthening sea surface temperature gradients (Inatsu et al., 2003). These changes lead to cooling within the stratosphere (Bengtsson et al., 2009) with a decreasing trend of 0.4±0.1°C over 100 years in the meridional temperature gradient (Gitelman et al., 1997), especially during winter due to strong Arctic warming. The reduced equator-to-pole temperature gradient results in a lack of upper-level westerlies and a decrease in mid-latitude cyclones (Brancome and Gutowski, 1992; Graham and Diaz, 2001; Hall et al., 1994; Iwao et al., 2012; Zhang and Wang, 1997). Because of the uncertainties in linking the primary cause of the EX storm trends to baroclinicity and greenhouse gas trends due to model limitations (Graham et al., 2013), it is too early to declare a robust trend of EX cyclones number and characteristics in the NP.

The variability in the EX cyclone trends dramatically influences the NP ocean environment. The upward trend of wave heights to the south of 40–45ºN after the 1950s (Graham et al., 2001; Trenberth, 1990; Trenberth and Hurrell, 1994) and their effect on long period swells since the 1980s in the eastern NP (Allan and Komar, 2000; Bromirski et al., 2005; Gemmrich et al., 2011; Mendez et al., 2010; Menéndez et al., 2008; Ruggiero et al., 2010) are consistent with increased wind speeds and changes in the structure of the wind field (Graham et al., 2013). On the other hand, a significant decrease in mid-latitude wind speeds results in 10-15% smaller waves at central and western lower mid-latitudes of the NP (Graham et al., 2013; Sasaki, 2014). Surprisingly, this decrease is related to westerly wind speed decreases in the southern flank of the main core rather than the northward shift of EX patterns (Graham et al., 2013). EX storms contribute to 50% wind and 60% wave variabilities along 40ºN (Stopa, 2013) due to an equatorward shift during winter (Chang et al., 2002; Eichler and Higgins, 2006). The maximum swell energy directed from the Aleutian Islands (Fan et al., 2014) does not show a easily discernable propagation pattern. Even though Bromirski et al. (2005) observed high wave heights with higher wind speeds of storms, the wind speed and wave height relation is too

complicated to draw a linear relation (Semedo et al., 2013). Wind direction, cyclone size, and frequency are as important as the magnitude of the wind speed in determining their effect on ocean wave spectra. Therefore, larger scale wave modeling simulations should be performed to model remotely generated swell effects to extend our knowledge of wind-wave interactions and air-sea momentum flux on the global wave environment. This would also allow us to compose more accurate responses to the global wave energy content (Zheng et al., 2016).

The consistent increase in extreme wave climate and its relation to EX cyclones (Wang et al., 2006) in the NP draws attention to swell generation. The swells show small dissipation traveling in deep water, conserving their period and group speed as they travel in the ocean basin (Alves, 2006; Collard et al., 2009; Snodgrass et al., 1966), and may contribute to the wave climate of distant islands like Hawai'i. The Hawaiian wave climate is dominated by high annual wave heights and long-period northwesterly swells during the winter months (Vitousek and Fletcher, 2008) generated by the EX storms near the Kuril and Aleutian Islands (Li et al., 2016). The wave periods increase from west to east due to the propagation of mid-latitude swells from the northwest in the northern hemisphere (Arinaga and Cheung, 2012). EX cyclone characteristic trends that influence Hawai'i's high surf zone trends remain uncertain. The main problem of uncertainty associated with the changes in EX cyclones and ocean swell environment, and their effect on the Hawaiian Islands' vulnerability, requires a correlation between strong winds and wave disturbances on far-reaching coastlines. This research aims to link the EX cyclone evolution with their effect on long-period waves by examining swell trends over 2007–2017. The research identifies strong EX cyclone event locations from a reanalysis dataset and uses wave modeling to hindcast swells over the years and validate the data with existing buoy datasets.

In the next section, the datasets used in the study to define strong EX storm locations and the validation buoy datasets are described. The methods used in the EX storm eye location detection algorithm, wave hindcast modeling criteria, and the statistical analysis are described. In section 3, the characteristics of swell trends found in the section 2 are discussed. In the final section, the results of EX storm-swell analysis and implications for future research are presented.

2. Methodology

The focus of this section is to explain the storm identification algorithm, wave model, and statistical methods used to determine EX cyclone generated swell trends. High-resolution wind data reduces errors in wave modeling. Therefore, selection of high-quality reanalysis datasets is crucial to accurately reproducing the global wind climate (Arinaga and Cheung, 2012; Caires et al., 2004; Chawla et al., 2013; Stopa et al., 2013b). The wind data between 1979–2017 and 2007–2017 are processed via the EX storm detection algorithm. Geopotential height and vorticity fields (Hoskins and Hodges, 2002) are analyzed to focus on synoptic spatial and small-scale features by eliminating the background flow of unfiltered pressures. The effect of individual storms is included by reducing the biases in conventional cyclone tracking algorithms. The wave model state is generated via third generation wave models and compared with buoy data. The datasets and methods used in this study are described in the following sections.

2.1 Datasets

2.1.1 Atmospheric Reanalysis Data

The atmospheric model used in this study is from the National Center for Environmental Prediction (NCEP) Climate Forecast System Reanalysis (CFSR). The CFSR provides higher accuracy upper percentile winds (Stopa and Cheung, 2014; Wang et al., 2016), which are vital for wave hindcasting the Hawaiian Islands (Stopa and Cheung, 2014). The CFSR global atmospheric resolution is about 38 km with 64 levels. CFSR is used to obtain global wind conditions because it includes coupled ocean, land, ice, and atmospheric models with the assimilation of observation time series products (Saha et al., 2014, 2010b). This study uses a spatial resolution of 0.5° grid for the NP between 120°W–120°E and 23°N–66°N from December 2007 to the end of March 2017, combining CFSR and CFSR version 2 (Saha et al., 2011, 2010a). The hourly forecast of the 6-hourly reanalysis set is used for temporal resolution. The data used are the geopotential height, pressure reduced to mean sea level (MSLP), and meridional (v) and zonal (u) wind speeds. These data from the reanalysis are used to identify the strong storm eye location using the storm identification algorithm. The meridional and zonal wind speeds, which are obtained in the marine field at 10 m above the identified storm centers, drive the wave hindcast modeling. The CFSR dataset winds show a strong validation with a thirty-year wave hindcast model performed by Chawla et al., (2013).

2.1.2 Tropical Storm Data

The northeast and north central Pacific hurricane database (HURDAT2) from the National Hurricane Center (NHC) and the Central Pacific Hurricane Center (CPHC) and west Pacific database from the Joint Typhoon warning center (JTWC) between 2007–2014 are used to eliminate the tropical storms and depressions in the EX storm detection algorithm. Both datasets provide best track data that contains tropical cyclone locations, central pressures, winds, and intensities at 6-hour intervals (Chu et al., 2002; Landsea et al., 2016).

2.1.3 In-situ Data

In-situ measurements from offshore buoys of the National Data Buoy Center (NDBC), Pacific Islands Ocean Observing System (PACIOOS) and the Coastal Data Information Program (Scripps Institution of Oceanography (SIO), 2013) are used to validate the EX cyclone detection and wave hindcast results. Hourly significant wave height, peak direction, peak wave period, wind speed and direction are used for verification of the cyclone model and validation of the wave model. Table 1 lists the coordinates, water depths and locations of the offshore buoys used for wave hindcast validation in this study. The data from remaining buoys referenced in the results section are used to correlate magnitude of wind speed correlation with the winds recorded by the algorithm and the buoy measurements at the buoy location. The correlation analysis to show significance and strengths are given to prove that, in fact, strong EX storms occurred in the area.

2.2 Methods for Analysis

2.2.1 EX-Cyclone Identification Algorithm

The cyclone detection algorithm is applied in the NP between the Tropic of Cancer (23° N) and the Arctic Circle (66° N) on a 0.5° × 0.5° latitude-longitude uniform grid during October to March of 2007–2017. Common cyclone identification methodologies used in the literature are based either on mean sea level pressure (MSLP) minima (Gulev et al., 2001; Löptien et al., 2008; Pickart et al., 2009), geopotential height minima (Blender and Schubert, 2000; Francis and Atkinson, 2012a) or a vorticity maxima (Hoskins and Hodges, 2002; Sinclair, 1994). The MSLP based cyclone detection can be less sensitive to powerful high latitude cyclones (Sinclair, 1994) and strong eddies generated from closed low pressures on the surface (Sinclair and Watterson, 1999). While MSLP is sufficient

for capturing slower moving large-scale systems (Hodges et al., 2003), relative vorticity can distinguish storms at early stages of their life cycle and capture the small spatial scale end of the synoptic range (Sorteberg and Walsh, 2008). Becaue the study area includes a high latitude domain where small-scale events frequently occur (Twitchell et al., 1989), relative vorticity is also used in the detection algorithm. Thus, the disadvantage of using unfiltered MSLP (Wang et al., 2006), which captures large scale events and strong background flows (Hoskins and Hodges, 2002), is mitigated.

The hourly MSLP, geopotential height at 925 hPa, and winds at 850 hPa are used for the cyclone detection algorithm to satisfy extreme local conditions within the boundary. The eye of the cyclone coordinates recorded are over the ocean. A cyclone location is recorded if the following parameters are satisfied within 9-grid diameter (approximately 500 km) to capture synoptic scale cyclone events. The constraints are as follows.

- MSLP<970 hPa at chosen grid coordinate
- Local minima of MSLP.
- Local minima of geopotential height at 925 hPa, which is low enough (approximately 800 m above the surface) to eliminate the effect of surface conditions while representing pressure distributions.
- Maxima of relative vorticity at 850 hPa, where friction is small.
- Relative vorticity $\geq 5 \times 10^{-5}$ s^{-1} based on Sinclair and Watterson (1999), who conclude that the local maximum within relative vorticity does not always project the surface pressure lows. The constraint is set to 5 CVU where CVU (cyclonic vorticity unit) is 10^{-5} s^{-1} in the Northern Hemisphere.

The relative vorticity ($\boldsymbol{\zeta}$) is calculated in Cartesian coordinates as

$$\vec{\zeta} = \left(\frac{\partial v}{\partial x} - \frac{\partial u}{\partial y}\right)\hat{k} \qquad (2.1)$$

where *u* and *v* are meridional (*y*) and zonal (*x*) wind speeds, respectively. This relative vorticity calculation is based on winds available at 850 hPa and not dependant on the MSLP, which reduces the biases due to the extrapolated field (Hoskins and Hodges, 2002).

The algorithm also eliminates historical tropical storms, which transitioned in to the detection search range, by removing the locations that correspond to the same location in HURDAT2 and JTWC databases. The automatic algorithm compares the time stamp and coordinates of the EX storm database with the HURDAT2 and JWTC and eliminates any similar tropical event period and location from the dataset as well as their active ~65 km/h (35-knot) wind radii maximum extent in the northeastern, southeastern, northwestern and southwestern quadrant. Thus, any wind noise within the area bound by tropical storm tracking is eliminated so that the analysis is not influenced by tropical storms, depressions, hurricanes, subtropical depression storms, or lows. The tropical cyclone databases are also used to validate the EX storm detection algorithm by comparing the recorded EX storm within their database.

The algorithm records the location of the cyclogenesis, input characteristics, and vector winds 10 m above sea surface, deepening rate, and intensity. A cyclone refers to a single low-pressure center identified at a specific location (grid point) and time. Overcounting is prevented by allowing only one cyclone at and around the diameter of any grid during 72 hours. Note that this study identifies the cyclone's eye and records it for use in the wave hindcasting model instead of tracking the lifespan of each cyclone.

2.2.2 Wave Hindcast Modeling

The wave hindcasting models, which are based on the wave action balance equation, used in this study consider the conservation of action density spectrum. The study uses WAVEWATCH III (WW3) version 5.16 (The WAVEWATCH III Development Group, 2016; Tolman, 1991) to evaluate the directional wave spectrum. WW3 is in good agreement with buoy measurements (Delpey et al., 2010) with less than 10º of directional and 1 s wave period error in wave partitions (Stopa et al., 2016) and reflects swell propagation (Hanafin et al., 2012).

One arcmin length global relief bathymetry data set from the National Geophysical Data Center called ETOPO1 (Amante and Eakins, 2009) is used to generate WW3 model computational grids. The horizontal datum of ETOPO1 is WGS 84 with a vertical accuracy of 10 m. The grids use a global shoreline database polygon of the GSHHS-Global Self-consistent Hierarchical High-resolution Shoreline with 1 km resolution for boundary conditions to develop rectangular grids. The bathymetry grid data are retrieved from ETOPO1, with a resolution of 1 min in latitude and

longitude. The bathymetry was linearly interpolated to a 0.5 arc degree model rectangular grid between 120ºW–120ºE and 0º–66ºN in the NP area. The nested domain has 0.05 arc degree resolution between 161ºW–154ºW and 18º–23ºN in the Hawaiian Islands.

The source terms considered in the WW3 wave model from Ardhuin et al. (2010) include wind-wave interaction (Grachev and Fairall, 2001), nonlinear wave–wave interaction, nonlinear swell dissipation (Ardhuin et al., 2010; Zieger et al., 2015), bottom friction (Ardhuin et al., 2010), depth-induced breaking (Battjes and Janssen, 1978), wind-wave generation (Janssen, 1991), and discrete interaction approximation to define nonlinear wave-wave interactions (Hasselmann et al., 1985; Komen et al., 1996). The fine frequency and angular resolution are set to capture low-frequency swells as well as high-frequency swells in the Pacific, with the goal of improving storm-swell modeling ability (Hemer et al., 2010). A total of 36 directional bands (10° resolution) for 50 logarithmic frequencies with 1.1 constant frequency ratio starting from 0.03–1.1 Hz are used for hindcast modeling to capture frequency and angular spreading. The work by Hanson and Phillips (2001) is used for spectral partitioning. The series of wave heights and peak periods are grouped into swell systems from the spectral partitioning of the directional wave spectrum. The swell systems represent time evolving wave components from the storm. Each observed EX storm event is matched against the swells in each swell system, using the deep water wave dispersion and great circle equations to calculate the group speed of the swell and minimum and maximum durations of the swell system. When an event is estimated to be within a 5-degree threshold of the swell system and traveling toward the source location within the estimated timeframe, the event is associated with that swell system.

2.2.3 Trend Analysis

Cyclone trends are obtained by examining the MSLP and geopotential height during 1979-2017. Swell trends are displayed by examining the change in significant wave height, wave period, and direction over 2007-2017. The magnitude estimate of the characteristics of swell trends, *TS*, are calculated using the robust trend calculations applied by (Aarnes et al., 2015; Sen, 1968; Stopa and Cheung, 2014; Wang and Swail, 2001; Young et al., 2011) with data at time j and k where $k<j$ for the ith month is

$$\mathrm{TS} = \mathrm{median}\ \frac{\mathrm{x_{ij}} - \mathrm{x_{ik}}}{\mathrm{j-k}} \tag{2.2}$$

for all data *x*. The Mann-Kendall test (Gilbert, 1987; Kendall, 1975; Mann, 1945) is applied to assess the monotonic trend H_a. The significance of the trends are assessed with the Mann-Kendall nonparametric test, which is used to identify significant results and the relation to randomness by eliminating gross errors and non-normality of the distribution (Wu et al., 2017). The non-parametric functionality of the test allows usage in nonlinear regression fitting. The method is less sensitive to gross errors because it has no distributional assumption. For the dataset $x_1, x_2, \ldots, x_n$ for n measurements, the number of the difference of positive and negative differences, *S*, is

$$S_i = \sum_{k=1}^{n_i-1} \sum_{j=k+1}^{n_i} sgn(\boldsymbol{x_{ij}} - \boldsymbol{x_{ik}}) \tag{2.3}$$

Because we focus on strong EX cyclone effects during winter and fall months, summer and spring effects (i.e., May, June, July, August and September) are treated as missing data and not considered. In other words, $sgn(x_{ij} - x_{ik})$ is equal to zero. Therefore, only six months are considered beginning in January with $i = 1$ to December $i = 6$. The data is used to calculate the monthly trend for each year with the mean of *S* equaling zero and the overall variance of *S* modified by (Hirsch et al., 1982) as

$$S' = \sum_{i=1}^{6} S_i \tag{2.4}$$

$$VAR(S') = \sum_{i=1}^{6} VAR(S_i) + \sum_{i=1}^{6} \sum_{l=1}^{6} cov(S_i, S_l) \tag{2.5}$$

$$VAR(S_i) = \left(n_i(n_i - 1)(2n_i + 5)\right)\Big/_{18} \tag{2.6}$$

where $\neq l$, $cov(S_i, S_l)$ is the covariance and n_i is the number of data points in the *i*th month. The standard normal variate *Z* is defined as follows

$$Z = \begin{cases} \frac{S'-1}{\sqrt{VAR(S')}} & if \quad S' > 0 \\ 0 & if \quad S' = 0 \\ \frac{S'+1}{\sqrt{VAR(S')}} & if \quad S' < 0 \end{cases}, \tag{2.7}$$

where the null hypothesis of randomness, H_0, is accepted when $|Z| < 1.96$, , using a tolerable probability of $\alpha = 0.05$. In addition to the Mann-Kendall test, the Pearson correlation and *p-value* significance for the trends are calculated. The Pearson's correlation coefficient is

$$\rho_{X,Y} = \frac{cov(X,Y)}{\sigma_X \sigma_Y} \tag{2.8}$$

where *cov* is covariance, and σ is the standard deviation for series *X* and *Y*. The swell and cyclone trend values are calculated by decomposing the data from their cyclic patterns. The time series, *y*, is assumed to have three components

$$y = T + S + I \tag{2.9}$$

where *T* is the non-seasonal deterministic trend, *S* is seasonal deterministic component and *I* is the stochastic irregular component. The additive model given in Equation (2.8) is de-seasonalized by subtracting a moving average from the original series *y*. A seasonal filter is then applied to the de-trended time series, *y*-*S*, to obtain a de-seasonalized series, which is used to find the trend using linear regression fitting (Findley et al., 1998).

2.2.4 Validation of Cyclone Events and Hindcast Waves with In-situ Data

The cyclogenesis creates a disturbance on the wave surface thus forming wind waves. Therefore, the expectation is that wind waves are generated around the eye of the cyclone. The significant wave heights, obtained from buoys, are correlated with the 10 m wind speed obtained from the cyclone identification analysis to verify cyclogenesis presence. A strong correlation is an indication that a strong storm is present in the area. A positive correlation in wind speed against significant wave height and average wave height indicates an increase in wind energy in the area, whereas a low correlation might be due to diurnal change in wind direction.

Typical statistical indexes are used to compare the wave hindcasting model results with buoy measurements. Using N as the number of paired measurements and reanalysis values, mean error (*ME*), *rmse*, bias, correlation, and scatter index and t-test are calculated for variable X, where the sub-indexes M and O indicate the model value and observation, respectively. The bias b is computed by

$$b = \frac{1}{N}\sum_{i=1}^{N}(X_{Mi} - X_{Mi}) \tag{2.10}$$

moreover, the correlation of determination, R^2, measures how closely the data is fitted to the model with the relation by

$$R^2 = \left(\frac{\sum_{i=1}^{N}(X_{Mi} - \bar{X}_{Mi})(X_{Oi} - \bar{X}_{Oi})}{\sqrt{\sum_{i=1}^{N}(X_{Mi} - \bar{X}_{Mi})^2 \sum_{i=1}^{N}(X_{Oi} - \bar{X}_{Oi})^2}} \right)^2 \tag{2.11}$$

where the overbar is used to indicate the average. The *rmse* measures the strength of the relation, which is given as

$$rmse = \sqrt{\frac{1}{N}\sum_{i=1}^{N}(X_{Mi} - X_{Oi})^2} \tag{2.12}$$

The scattered index is given by

$$SI = \frac{1}{\bar{X}_O}\sqrt{\frac{1}{N}\sum_{i=1}^{N}((X_{Mi} - \bar{X}_{Mi}) - (X_{Oi} - \bar{X}_{Oi})^2} \tag{2.13}$$

The distribution of the hindcast and measured data are demonstrated with quantile-quantile (Q–Q) plots.

3. Results

The results given in this section present the EX cyclone and generated swell characteristics and patterns obtained from the wave model and buoy measurements. The trend calculations are applied to the moving averages and refer to a rate. The trend difference refers to a difference in the height of trend line.

3.1 EX-Cyclone Events

The validation of the EX-identification algorithm shows ocean disturbances and strong correlation. The represented strong EX storm event in Fig. 2.1a, which highlights the geopotential low, is detected using the algorithm. The wind speed magnitude recorded at the buoy location of NDBC 46075 (53.983ºN, -160.817ºW) is plotted against the wind measurements from the buoy. The time series of the wind magnitude (Fig. 2.1) demonstrates similar patterns and peaks between wind speed recorded from CFSR and wind speed recorded via buoy on December 25th, 2015.

The storm event MSLPs over the 38 years (1979-2017) is plotted in Fig. 2.2. The linear trend of the average of the MSLP and geopotential heights for each year (Fig. 2.2) demonstrate an average decrease of 0.67 hPa, a rate of 0.02 hPa/year for the MSLP, and a rate of 0.26 m/year for the geopotential height. The fluctuations in MSLP and geopotential height are stable after the 2000s. The last ten years show a linear decline with an average MSLP decline of 3.34 hPa and a rate of 0.372 hPa/year, and an average geopotential height of 23.9 m and a rate of -2.6 m/year. The number of strong EX cyclones over the years showed a significant increasing trend of 7.3/year. The rate increase in the magnitude of the trend emphasizes the need for careful examination of the last ten years of cyclonic data.

Figure 2.3 depicts the six-month range of each event from November till the end of December for ten years. The increase in storms concentrated in the NP during 2007–2017. The number of storms increased during the strong El Niño seasons of 2009–2010 and 2015–2016. During the strong La Niña seasons of 2007–2008, 2010–2011, and 2011–2012, the number of events is small compared to non-ENSO seasons and the locations of these events move poleward. A high concentration of events is observed around the 43-45ºN latitude (Fig. 2.3). The number of events are plotted against Multivariate ENSO Index (MEI) (Wolter, 2018) and Pacific Decadal Oscillation (PDO) (NOAA National Center for Environmental Information, 2018) to show a correlation (Fig. 2.4). The MEI and PDO indices show the monthly sea surface temperature anomalies in the NP and show similar patterns in the number of strong EX storm events over 2007-2017.

The latitude range of events over the last ten years demonstrates that the average concentration moved equatorward during the El Niño seasons and poleward during La Niña seasons (Fig. 2.5a). The average latitude moved northward 2.7° over ten years. The concentration of events is in the

northeast Pacific and the Aleutian Islands. The events show a westward move of 4.65° within the last decade (Fig. 2.5b).

The average cyclone counts and intensity over the last 38 years (Fig. 2.6a) show that most of the events concentrate around the 965–970 hPa level. The last ten years (2007–2017) gives a mid-range value between 1987–1997 and 1997–2007. For the last ten years, these events show a wide range in the MSLP concentration (Fig. 2.6b). The variation may be the result of ENSO events and seasonal fluctuations. The average number of storm events per month shows that the EX events increase consistently between October until February, followed by a decrease in March (Fig. 2.7). This increase confirms that the greatest number of strong cyclones most likely occur during the December-January-February time range.

The EX cyclone generation locations are correlated to demonstrate how the swell systems reach Hawai'i. Among the 1319 swell systems, 319 swell systems are detected in 2007-2017. The swell systems represent 24.18% of the swells generated during the modeled period. The Pearson and Spearman correlation given in Table 1 shows a significant correlation between the strong EX events and swells. The correlation relationship showed a statistically significant positive correlation between significant wave height and peak period. The results also show a strong correlation between MSLP and geopotential height. The correlation was not significant between the peak period and event parameters. The location of the most dominant swells generated from the EX events are detected around the Kuril and Aleutian Islands. The events generated above the Aleutian Islands do not transfer much of their energy into the Pacific due to a number of small islands within the area that act like a barrier. The number of strong EX storm events and associated swell systems are correlated using linear and quadratic regression analysis (Table 2.2). The *p-value* < 0.05 shows statistically significant association and standard deviation of the distance between the data values, *Sd*, and percentage variation of the response, R^2, indicates a better fit with quadratic equations.

3.2 Swell Systems

Figure 2.8 shows the time series of the swells generated by EX storms, which reach the northwest location of O'ahu (201.85ºE 21.75ºN). The model requires an average of three days to spin up and runs from October until the end of March of each year span. The peak over threshold analysis shows that significant wave height reaches over 3.63 m about 70 times (Fig. 2.9). A

maximum significant wave height of 7 m with a 17.1 s peak period coming from 330º is observed during an intense El Niño event when the geopotential height dropped to 329.6 m. The peak wave period ranges between 13-18 s. The direction of the swells is mainly from 325-330º and EX storm events mostly generate below the Aleutian Islands. The scattered swell data and histograms of the wave characteristics are given in Fig. 2.10. The distribution of the swells is mainly dominated by an average of 1.26 m, at 325-330° and a 13.41 s peak period.

The swell direction rose for each season demonstrates the high swell events shift from the northwest to the north from fall to winter (Fig. 2.11). The spring wave direction rose does not reflect the total change because only March is included. Although there is no significant change in direction from winter to the month of March, the probability of observing the highest events decreases. The dominant direction reflects a meridional shift in EX cyclones. The strong EX cyclone generated northwest swell characteristic are an average of 2.18 m, direction of 325°, and a peak period of 17.68 s. These annual extremes are due to strong EX cyclones.

The maximum value of the significant wave height de-seasonalized trend of the swells (Fig. 2.12) shows most of the maximum changes observed around 0.40–0.45 m except for January and February, when the maximum trend difference reaches 0.65 m. The low trend slope differences behind the islands indicate the sheltered zones from the north swell effects. The non-parametric trend of swells shows that the highest activity is observed in February (Table 2.4) for the northwest location of Oʻahu (201.85ºE 21.75ºN). The Mann-Kendall test results show no significant trend during November and December. However, significant trends exist in other months, especially the high swell energy months of January and February. The maximum value of the peak period de-seasonalized trend of the swells (Fig. 2.13) shows the movement of the strong swells throughout the months. The peak period trend slope differences are highest in October, which means that there are more strong EX storms in this month. The strong EX storm belt moves toward the equator during the winter making the trend slope differences smaller as the swells travel a shorter distance then in fall. The EX storm belt is closest to the Hawaiian Islands during February. The Mann-Kendall test results for the associated peak periods on the northwest location of Oʻahu (201.85ºE 21.75ºN) show significant trends every month except December and February. The average maximum value wave trend of each grid point around the Hawaiian Islands (Fig. 2.14) shows the similar sheltering effect of the islands. The highest significant wave height slope differences are located northwest of Kauaʻi.

Figure 2.15 shows an example of the strong swell event on February 22, 2016. Twelve swell systems reached Oahu during February 19–26, 2016. Among those swells, five swells affected the area on Feb. 22, 2016 in the directional spectrum. The peaks of the events are easily seen in Figs. 2.16 and 2.17. The swells reaching this location are grouped into five swell systems using spectral partitioning by Hanson and Phillips (2001) (Fig. 2.17). Figure 2.18 shows that there are four swells generated by strong EX cyclones out of the 12 swells given in Fig. 2.15. The strong EX cyclone events associated with the swells in Fig. 2.18 are generated in the northwest direction.

The time series distribution of the peak of the daily swells is decomposed to show that a de-seasonalized trend of the swells is generated by strong EX cyclones in the northwest of Oʻahu (201.85ºE 21.75ºN) (Table 2.6). Northwest of Oʻahu the maximum significant wave height rate is +0.022 m/year and the peak period rate is +0.073 s/year (Table 2.5). The maximum trend difference in significant wave height is 0.51 m and the peak period is 1.72 s over 2007-2017. During 2007-2017 the change in average significant wave height is 0.36 m and the average peak period is 1.43 s for the area northwest of Oʻahu. The most observed direction ranges between 325-330°. The Mann-Kendall results indicate the significance of the daily series trend. The maximum average of the wave trend time series of significant wave height and peak period shows the linear trend for the de-seasonalized series (Fig. 2.18). The non-parametric trend test results also show a close correlation using the de-seasonalized trend method. The rate of increase in the strong EX-generated swell on the north shore of Oʻahu is higher than the overall trends in the same area.

The WW3 model results are validated with buoy data (Table 2.7). The time series distribution, QQ-plots (Fig. 2.19), and error metrics prove a high R^2 shows closely fitted regression with true predictions in the swell system decomposition. The model has high regression at the northwest facing buoys of Kauaʻi and Oʻahu. The period correlation is lower than wave height correlations of the primary swell. The model is less scattered, however, and showed higher bias around the refracted zones. The highest errors are observed in the sheltered zones. The high *rmse* in peak period indicates rough partitioning of the swell systems. Although modeling applications are advanced enough to capture the wave distribution on interisland channels and headlands, northwest swells are still overestimated in sheltered areas (Li et al., 2016).

4. Discussion

The accuracy of the EX detection algorithm depends on the reanalysis data. CFSR is known to show more cyclones of moderate intensity than other datasets (Wang et al., 2016). CFSR's overestimation of the wind speeds especially near Alaska and in the northeast Pacific (Stopa and Cheung, 2014) can cause biases in the wave modeling.

EX cyclone location detection is advantageous in detecting all of the EX cyclonic locations for identifying individual cyclones and using approaches like band-pass filtering, which cannot single out the cyclone tracks but measures the baroclinic fields (Wallace et al., 1988). Because the method looks for the local minima and maxima of the chosen grid fields, the detected locations closer than the chosen detection radius to the boundaries are biased. An alternative is to either eliminate the events inside the chosen grid radius of the boundaries or extend the boundary regions out further than the desired boundary. The method does not track cyclones due to the uncertainty in determining the individual storm duration and swell spin-up time, isolation of the event, and high computational cost (Alves, 2006). Isolating an individual storm location instead of using a segmented wind field creates a duration-limited wave generation problem in large ocean basins. This problem is reduced by correlating the peak direction of the swells with the event locations by performing backtracking for the wave hindcast model using the dispersion equation. The deep water dispersion relation has high accuracy along the great circle paths; however, tends to overestimate when it reaches poleward.

The swell dissipation and propagation (ST4 package) of WW3 displays the swell dissipation well in high wave energy environments like the Pacific Ocean (Bi et al., 2015). Even though ST4 results give a better representation of extreme waves in swell-dominated areas (Shimura et al., 2015), the attenuation rate of swell energy can be improved to provide a better representation of frequency dispersion and angular spreading in tropical and sub-tropical areas with empirical tuning (Jiang et al., 2016). A limit to the study is that it does not consider the strong current effect on swell propagation. The relatively coarse resolution is not enough to represent the refraction in the protected shores. However, the nested integration of nearshore wave models can be applied to fine tune future studies. The WW3 northern hindcast boundary is cut at the Arctic Circle (66°N) to eliminate the numerical instability due to the time step convolution at high latitudes (Hanafin et al., 2012).

The comparison of the hindcast results with buoy observations shows good representation for wave systems on north to northwest facing shores. The spectral resolution for direction is fine enough to allow for spatial propagation, reducing the garden sprinkler effect. However, the difference can be higher for breaker heights and dominant wave periods of large swells (Businger et al., 2015). Therefore, in this study a comparison is made in deep water to eliminate wave-breaking effects. The results are consistent with Chawla et al. (2009), who show an overestimation of the wave heights. The model displays a shadowing of the swells resulting from the islands. The lack of diffraction in the model and abrupt changes in the bathymetry overestimates interisland channels and headlands and underestimates sheltered areas, as demonstrated by Li et al. (2016) for multi-state modeling. In the future, the WW3 model will need appropriate adjustment to represent the diffraction around small island chains.

The spectral partitioning in directional wave spectra requires swell angle and spectral distance threshold to separate the adjacent peaks. The automated individual spectral spread for a fixed angle may lead to the formation of a number of swell systems.

The results confirmed the results of Li et al. (2016) who showed that in a boreal winter, the intense storms that generate swells originate near Kuril and Aleutian Islands reach Hawai'i. The El Niño Southern Oscillation effect (Stopa and Cheung, 2014) on the increased intensity of the north swells (Aucan, 2006) correlates with the intensity of cyclonic events. The intensity of the storm events decreases during ENSO events, ranging from 30-60°N latitude during the winter (Hanafin et al., 2012). In the last ten years, the trend of the front of the EX cyclones moves poleward at a rate of 0.30°/year, validating arguments for poleward intensification (Fyfe, 2003; Yin, 2005). The strong El Niño event also demonstrates fluctuations in storm-generated swells. The East Pacific pattern index (EP) between the Aleutian low and Hawaiian high (Allan and Komar, 2000) provides a better explanation for the ENSO events. The meridional location shift in the winds moves west at 0.12°/year but shows a more intense value of 0.52° per year in the last ten years due to strong ENSO events. A significant westward shift is observed during the La Niña years. The results also confirm that the monthly intensity of the cyclones increases from November with the greatest intensity during February.

The swells propagating to the Hawaiian Islands show seasonality. The trend taken for de-seasonalized data shows a substantial increase in the significant wave height of 0.51 m and 1.72 s peak period in 2007–2017 at northwest of O'ahu. The numerical errors on swell dissipation and wave growth affect the accuracy of the hindcast results. The maximum swells align with Li et al. (2016, 2012) and show high trends in the region north of the islands where the maximum wind-sea energy of the cyclones are generated. The swell period ranges between 13–18 s and has cyclonic peak directions. The change in the strong EX storm-generated swells are larger than the trend change of the all swells approaching northwest of O'ahu. The significant change in the swell heights shows that statistical representation of the swells should be examined at a regional or local level (Hanafin et al., 2012). Accurate swell climate projections should include a large basin model for local-scale results.

The liner trend calculations are sensitive to the duration of the data. The rates should be interpreted as an indication of the general behavior (Graham and Diaz, 2001) of the cyclones and swells. The non-parametric tests, such as Mann-Kendall, assess significant change in the trend without being affected by the non-normality of the distribution (Wu et al., 2017). The de-seasonalized wave height and period data capture the significant trend changes over the years. The multi-modal state results indicate that as the wave period and height decrease for the Hawaiian Islands, while the number of strong swells increases at mid- to high latitudes (Sasaki, 2014). Thus, although the enhanced effect of the trade winds in the eastern equatorial Pacific with La Niña weaken swells propagated from mid-latitude NP during 1992–2012 (Sasaki, 2014), the strong EX cyclone-generated swells increase during 2007–2017.

5. Conclusion

The research focuses on strong EX cyclone characteristics and their impact on the trends of swells for the Hawaiian Islands. The strong cyclones are defined by a three-constraint detection algorithm using a CFSR reanalysis dataset. The existence of the strong El Niño events directs attention to the last decade, where the MSLP and geopotential height decline are 3.34 hPa and 23.85 m during 2007-2017, respectively. The boreal winter, when strong EX cyclone concentration is the greatest in February, generates significant swell wave heights of up to 7 m and peak period of 17.2 s. The EX events intensify during the El Niño season and move equatorward. During the last

decade the strong EX cyclones show a 2.7° northward and a 4.65° westward shift. The EX events are observed to consistently increase during the winter months, reaching a peak number of events in February. The correlation between EX cyclone and high swell system are observed, with generating 24% of the total swells generated during the last decade.

The de-seasonalized trend of the swell characteristics shows a significant increase in significant wave height and peak period at 0.51 m and 1.72 s northwest of O‘ahu, respectively. The direction shows a cyclonic pattern but remains consistent with most of the dominant direction changes from 325-330°. The intense concentration of EX cyclones that generates high-energy swells that propagate to the Hawaiian Islands originates south of Aleutian Islands. Even though the mid-latitude cyclones weaken (Sasaki, 2014), our study shows that the number of strong EX cyclone generated swells significantly increases.

The study has model limitations in storm tracking, swell dispersion, and underestimation in diffraction in sheltered areas that require further improvement. The study demonstrates that the swell variability of a local region can only be explained through a global model to eliminate duration-limitation of the swell growth. Swell trend studies will give a better understanding for wave exposure, especially for the small islands of the Pacific where the potential risk high for the coastal infrastructure, ecosystem, and economic resources.

Table 2. 1: Locations and temporal coverage of the CDIP buoys used in the research.

CDIP Buoy	Latitude (ºN)	Longitude (ºW)	Water Depth (m)
202-Hanalei	22.285	159.574	200
106-Waimea	21.671	158.117	200
098-Mokapu	21.415	157.678	88
187-Paunela	21.018	156.425	200
188-Hilo	19.780	154.970	345

Table 2. 2: The strong EX-cyclone event and associated swell system correlation over 2007-2017. The values in bold show significant correlation. Hs: Significant wave height, Tp: peak wave period, GHP: geopotential height, MSLP: mean sea level pressure.

	Hs		Tp		GHP	
	Pearson	Spearman	Pearson	Spearman	Pearson	Spearman
Tp	**0.282**	**0.256**				
GHP	**0.18**	**0.262**	0.036	**0.111**		
MSLP	**0.153**	**0.222**	0.012	0.056	0.959	0.853

Table 2. 3: Regression analysis between the number of strong EX-storm events and number of associated swell systems. *Sd:* standard deviation of the distance between the data values, R^2: percentage variation of the response, and *p-value* < 0.05 indicates significant correlation.

Source	*Sd*	*R^2 (%)*	*p-value*
Linear	7.13	43.35	0.038
Quadratic	5.61	69.32	0.045

Table 2. 4: Descriptive statistics of monthly swell wave height and Mann-Kendall test results the northwest location of O'ahu (201.85ºE 21.75ºN). The *p-value* < 0.05 indicates a significant trend.

Month	*Min(m)*	*Max(m)*	*Mean(m)*	*Stdev(m)*	*p-value*
Oct	0.2	3.49	1.03	0.61	**<0.05**
Nov	0.2	5.1	1.28	0.72	0.16
Dec	0.2	5.45	1.45	0.85	0.056
Jan	0.21	6.22	1.83	1.09	**<0.05**
Feb	0.2	6.95	1.64	0.99	**<0.05**
March	0.2	6.04	1.36	0.88	**<0.05**

Table 2. 5: Descriptive statistics of monthly swell peak period and Mann-Kendall test results at the northwest location of O'ahu (201.85ºE 21.75ºN). The *p-value* < 0.05 indicates a significant trend.

Month	*Min(s)*	*Max(s)*	*Mean(s)*	*Stdev(s)*	*p-value*
Oct	5.29	24.96	11.02	3.26	**<0.05**
Nov	5.52	22.84	12.18	3.51	**<0.05**
Dec	5.53	24.87	12.28	3.10	0.92
Jan	5.77	26.17	13.27	2.76	**<0.05**
Feb	5.80	24.03	13.15	2.85	0.10
March	5.89	23.35	12.03	3.12	**<0.05**

Table 2. 6: Trend changes of the swell wave height and peak period over a 2007-2017 at the northwest of Oʻahu (201.85ºE 21.75ºN). Rate: slope of the trend line, Diff: difference between the values at the highest and lowest point of the linear slope height.

	Hs		*Tp*	
De-seasonalized trend	Rate (m/yr)	Diff (m)	Rate (s/yr)	Diff (s)
Max	0.022	0.51	0.073	1.72
Min	0.010	0.23	0.053	1.23
Average	0.016	0.36	0.062	1.43
Thiel-Sen trend	Slope (m/yr)	Diff (m)	Slope (s/yr)	Diff (s)
Max	0.021	0.50	0.071	1.64
Min	0.005	0.13	0.054	1.24
Average	0.013	0.32	0.057	1.33

Table 2. 7: CDIP buoy and WW3 model results comparison of primary swells between 2015-2016.

	HS				**TP**			
CDIP BUOY	*Bias (m)*	*rmse (m)*	*SI*	R^2	*Bias (s)*	*rmse (s)*	*SI*	R^2
202-HANALEI	-0.46	0.53	0.24	0.95	2.75	8.74	1.0	0.57
106-WAIMEA	-0.67	0.75	0.35	0.78	1.04	5.23	0.76	0.28
098-MOKAPU	-0.72	0.79	0.31	0.78	2.24	6.84	0.9	0.08
187-PAUNELA	-0.56	0.61	0.24	0.86	1.39	7.02	0.99	0.48
188-HILO	-0.79	0.87	0.29	0.59	-0.72	1.60	0.20	0.44

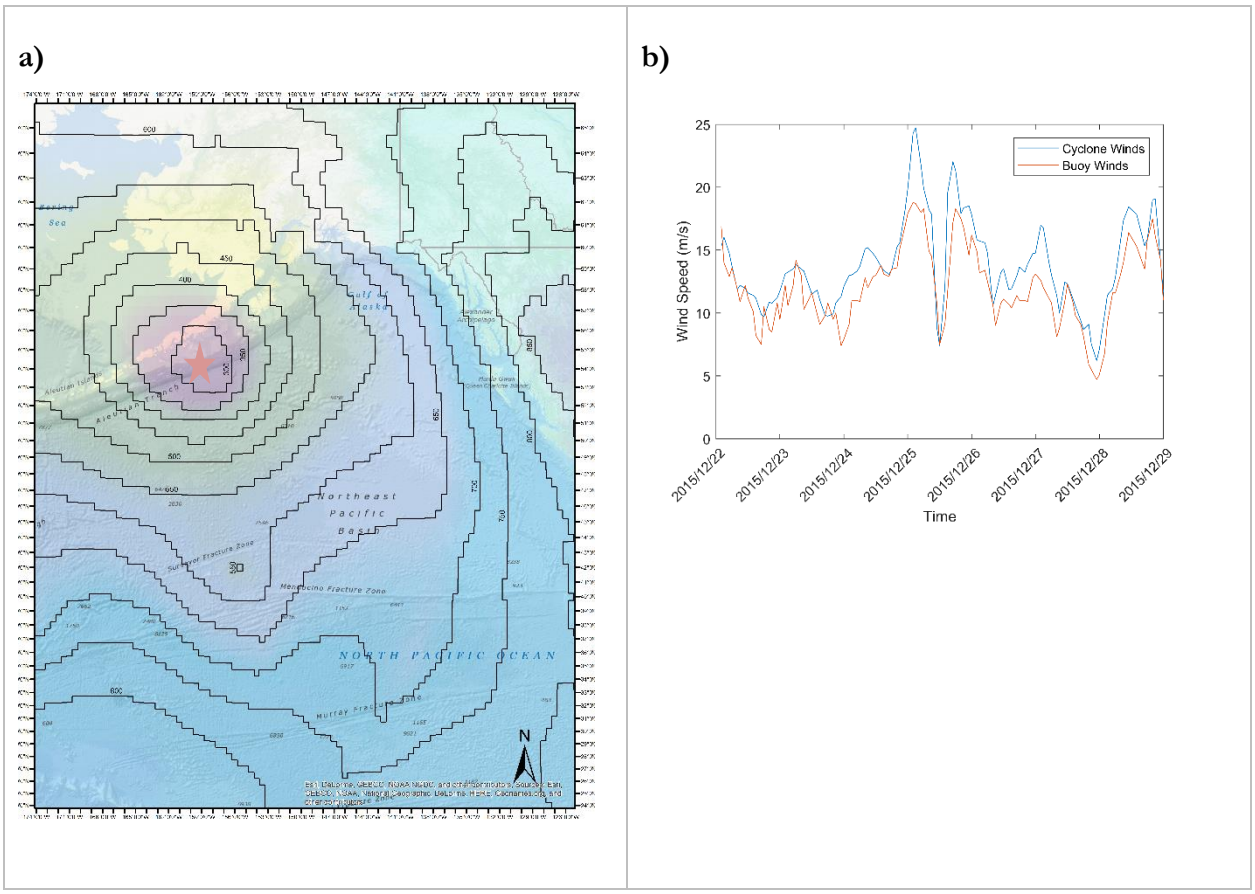

Figure 2. 1: EX-storm identification algorithm validation. Location of the detected event in geopotential height map (a) and wave and wind disturbances plot of the wave hindcast results of algorithm and wind measurments from buoy (NDBC 46075, marked with star on Fig. 2.1a) (b) on December 25th, 2015. The map is 174°W-125°W and 24°N-66°N with 1° intervals.

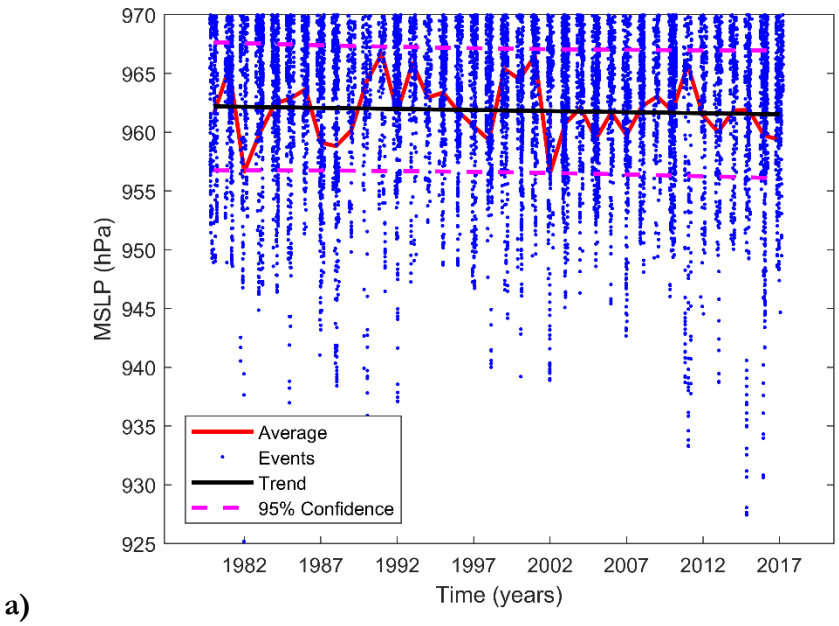

a)

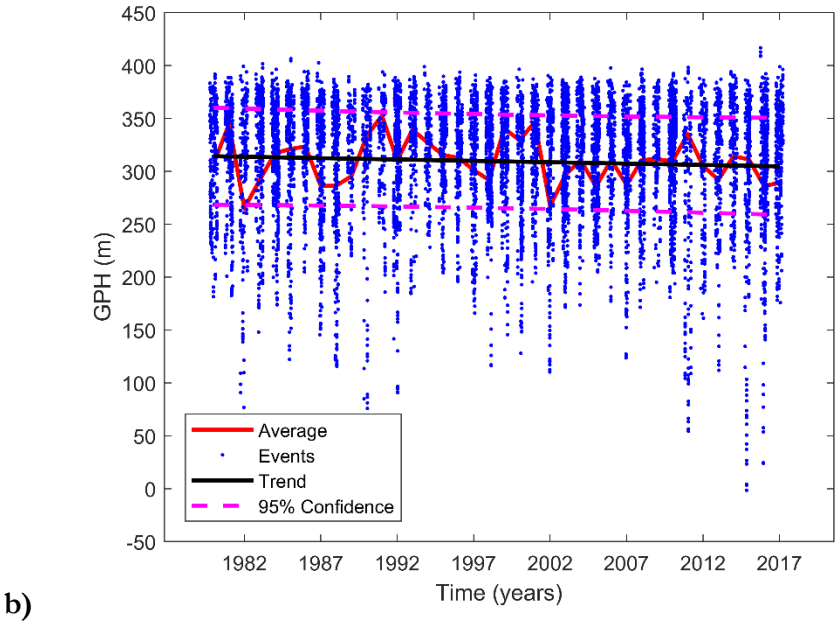

b)

Figure 2. 2: Change in strong cyclone MSLP (a) and geopotential height (b) over 1979-2017. The red line represents the yearly average of the MSLP and geopotential height (GPH).

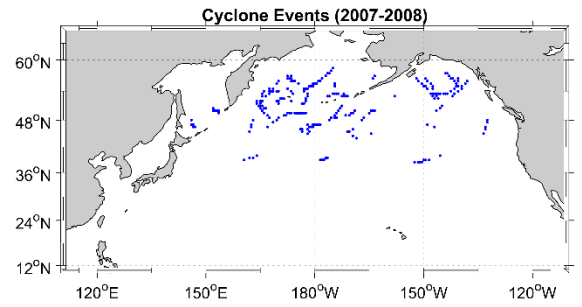

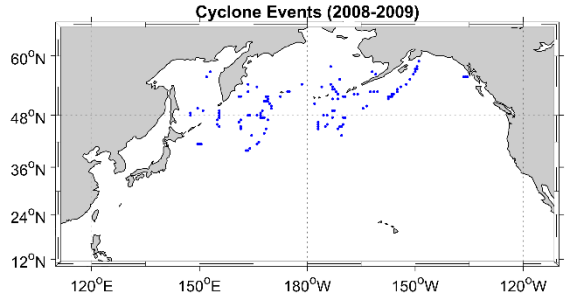

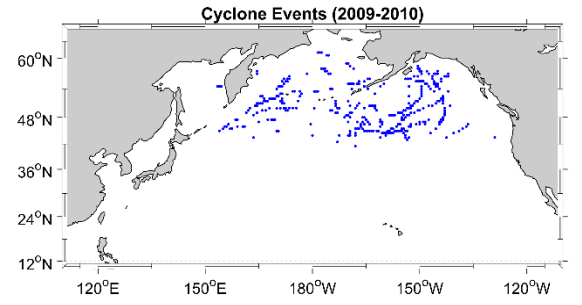

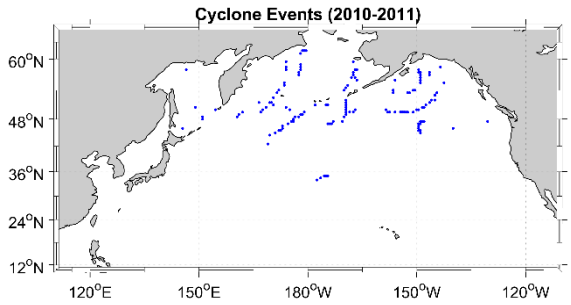

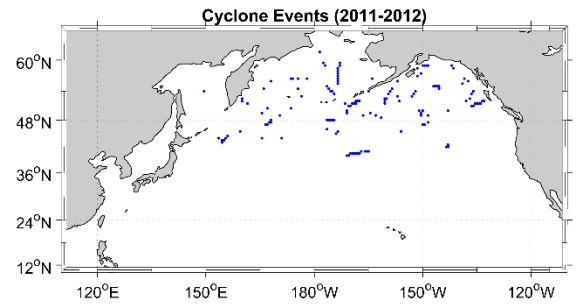

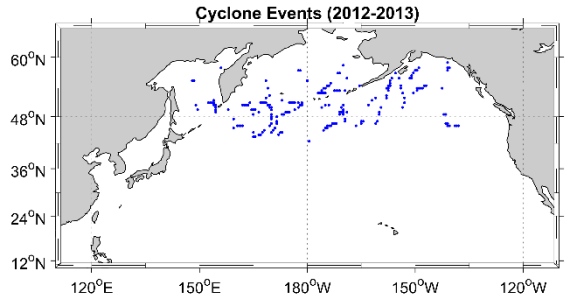

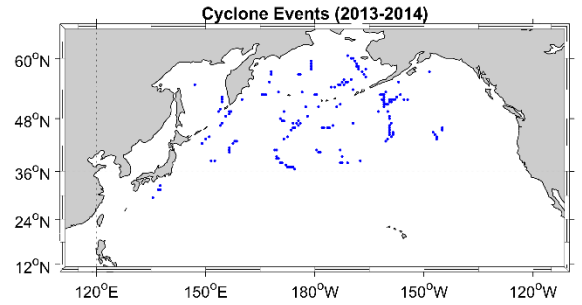

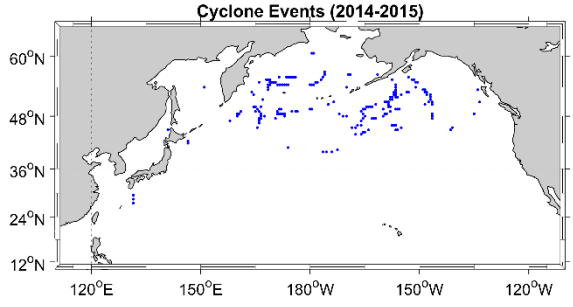

Figure 2.3 continues

Figure 2.3 continues

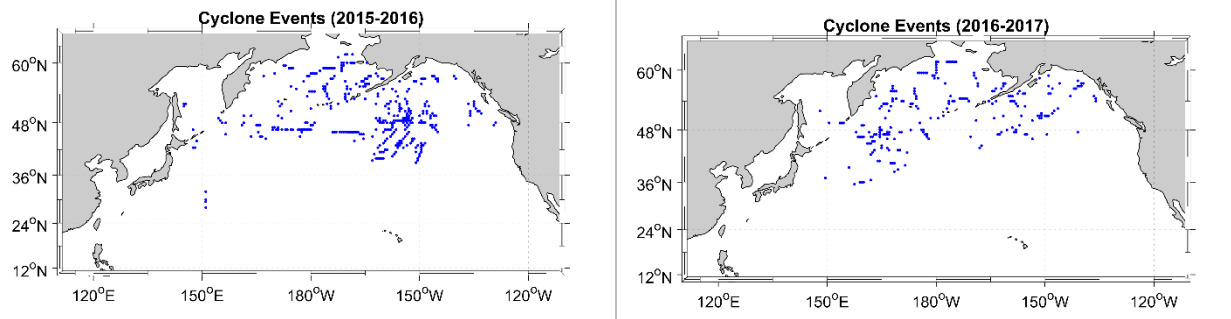

Figure 2. 3: Location of the events detected between November to December for the 2007-2017 from the EX-storm detection algorithm.

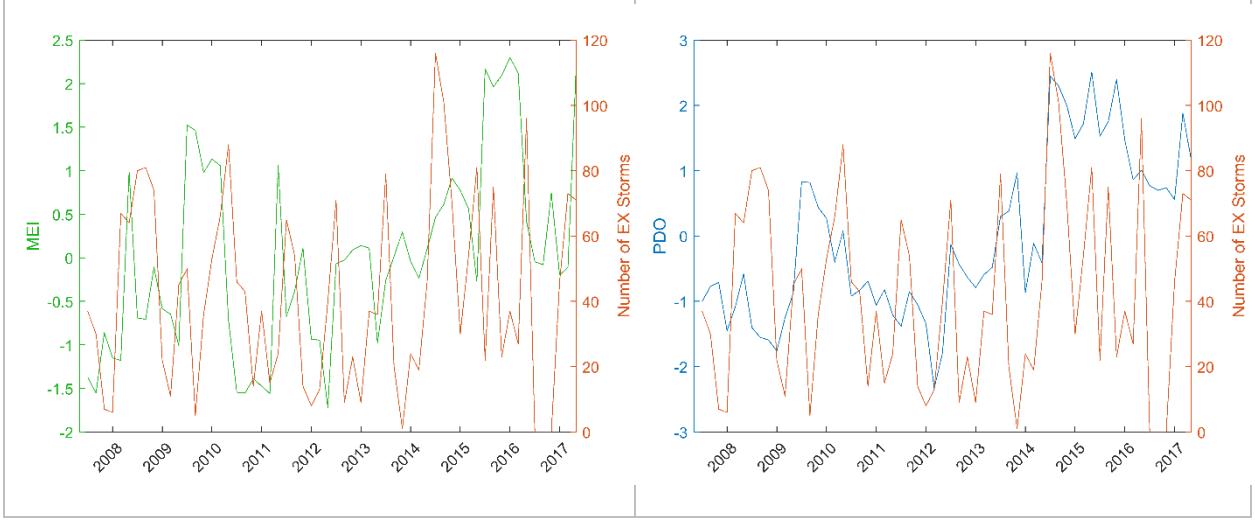

Figure 2. 4: Multivariate Enso Index (MEI) (left) and Pacific Decadal Oscillation (PDO) (right), and number of strong EX-storm events during 2007-2017.

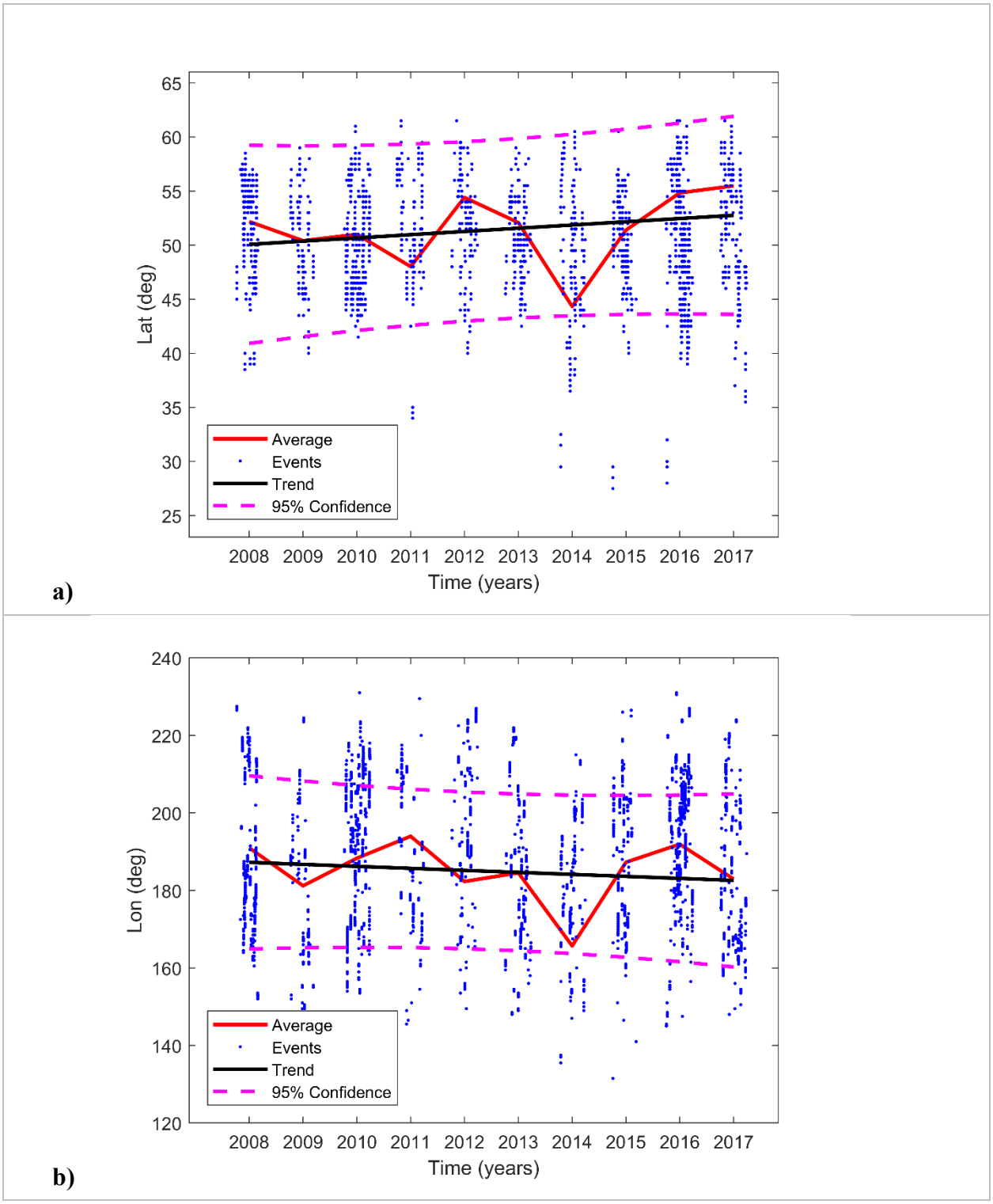

Figure 2. 5: Zonal and meridional cyclone trends between 2007-2017.

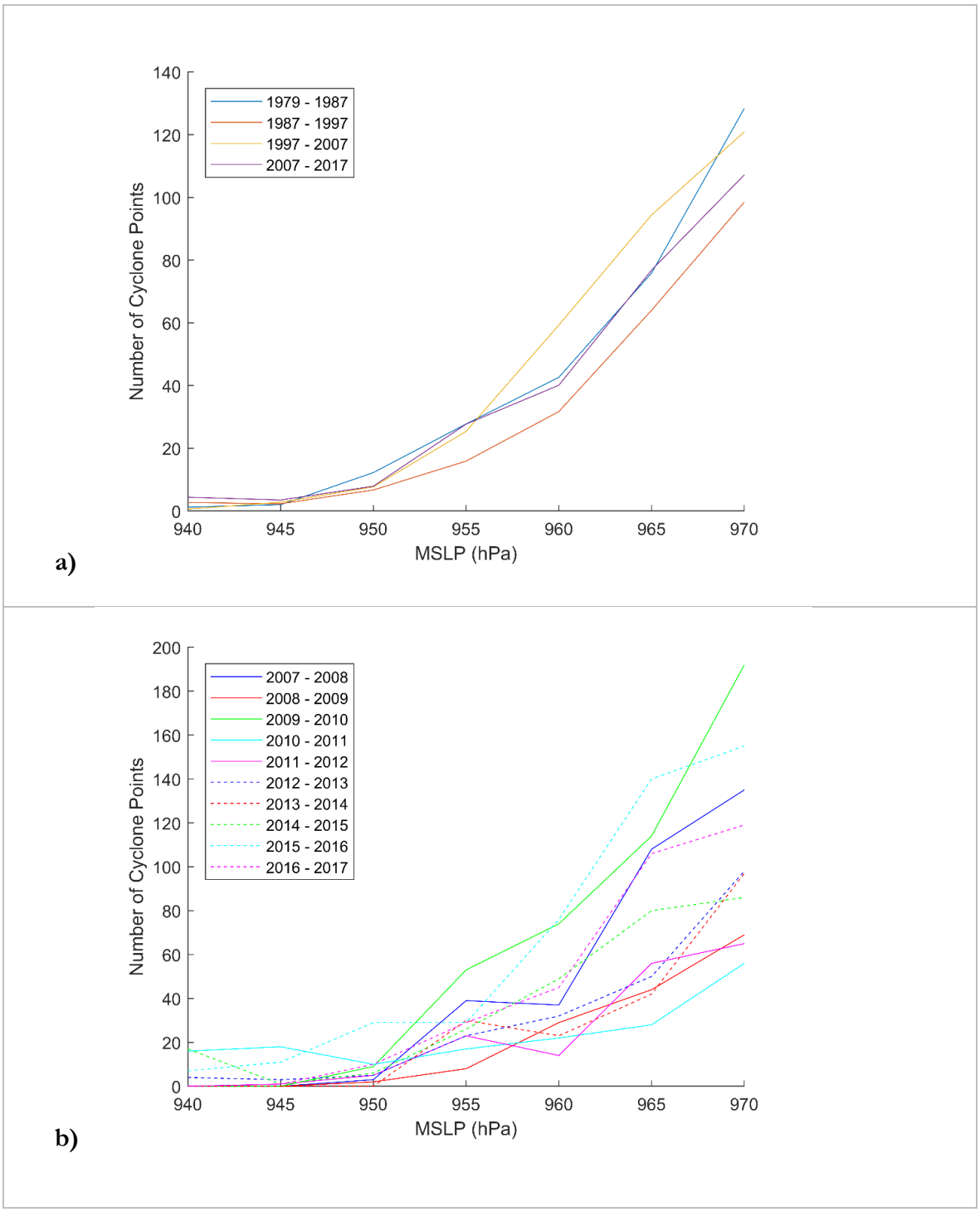

Figure 2. 6 Cyclonic location count and MSLP distribution over 1979-2017 (a) and 2007-2017 (b). The lines represent the average range for ten years in (6a). The total number of events at each MSLP is given in (6b).

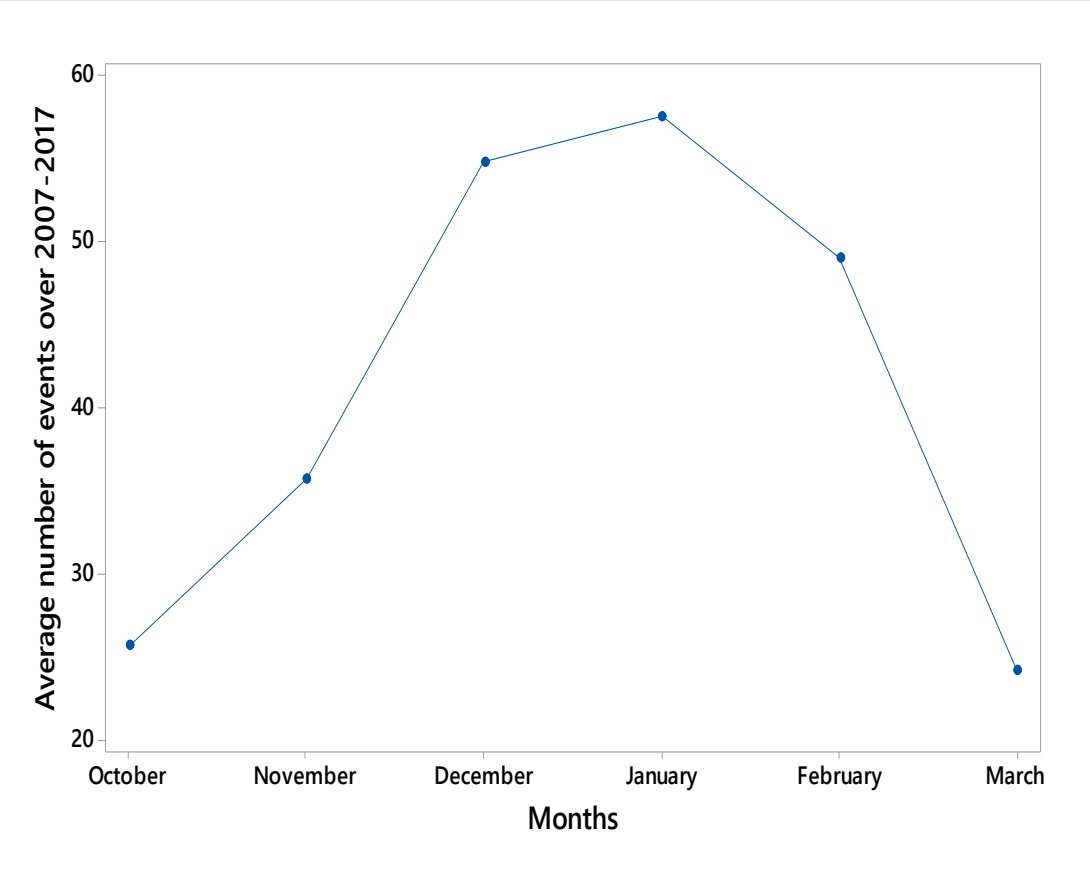

Figure 2. 7: Average number of strong storm events per month over 2007-2017.

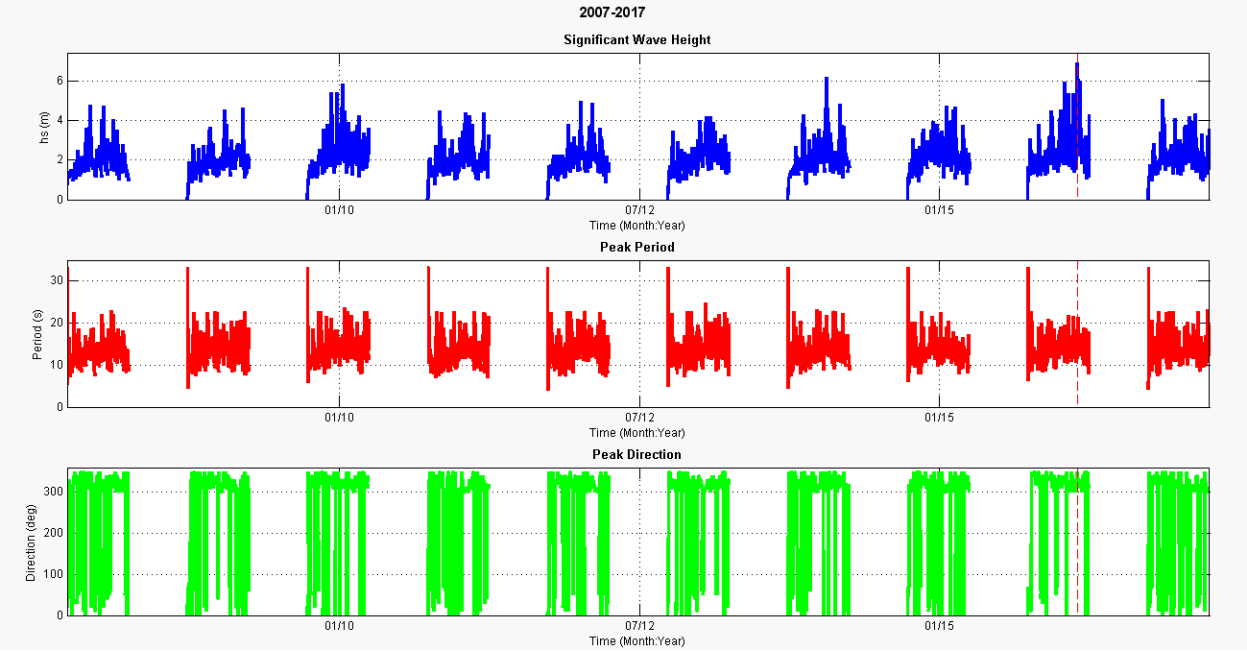

Figure 2. 8: Time series of the wave characteristics for October-March months over 2007-2017 at the northwest location of O'ahu (201.85ºE 21.75ºN).

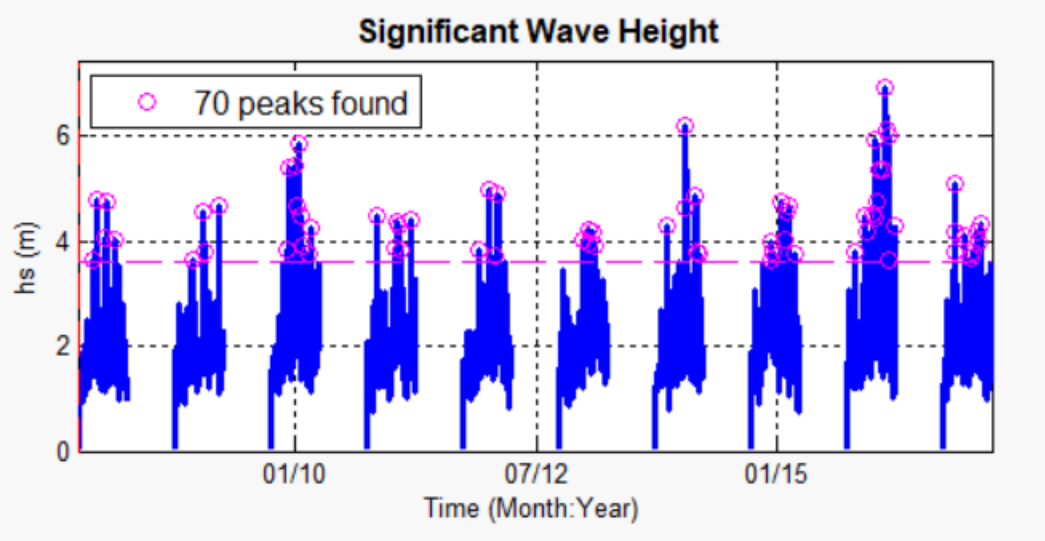

Figure 2. 9: Peak over threshold analysis of 2007-2017. The threshold calculated is 3.63 m; the northwest location of O'ahu (201.85ºE 21.75ºN).

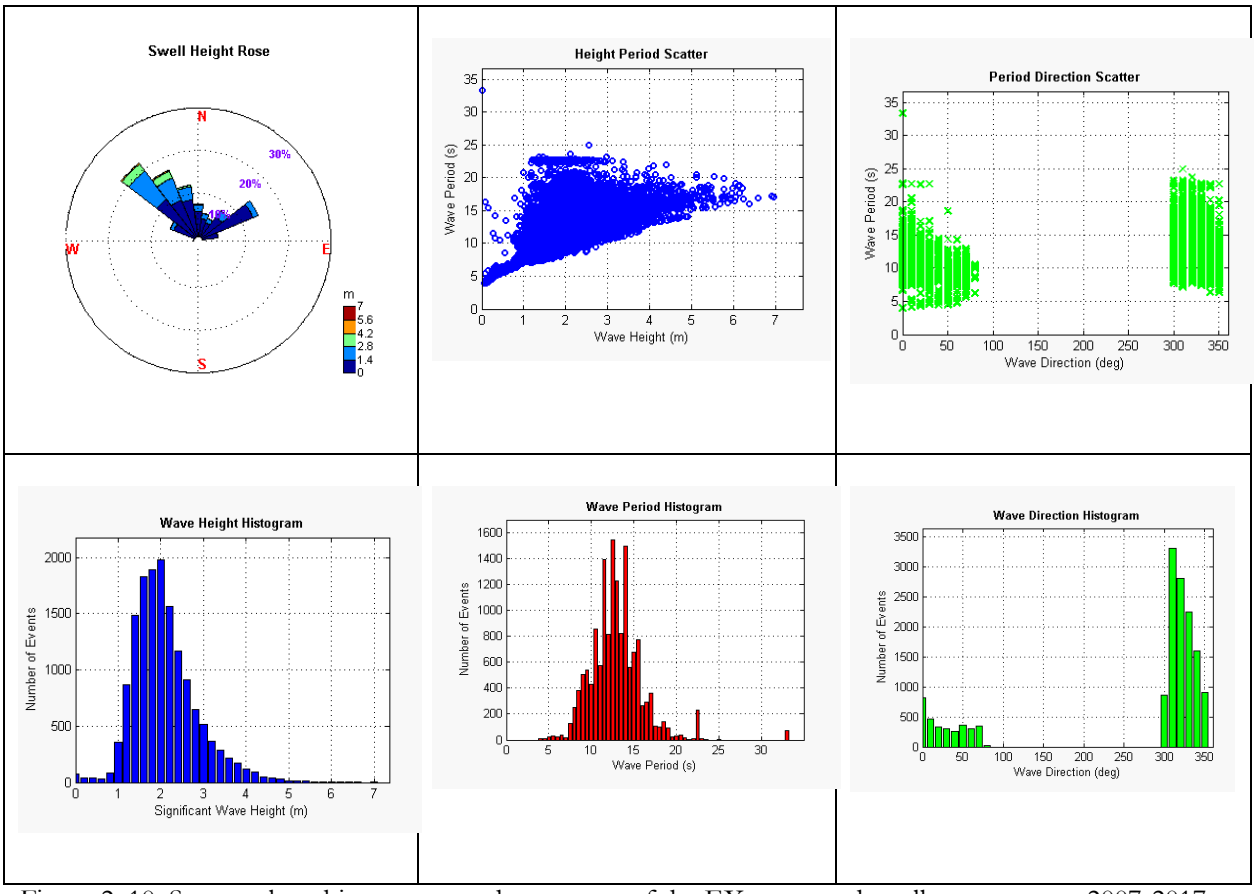

Figure 2. 10: Scatter plots, histograms, and wave rose of the EX-generated swell systems over 2007-2017 at the northwest location of O'ahu (201.85°E 21.75°N).

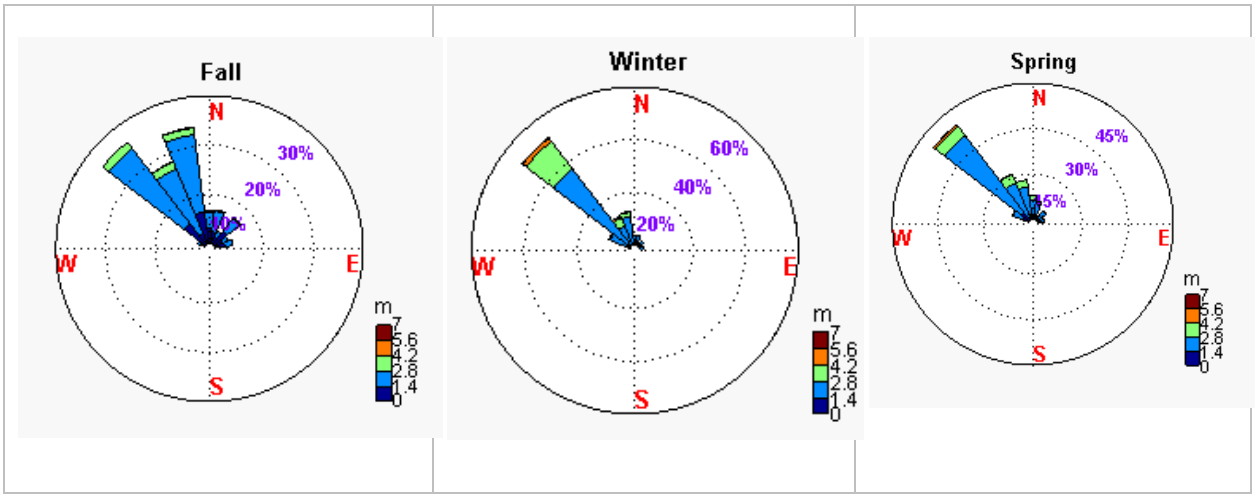

Figure 2. 11: Seasonal swell height rose at the northwest location of O'ahu (201.85°E 21.75°N) over October-March 2007-2017.

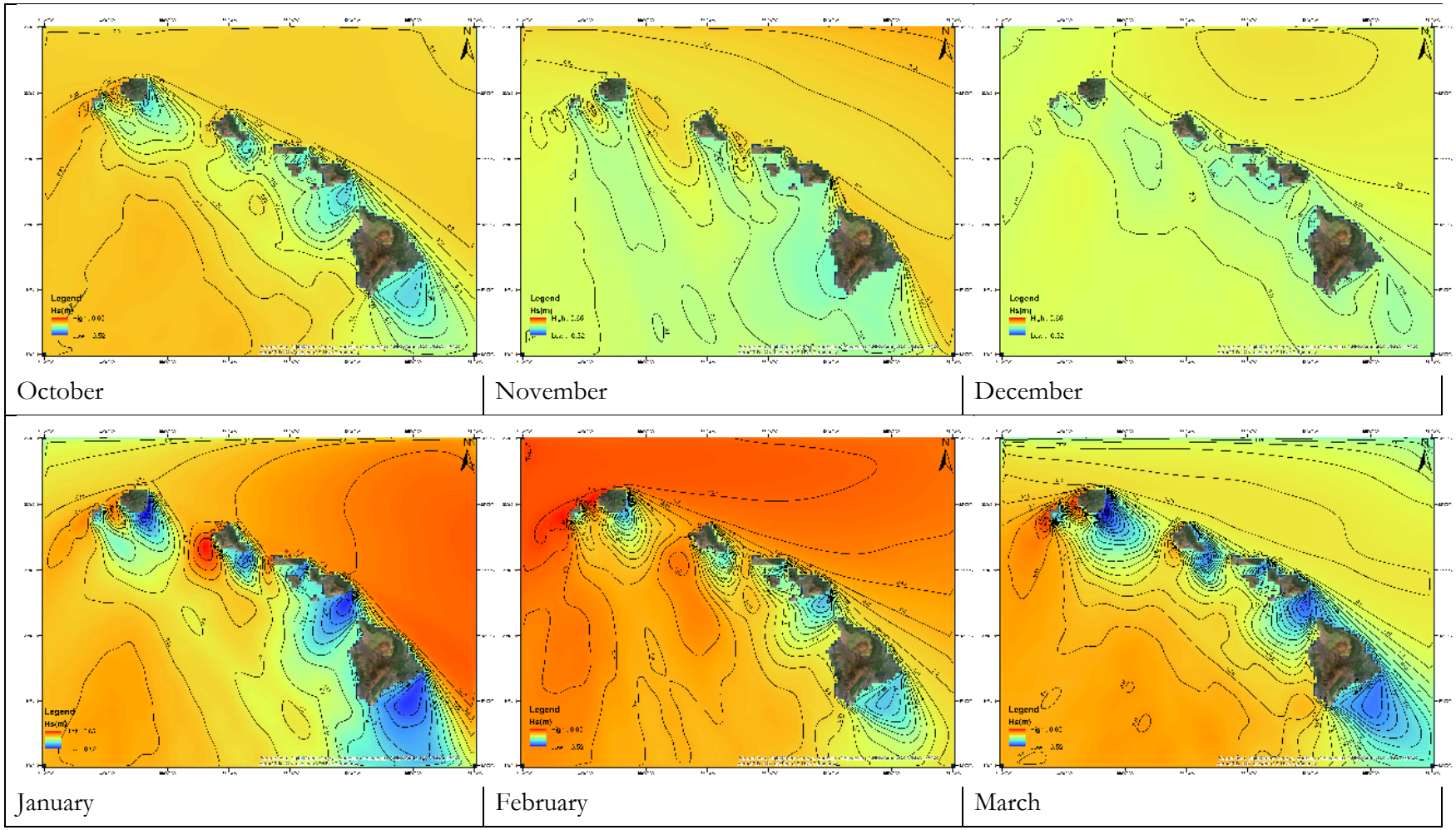

Figure 2. 12: Monthly maximum daily significant wave height de-seasonalized slope differences of the trend of swells approaching the Hawaiian Islands during 2007-2017. The legend ranges between -0.52 and 0.65 m. The contour lines are drawn for every 0.05 m. The map is 161°W-154°W and 18°N-23°N with 1° intervals.

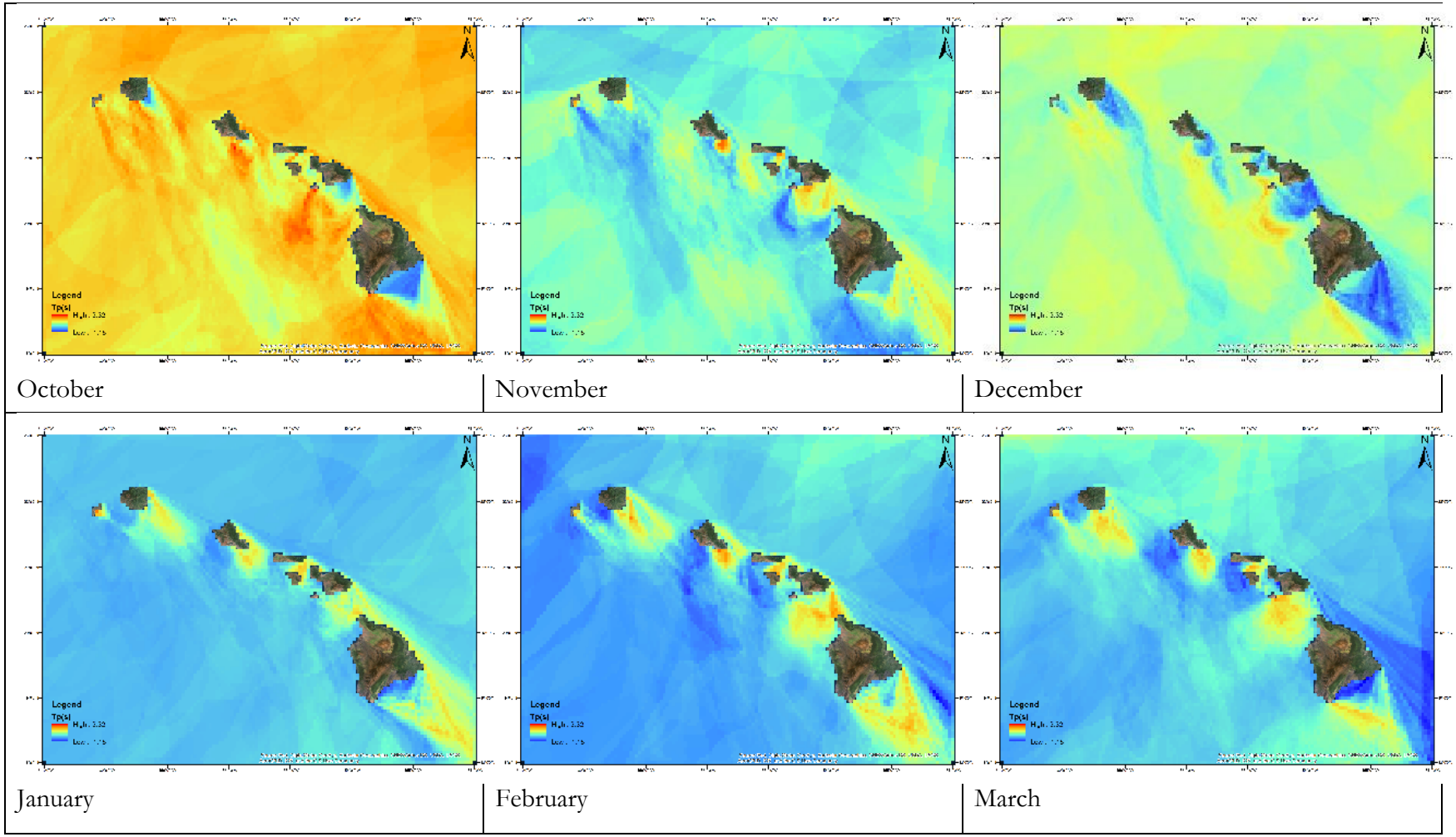

Figure 2. 13: Monthly maximum daily peak period de-seasonalized slope differences of the trend of swells approaching the Hawaiian Islands during 2007-2017. The legend ranges between -1.15 and 3.32 s. The map is 161°W-154°W and 18°N-23°N with 1° intervals.

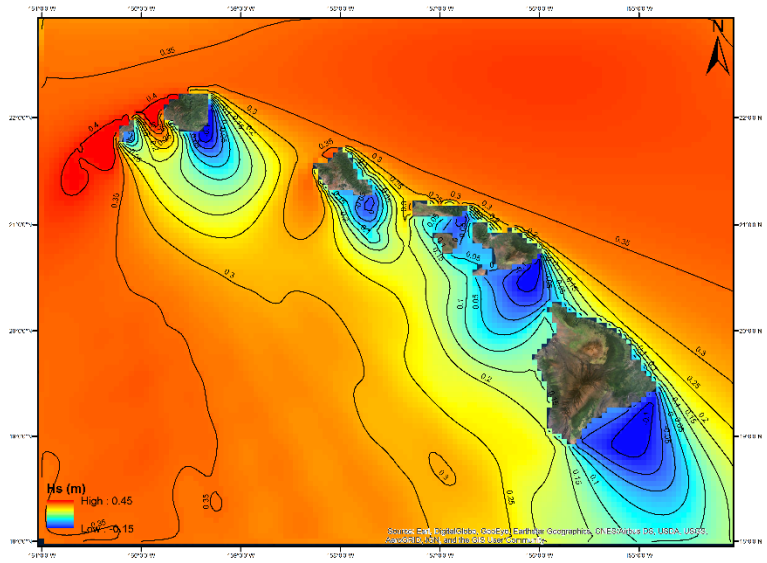

a)

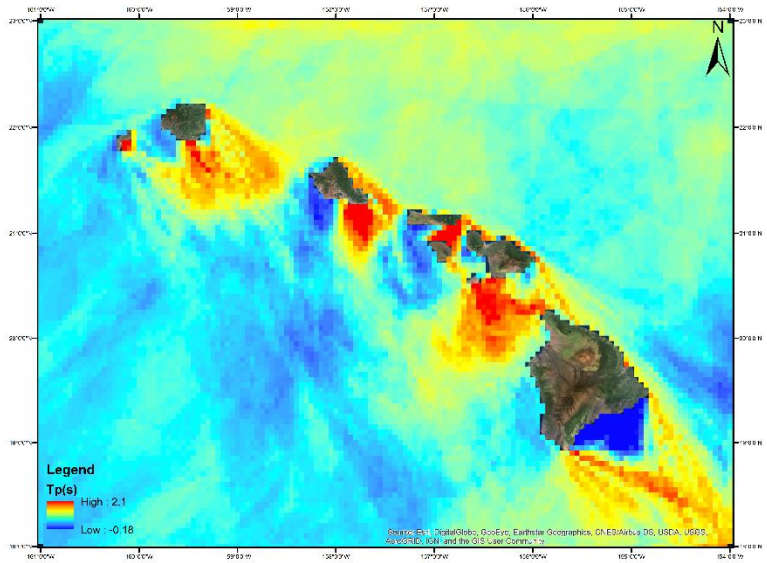

b)

Figure 2. 14: Trend contour maps of the slope difference of maximum significant wave heights (a) and peak period (b) according to the deseasonalized trend between 2007-2017. The legend ranges between -0.15 and 0.45 m for Fig. 2.14a and -0.18 and 2.11s for Fig. 2.14b. The map is 161°W-154°W and 18°N-23°N with 1° intervals.

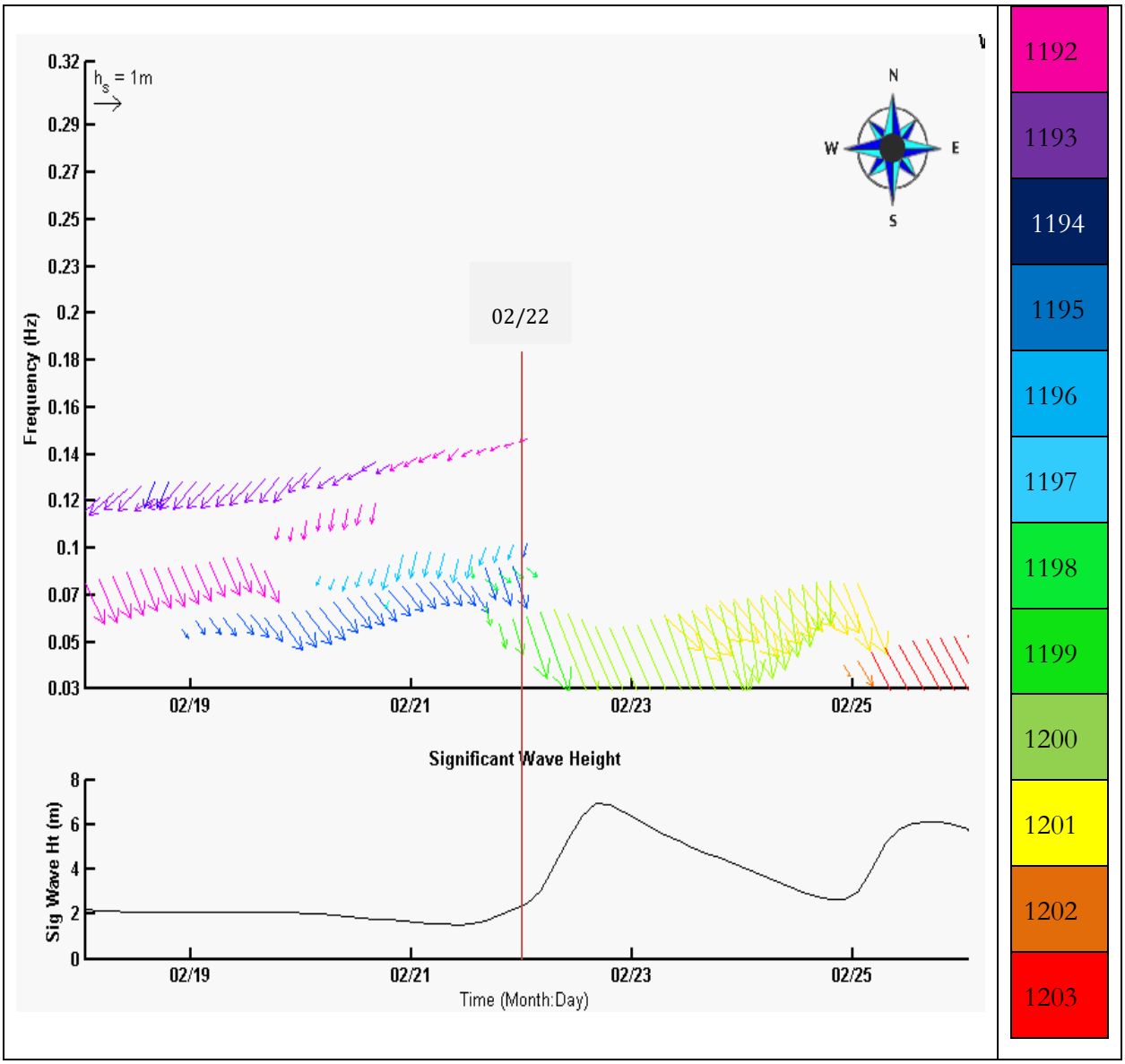

Figure 2. 15: Swell systems generated from WW3 affecting northwest O'ahu (201.85°E 21.75°N) during Feb. 19-26, 2016. During the peak event day of Feb. 22, 2016, five swell systems affected the area. The arrows show direction and their length indicates the wave height. The swell systems are color coded

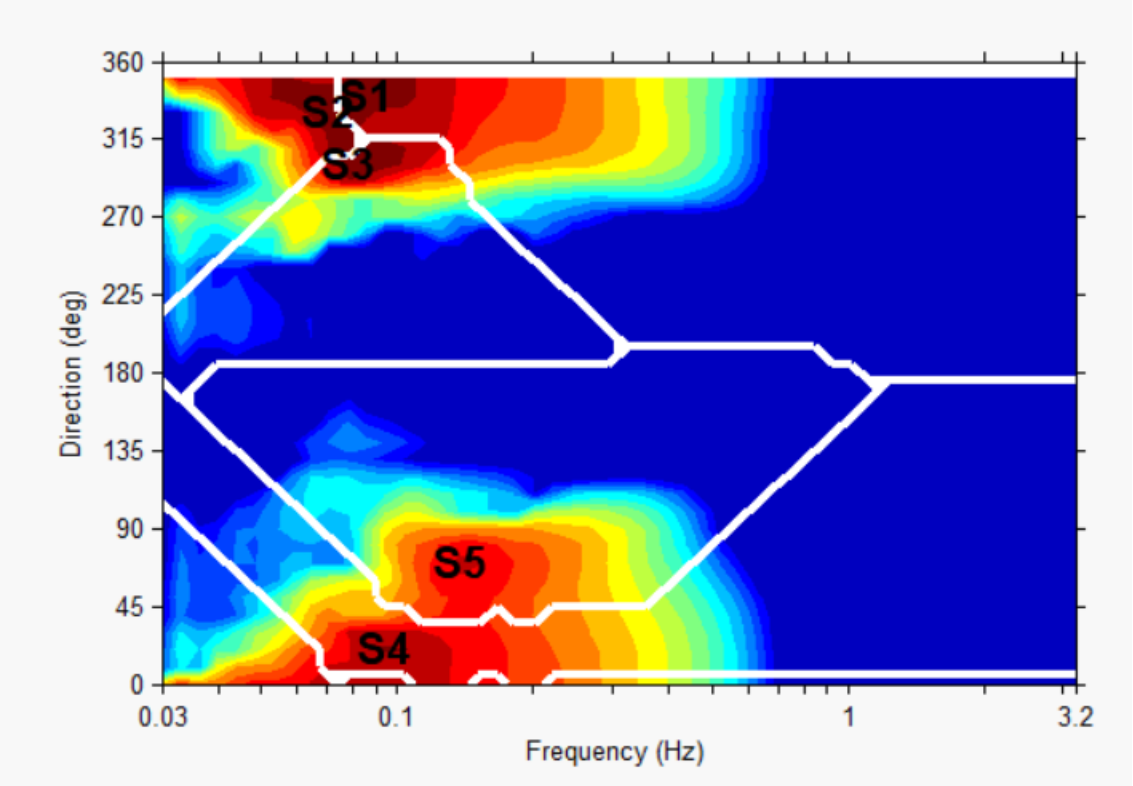

Figure 2. 16: Swell partitioning of the 2D directional spectra on Feb. 22, 2016. The five swell events from Fig. 2.14 are shown.

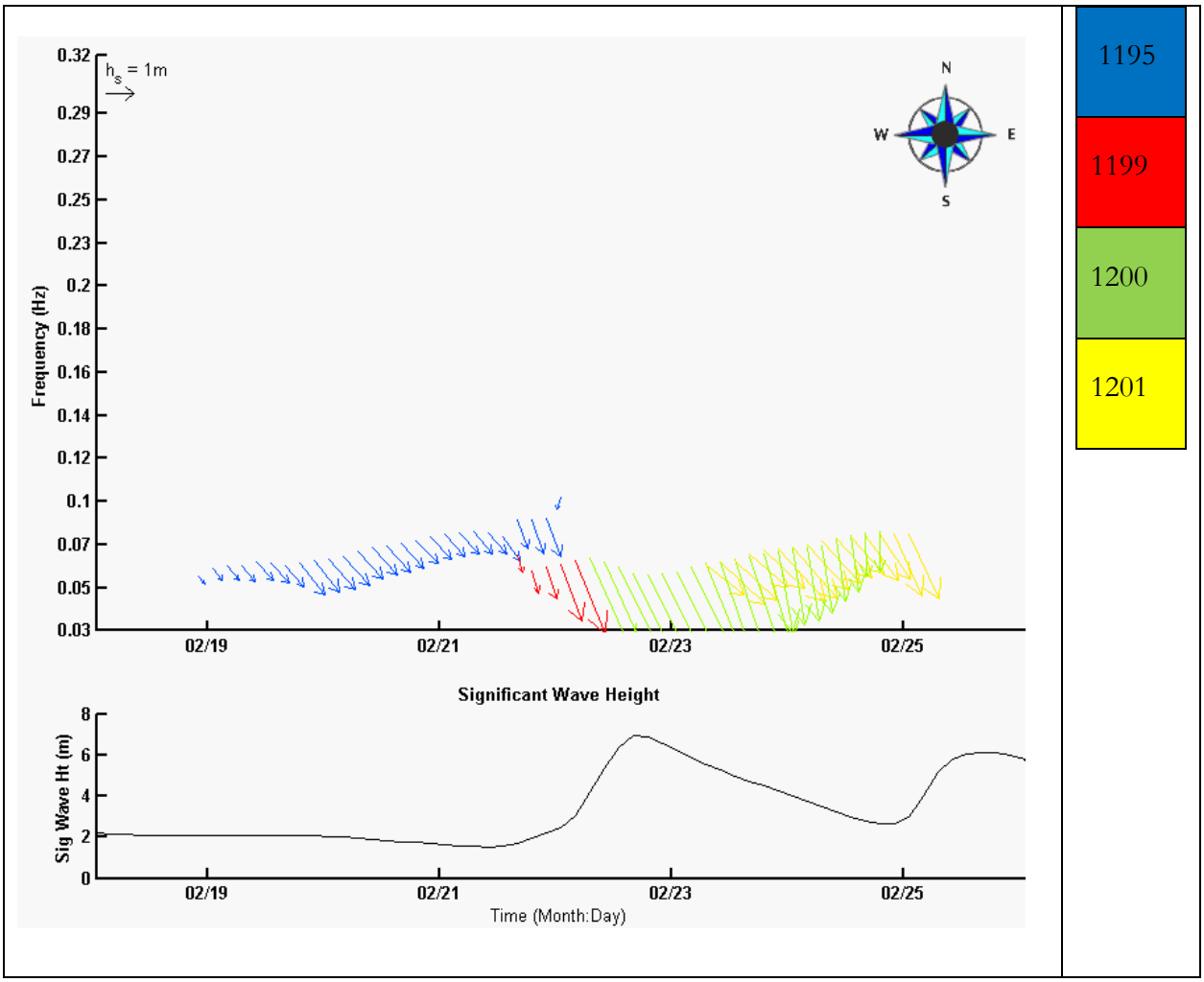

Figure 2. 17: Swells generated by strong EX-cyclones. The four events are the most dominant when compared to the medium EX-generated swells. Swell 1199 (red) is the primary swell system generated by EX-cyclone event.

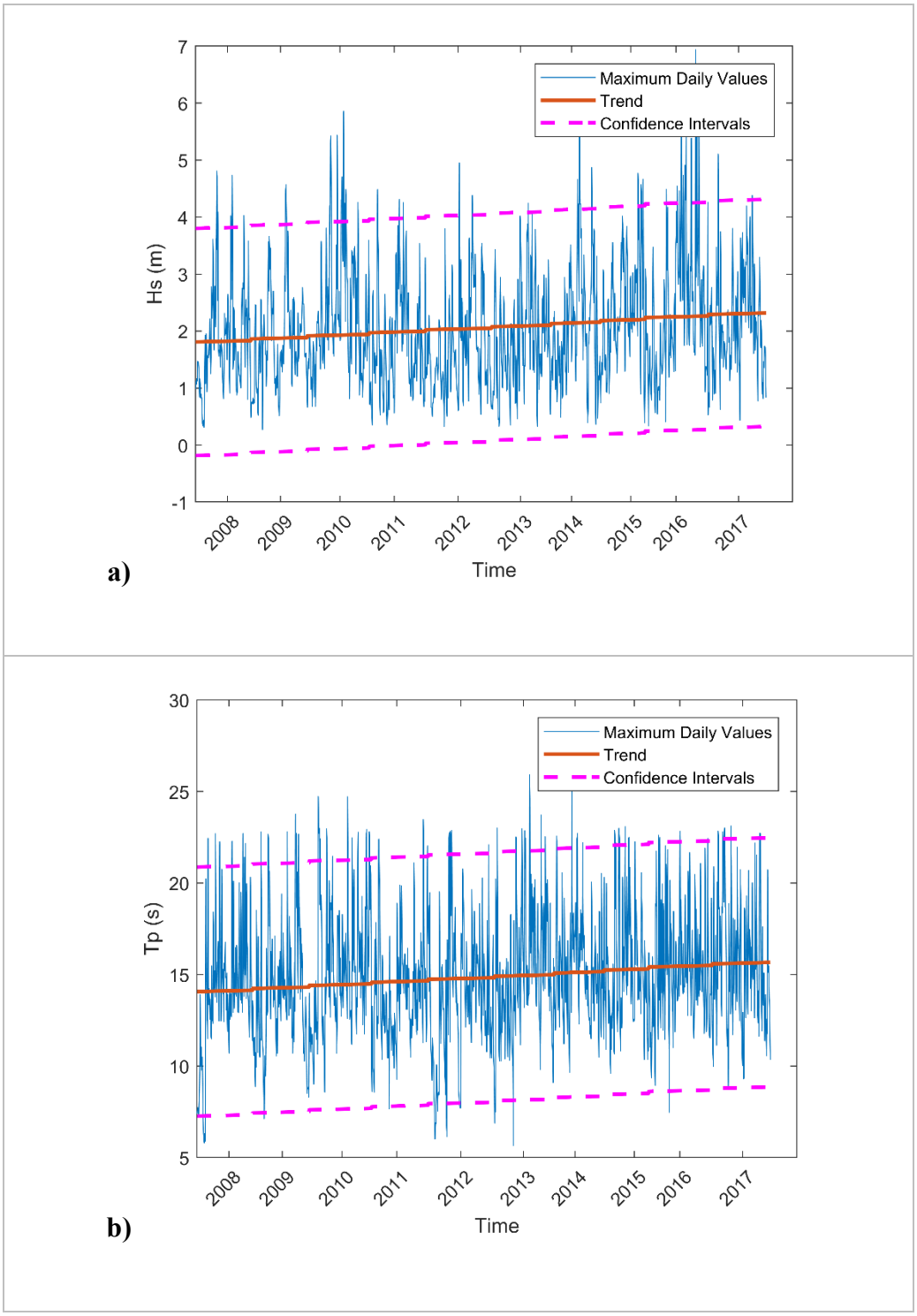

Figure 2. 18: The de-seasonalized series and trend of maximum values of significant wave height (a) and peak wave period (b) during 2007-2017 at northwest of O'ahu (201.85°E 21.75°N).

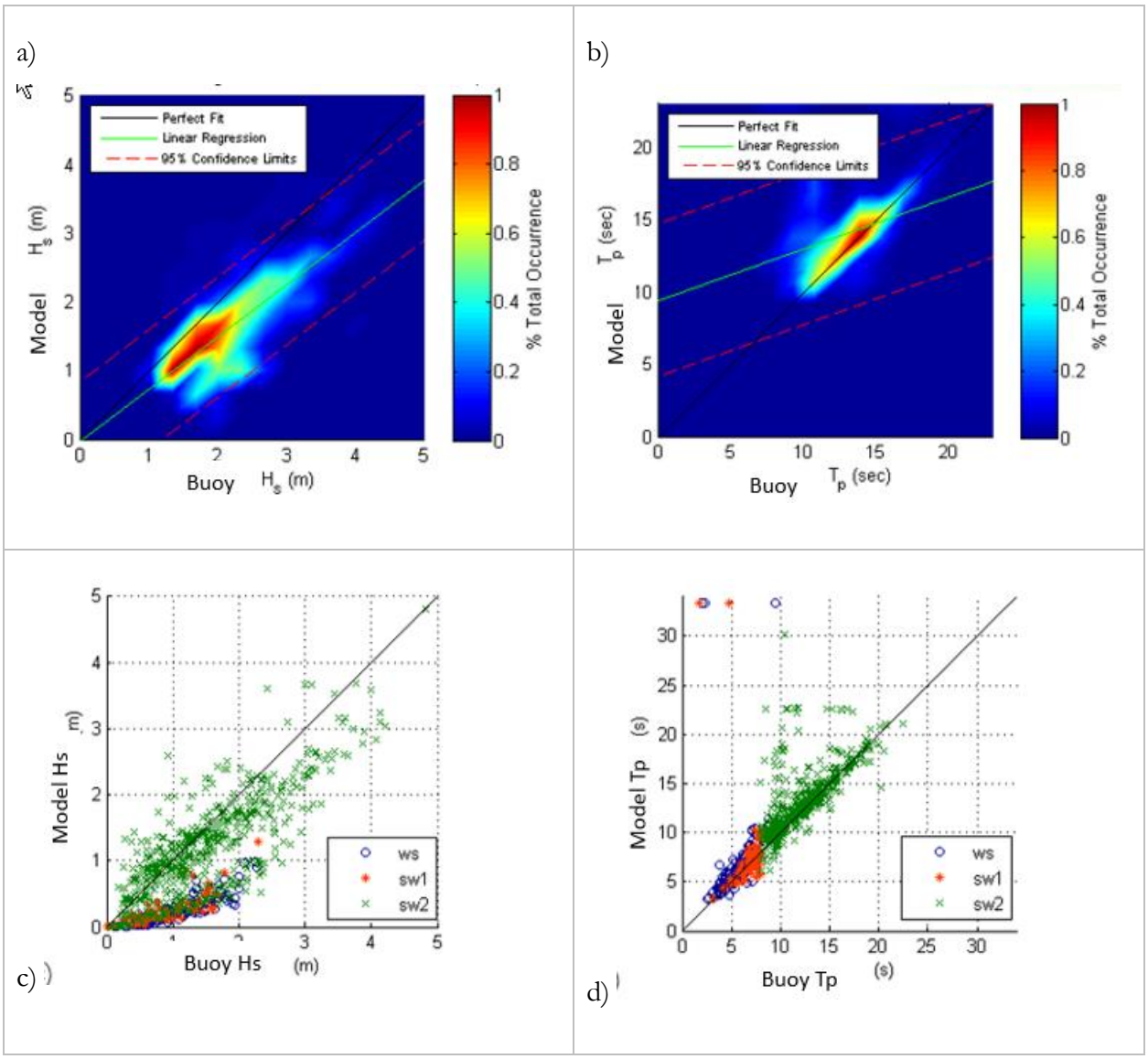

Figure 2. 19: Validation graphs of Waimea-106 CDIP buoy and WW3 model. The buoy is decomposed to wind sea (ws), primary swell (s1) and secondary swell (s2) at a time. QQ- contour plot of wave height (a), decomposed QQ plot of wave height (c) and peak period (b) and decomposed peak period (d) are presented between October-January of 2015-2016.

CHAPTER 3. Coastal Exposure of the Hawaiian Islands using GIS-based Index Modeling

The material presented here is a version of an article by Yaprak Onat, Michelle Marchant, Oceana Francis and Karl Kim that was published in Coastal and Ocean Management.

High energy wave environments intensify the impacts of sea level rise and create threats to island communities, which require measures to prevent the loss of lives and assets. There is a need to identify hazard-prone sites in order to mitigate and reduce threats. In this study, the overall coastal exposure of Hawai'i's shoreline, accounting for topography, bathymetry, wave, surge, and sea level rise is estimated along with interactions with natural habitats, coastal defense structures, and human activities. We quantify coastal exposure using the Integrated Valuation of Ecosystem Services and Tradeoffs (InVEST) model, which provides relative comparisons between shoreline segments to identify the most hazardous locations in the state. The study includes estimates of the probability of erosion and calculates exposure index metrics for at-risk areas. Although the average exposure index of the islands is at the low to medium vulnerability level, an alarming 34% of the state has moderate to high vulnerability. Geomorphology and wave exposure cause the high levels of risk. Maui, O'ahu, and Kaua'i are the top three most vulnerable islands. While geomorphology is most important in influencing vulnerability on O'ahu and Kaua'i, sea level rise and surge potential are the most influential factors on Maui and Kaho'olawe, respectively. Although high wave energy affects all the Hawaiian Islands, Lana'i and Kaua'i are especially influenced by wave exposure while O'ahu has the most eroded shorelines. Natural habitats serve as barriers to the adverse effects of exposure and reduce vulnerabilities. The observed probability distribution of the exposure and erosion indices for islands is also provided. By understanding which shorelines are most sensitive and the dominant factors affecting their vulnerability, policymakers can promote public awareness and support planning, design, and implementation of adaptation strategies.

1. Introduction

Island communities, whose economies and livelihoods depend on coastal assets and opportunities, are highly susceptible to changes in climate. Consideration of the biophysical and socio-economic effects of climate change (Doukakis, 2005) enables island communities to develop hazard management strategies in response to their vulnerabilities (Kim et al., 2015; Torresan et al., 2008). Identifying and assessing highly vulnerable areas (Torresan et al., 2008) as well as the contributing factors to vulnerability are necessary groundwork in developing a strategy for surviving inundation, erosion, degradation, flooding, and salinization caused by sea level rise (SLR) (Tysban et al., 1990).

Recent studies on global mean surface temperature (Rahmstorf, 2007) and the polar ice sheet melt (Pfeffer et al. 2008) call attention to SLR rates and their impact on the shorelines. The studies also indicate a likely acceleration in SLR rates with increased global warming (Church and White, 2006; Jevrejeva et al., 2008; Merrifield et al., 2009). According to the IPCC AR5, the average global SLR rates increase to 0.47 m by Representative Concentration Pathways (RCP) 4.5 and 0.63 m by RCP 8.5 by 2100. However, recent studies (Kopp et al., 2016, 2015; Mengel et al., 2015; Slangen et al., 2014; Sweet et al., 2017) showed that the previously reported low probability distributions fail to capture uncertainties in future predictions (Sweet et al., 2017) and that global SLR rates are 0.3-0.5 m higher within the Hawaiian Islands under an intermediate-high scenario (1.5 m global mean SLR by the year 2100) due to static equilibrium effects (Sweet et al., 2017). On the other hand, Parker, (2017, 2016) indicates that the impact of multi-decadal oscillations and subsidence decelerate the SLR rates of the Hawaiian Islands. Despite the debate between future SLR scenarios, we need a better understanding of past conditions to allow for future planning. Therefore, we include the relative sea level recorded by the tide gauge measurements, which capture past rates more reliably than model scenarios (Parker, 2016; Parker et al., 2013; Parker and Ollier, 2016a). These measurements should include the subsidence rates, record length, and oscillations in the recording period (Baker and McGowan, 2015; Chambers et al., 2012; Mazzarella and Scafetta, 2012; Parker and Ollier, 2016b; Scafetta, 2014).

The coastal vulnerability index (CVI) is widely used to assess shoreline vulnerabilities (Cooper and McLaughlin, 1998; Gornitz, 1990; Thieler and Hammar-Klose, 1999) by identifying risk-prone

areas undergoing physical changes and impacts due to SLR (Rangel-Buitrago and Anfuso, 2015; Thieler and Hammar-Klose, 1999). The CVI measures the exposure, sensitivity, and adaptive capacity of a community (IPCC AR4, 2007). Different approaches summarized in Nguyen et al., (2016) comprise both the biophysical and social dimensions of vulnerability to assess complex coastal vulnerability determinants relative to SLR, such as climate forcing and socioeconomic factors (Boruff et al., 2005; Mclaughlin and Cooper, 2010; Szlafsztein and Sterr, 2007), and coastal sensitivity (Abuodha and Woodroffe, 2010). Defining the indicators which identify the vulnerability of a region is a challenge because different parameters protect the shoreline at different levels (Denner et al., 2015). Within the scientific community there is no commonly accepted validation for exposure results (Nguyen et al., 2016). Researchers integrate weighted index calculations with an analytic hierarchy process (AHP) (Duriyapong and Nakhapakorn, 2011; Le Cozannet et al., 2013; Mani Murali et al., 2013) and fuzzy AHP (Özyurt and Ergin, 2010; Tahri et al., 2017) to reduce the subjectivity of the indicator (Balica, 2012). Although these approaches are a good attempt at dealing with uncertainty in the decision-making (Tahri et al., 2017), it can be an overwhelming process in the preliminary stages of the CVI application. The CVI application proposed by Gornitz, (1990) and Thieler and Hammar-Klose, (1999) is a standardized measure for relative SLR vulnerability assessments and widely used. The method can be modified by using percentile ranges instead of actual values (Shaw et al., 1998). The GIS is an efficient tool used to measure the impact on hazard prone areas to flooding (Lawal et al., 2011) and erosion (Rizzo et al., 2017). The GIS application of the CVI displays the frequency distribution of the index variable. CVI mapping is also used to support planning and decision making in response to climate change (Kelly et al., 1994; Onat et al., 2018a) and to integrate ecological and social functions into ecosystem-based management (Mangubhai et al., 2015; Yoo et al., 2014) for the future (Denner et al., 2015; Musekiwa et al., 2015). Spatially explicit models like the Integrated Valuation of Ecosystem Services and Tradeoffs tool (InVEST) show the impact of the changes in the ecosystem (Natural Capital Project, 2008). The overlapping analysis of the InVEST model is used to understand the interaction of coastal habitats with SLR (Arkema et al., 2013a; Onat et al., 2018a), modeling ecosystem services for coastal zone planning (Arkema et al., 2017, 2014, Guannel et al., 2016, 2015; Guerry et al., 2012), and protection against climate stressors (Cabral et al., 2017; Elliff and Kikuchi, 2015; Langridge et al., 2014; Vogl et al., 2016). A better understanding of the vulnerability of the shorelines from coastal stressors leads to improved climate change adaptation plans (Onat et al., 2018a).

The motivation for this study comes from the need to define the current vulnerabilities and quantify the change in vulnerabilities due to SLR and climate change. The exposure and sensitivity of the region to climate events can also be better estimated with more in-depth knowledge of coastal vulnerabilities. Another vital aspect is that the most exposed areas are identified from critical physical parameters that affect the vulnerability of the shoreline, which are needed to prioritize different adaptation measures.

There are three main goals for this paper. The first goal is to identify which environmental parameters most affect Hawaii and understand the linkages between them. Even though coastal hazard risk and inundation maps display historical event impacts, more information is needed because the perception of risk may be inaccurate, especially in highly susceptible areas. Exaggerated risk causes public fear and desensitizes the community to likely scenarios (Bolter, 2013). This study also demonstrates the contribution of shoreline attributes to exposure. It addresses the gaps in inundation or hazard maps by considering natural and anthropogenic processes (Bolter, 2013), as well as their interactions with population and infrastructure to define vulnerability (Wu et al., 2002). The second goal of the study is to reduce uncertainty when prioritizing vulnerable coastal systems and determine effective linkages between vulnerability assessment and development planning. The third goal is to show what factors reduce resilience in specific regions through inspection of the input values affecting exposure and vulnerability, which addresses the most critical underlying factors affecting vulnerability.

The next section explains the unique characteristics of the Hawaiian Islands and the SLR influence over the shorelines. The methods used to define exposure metrics and conduct the statistical analysis are described in Section 3. The vulnerability of each shoreline segment is quantified using CVI. The research considers topography, bathymetry, wave and surge exposure, SLR, and the impact of natural habitats, coastal defense structures, and population by evaluating and illustrating the degree of change in exposure. Section 4 covers the results and discusses the characteristics of input vulnerability and exposure metrics are provided. The research presents assessments of vulnerability that policymakers can use to select appropriate adaptation and mitigation strategies. We investigate the characteristics of vulnerability and exposure metric distributions and comparing the differences between them. Also presented are the habitat, coastal defense structure, and population density effects for island exposure, and typical characteristics of

the most vulnerable locations for each island. In the final section, the results of the CVI analysis and the implications for research, planning, and development are presented.

2. Study Area

The study area covers the shorelines of the seven main Hawaiian Islands – Kauaʻi, Oʻahu, Molokaʻi, Lanaʻi, Maui, Kahoʻolawe and Hawaiʻi (Big Island) (Fig. 3.1). The islands are the result of hotspot formations and include beaches formed from sandy, alluvial deposits, coral reefs and volcanic bedrocks (Romine and Fletcher, 2012). Surrounded by fringing reefs, the islands have diverse habitats due to the tropical environment. The Hawaiian Islands are under the influence of high energy waves (Moberly and Chamberlain, 1964; Vitousek and Fletcher, 2008) and tropical storms, and undergo shoreline changes due to erosion (Romine and Fletcher, 2012). Prediction of climate change effects is challenging due to the islands' complex natural and geographic formations (Eversole and Andrews, 2014). Coastal areas have been urbanized by tourism, housing developments, and roads and utilities connecting these coastal communities.

The SLR projection for Hawaiʻi is highly variable due to local isostatic response (Caccamise, 2003; Church et al., 2004; Richmond et al., 2001; Romine and Fletcher, 2012) originating from the volcanic formation of the islands, which creates disparity in historic sea level across the state (Fletcher, 2000). Long-term trend measurements from tide measurements, which include GPS station corrections, show that the Big Island and Maui have higher rates of SLR (1.8 mm/yr and 2.02 mm/yr, respectively), while Oʻahu and Kauaʻi have a SLR rates of 1.43 and 1.47 mm/yr, respectively (Yang and Francis, 2018). The differences in SLR rates are from the sinking of Hawaiʻi and Maui, due to the flex caused by the weight of geologically young volcanic material on the underlying crust, while Oʻahu and Kauaʻi are outside of the subsidence zone (Fletcher, 2000; Richmond et al., 2001; Romine et al., 2013).

Sea level rise adversely contributes to existing hazards in the state. Hawaii faces risks of coastal erosion, SLR, tropical storms, flooding, high wave events, volcanic and seismic activity and tsunamis (Fletcher et al., 2012; Richmond et al., 2001). Fletcher et al. (2012) and Richmond et al. (2001) developed hazard intensity maps using historical evidence to rank the occurrence and magnitude of the natural events, including the geologic character and morphologic slope of specific coastal segments. According to Fletcher et al. (2012) and Richmond et al. (2001), Hawaiʻi experiences heavy

rainfall and flooding due to high wave events at least once a year. There are four main wave events affecting Hawai'i year round: trade winds on the east-northeast side, which cause events up to 3.6 m high; southern swells, which cause events up to 2 m high; the passage of extratropical low-pressure systems (Giambelluca and Schroeder, 1998) associated with Kona storms from the south to southwest, which cause events up to 4.5 m high; and north Pacific swells, which cause events up to 7.7 m high (Vitousek and Fletcher 2008). Additionally, tropical cyclones have created waves between 1.2 m and 4.5 m high (Vitousek and Fletcher, 2008). The high wave events along the shorelines combined with tides can cause flooding, the impact of which can be increased by SLR (Caldwell et al., 2009).

Sea level rise can also result in beach narrowing and sand volume loss due to erosion (Dail et al., 2000). Historical aerial photos of erosion reveal that the state has an average loss of -0.11 ± 0.01 m/y (Hwang, 1981; Makai Engineering, Inc. and Sea Engineering, 1991; Romine and Fletcher, 2012; Sea Engineering Inc., 1988). Beach narrowing was observed in 25% of O'ahu beaches and 33% of the Maui beaches (Coyne et al., 2012; Fletcher et al., 1997). Fletcher et al. (2012) and Romine and Fletcher (2013) found that Maui is experiencing higher erosion rates compared to O'ahu and Kaua'i. A finite amount of sand reserves (Richmond et al., 2001) also creates obstacles in maintaining beaches, especially with SLR, which contributes to the long-term erosion rates (Fletcher et al., 2011; Zhang et al., 2004). Loss of beach can also submerge ancestral lands and degrade cultural resources (Kane et al., 2014). By incorporating long-term sediment processes based on historical trends, Anderson et al. (2015) and Romine and Fletcher (2013) found that by 2100 the average shoreline may be reduced by as much as 2.5 times over historical levels due to SLR.

Hawaii has unique coastal ecosystems susceptible to climate change impacts due to their location and geological formations. Reefs mostly start at approximately 1.2-1.8 m water depth (Richmond et al., 2001) and play a significant role in maintaining coastal ecologic health (Bowler et al., 2010; Guannel et al., 2016, 2014), as well as protecting shores from wave action (Eversole and Andrews, 2014) and coastal hazards (Chen et al., 2007; Costanza et al., 2008; Guannel et al., 2016; Mcivor et al., 2012). Guannel et al. (2015, 2016) showed how natural habitats reduce erosion and defend against the severe effects of SLR. If precautions are not taken, SLR impacts will accelerate after a critical sea level elevation is reached, resulting in further habitat loss (Kane et al., 2014). Such a "tipping point" should be avoided.

3. Methodology

3.1 CVI and Coastal Vulnerability Model InVEST

The coastal vulnerability index (CVI) for shoreline segments, statewide, was developed using GIS. The CVI is an effective method to characterize which shoreline segments are most vulnerable due to which factors (Gornitz, 1991; Thieler and Hammar-Klose, 1999).

An open-source GIS-based program developed by the Natural Capital Project called Integrated Valuation of Ecosystem Services and Tradeoffs tool (InVEST) Version 3.3.2, is used to assess the coastal vulnerability of shorelines throughout the state. The model uses the index defined by Gornitz (1990) and extended by Thieler and Hammar-Klose (1999). The variables include geomorphology, shoreline erosion/accretion rates, coastal slope, relative SLR, mean significant wave height and mean tidal range. These are classified according to relative ranking and multiplied to obtain an exposure index. Thieler and Hammar-Klose (1999) reduced the number of input variables to increase the CVI method's usefulness. The method used within the InVEST model uses a percentile range application, which provides simplicity, clarity and applicability to diverse settings. The hierarchical structure of the CVI map generation includes data collection, categorizing the data, digitizing or modifying the layers, ranking the biophysical parameters to apply in InVEST and obtaining the exposure index (Fig. 4.2). The user can generate and manipulate the obtained exposure index values and generate specific maps via GIS. It is widely used by the U.S. Geological Survey (USGS) and others to define the vulnerability of shorelines and communities to sea level and changes in exposure to different hazards, relative to each other.

The biophysical factors include geomorphology, relief (elevation), sea level rise, wave and wind exposure, surge potential, and natural habitats, which are used to define coastal exposure (Sharp et al., 2016). The index combines input variables defined according to ranking criteria (Gornitz, 1990; Thieler and Hammar-Klose, 1999; Sharp et al., 2016) in the InVEST model to calculate the coastal exposure index (EI) for each shoreline segment. The relative coastal EI for each 250 m shoreline segment is calculated by

$$EI = \prod_{i=1}^{n} (R_n)^{1/n} \quad (3.1)$$

where *R* is the rank of the variable and *n* is the number of variables. The erosion index (ErI) is the geometric mean of geomorphology, habitats, and wave exposure. The ranks range from 1 for low exposure to 5 for high exposure. Table 4.1 shows the input layers used in the analysis, which are also ranked as described by Sharp et al. (2016). The distribution of the input values is ranked according to their percentile ranges. If an input value ranges in the highest 100-80 percentile, it is ranked 5 (very high). Similarly, the 80-60 percentile is ranked 4 (high), 60-40 percentile is ranked 3 (moderate), 40-20 is ranked 2 (low), and less than 20 percentile is ranked 1 (very low). The method of ranking input exposure index is given in Appendix A. The projections of the original shape and raster files are converted to WGS 1984 UTM Zone 4N.

The nine contributing layers contained in Table 4.1 are weighted equally to compute the exposure of the area. The layers are ranked again from 1 (low) to 5 (high) as inputs for the spatial vulnerability model. Each layer uniquely contributes to the general coastal EI.

3.2 Data Sources and Input Layer Generation

The mean elevation of the shoreline within a 5 km radius from the digital elevation model (DEM) is used to define the average elevation of the coastline segment (Sharp et al., 2016). Elevation data with fine resolution play a significant role in defining the soil and vegetation available in the area, which is needed to determine SLR impacts (Cooper, 2014). Because 250 m is smallest resolution of the model, the resolution of the input data layers (Table 1) is sufficient to calculate the exposure indices. Although a higher resolution model of more than 250 m would be desirable, the chosen resolution is enough to contribute to EI calculations for beach segments. The relative SLR changes are used to include both the eustatic SLR and local tectonic movements of the island chain. Maui and Hawai‘i have high rates of SLR at 2.02 and 1.8 mm/y, while SLR is roughly 30% slower around Kaua‘i and O‘ahu, at 1.47 mm/y and 1.43 mm/y, respectively (Yang and Francis, 2018). Another contributing layer, geomorphology, includes coastal defense structures to designate necessary shorelines (Arkema et al., 2013b). While the ErI can be calculated without the impact of these defense structures, the general erosion index assumes the structures are fully functional, which leads to underestimation of the recent conditions (Arkema et al., 2013b).

The wind wave and storm surge potential come from the compiled eight-year wave hindcast data using WAVEWATCH III (Tolman, 2009). Wind exposure is calculated by using relative exposure

rankings (Keddy, 1982), which include the multiplication of the fetch distance, average of the highest 10% wind speed, and percent of all winds in the record for each sector formed by dividing the shoreline segment into 16 equiangular sectors (Sharp et al., 2016). The shoreline segment's wind exposure is related to wave and surge potential. The wave potential is ranked using the maximum of the weighted average wave power of swells and locally generated waves in each equiangular sector. The wind and wave exposure equations are given in Appendix B. The model uses depth and fetch threshold to determine whether the shoreline is sheltered or exposed (Sharp et al., 2016). Any fetch and depth over a threshold of 60 km or 10 m (estimated by calculating average depth of shallow estuaries), respectively, is considered a sheltered shoreline. The islands are under the effect of trade winds from the east to the northeast (Stopa et al., 2013a), with an average wind speed of 8-12 m/s during May-June (Stopa et al., 2013b), while Kona storms are more influential during the winter months (Yang and Chen, 2003a).

The mountainous formation generates high-speed wind channels (Smith and Grubišić, 1993; Yang and Chen, 2003b), which result in local wind wave energy with long fetch distances (Stopa et al., 2013b). Stopa et al. (2013b) states that the median wave parameters of swells during the winter months are 3 m and 11 s, whereas, the median wind waves during the summer months are 1-2 m and 7 s, which increases up to 2.5 m with the trade winds speed increases in the 'Alenuihaha Channel. Thus, the northwest swells can generate 35-50 kW/m of wave power (Stopa et al., 2013b). In addition to wind exposure, the surge potential uses the horizontal distance from the edge of the continental shelf to the land boundary to define the vulnerability.

Natural habitats along the shoreline dissipate wave energy (Ferrario et al., 2014; Kobayashi et al., 1993). The polygon file created from Table 3.1, which was combined with the user-defined natural habitat type input ranking and maximum protective distance influenced by habitat, accounts for the maximum protection that habitat can provide for the shoreline segment. Thus, the protective power of the habitat in the area increases with the number of habitats that affect the area. The input ranking is lowest for fixed natural habitats like reefs, coastal forests, or dunes that absorb the energy of incoming water column and reduce its energy (Sharp et al., 2016). Seasonal and flexible habitats like kelp or seagrass have higher rankings because they encourage sediment accumulation over time, however, reducing the flow of water is less effective at protecting the coastal area than the lowest ranked habitats (Sharp et al., 2016). We measure the maximum protective distance along the

shorelines for each habitat by using the median for each habitat area. We found eight common habitats, which include reefs, coastal forests, dunes, brackish salt marshes, freshwater marshes, swamps, vegetative low banks, and mangroves (Table 3.2). The user-defined values in Table 3.2 are calculated by measuring ten maximum distances observed around the islands via ArcGIS and taking their average. Even though this measure assessed which shoreline segment is protected according to different habitats, it simplifies the effect of the natural habitat layer for EI calculations by not including depth, channel configuration, soil type, which could influence protection of the segment (Arkema et al., 2013b).

3.3 Statistical Analysis

The research presents the histograms and probability distribution using curve-fitting methods for both input variables and EIs. The GIS files from Table 4.1 are used in the InVEST model. Moran's I spatial analysis is performed to show significant clustering for each island. Descriptive statistics and ANOVA are performed to demonstrate the statistical significance of the differences between segments and types of environments. The group mean differences are used to establish the significant high vulnerability locations as well the differences among factors associated with vulnerability. The group means are considered significantly different when the $p\text{-}value < 0.05$. The Tukey-Kramer test is used to demonstrate which vulnerability metric among the islands is different from each other.

4. Results and Discussion

Input vulnerability metric distributions and exposure indices are calculated to demonstrate the potential susceptibility of the shoreline to climate stressors. The results include the following: i) traits of input vulnerability and resulting exposure metrics; ii) causes of vulnerability in each metric that affect impacts; and iii) significant differences in the metrics. The maps presented here demonstrate which shoreline segment is more likely to be influenced by SLR, wave, and surge exposure.

Out of the seven Hawaiian Islands considered in our study, the most extended shorelines belong to Hawai'i and O'ahu. Throughout the state's coastal areas, a total of 31.42% of all the shoreline segments are exposed to climatic forces (Table 3.3). The distribution of the exposed shorelines

(Onat et al., 2018b) reveals that although Molokaʻi and Maui have diffraction zones with reduced trade wind waves and North Pacific swells, Lanaʻi and Kahoʻolawe have the highest exposure rates due to headland formations on their shorelines. Lanaʻi and Kahoʻolawe are also exposed to southern swells and Kona storm waves. Hawaiʻi Island follows a similar pattern in that it is exposed to trade winds and southern Kona storms; it also has more headland formations than all the other islands combined. Kauaʻi, on the other hand, has more bays and pocket beaches and is less exposed than Hawaiʻi due to its geomorphology, location, and position. Oʻahu is the most sheltered island due to its many protected bays in comparison to the other islands.

4.1 Characteristics of Input Vulnerability Metrics

The upper and lower limits of each input vulnerability metric value are ranked according to the percentile ranges (Sharp et al., 2016) for each island. The range of the input vulnerability metric values is different for each island. The frequency distributions of the input vulnerability metrics are shown in Fig. 3.3 to help visualize the differences between inputs and the contribution of each metric to the overall exposure of the island (Table 3.3). The average and standard deviations of each vulnerability metric indicate that geomorphology has the highest mean at Kauaʻi, Oʻahu, Lanai, and Molokaʻi, whereas SLR has highest mean at Maui and Kahoʻolawe. The geomorphology varies significantly on Kauaʻi, Oʻahu, and Molokaʻi. The mountains on Kahoʻolawe increase the average elevation of the coasts, even though Kahoʻolawe's coasts are not the highest among the islands. The mountainous formation of the islands increases the resistance of the shorelines, creating a moderate level of vulnerability. The reef formations around the islands are leading contributors to the low vulnerability averages. The mean strengths of each input vulnerability among the different islands show that there is higher value variability in input vulnerability indices. The island group means of SLR, geomorphology, and natural habitat input indices indicate a broader range spread of the group means. The island groups' exposure to similar wave trends result in means that represent low variability. Similarly, surge, which varies slightly with local continental shelf width, shows a smaller F-value that represents low variability in the islands. Thus, high F-value results reject the null hypothesis that each island input vulnerability mean is equal. The comparison F-value results using the ANOVA of the related metric among all the islands showed a significant difference, $p\text{-}value < 0.05$ (Table 3.3). This proves that the islands have a very diverse reaction to the biophysical variables and demonstrate the variability of each island's contributing vulnerability metric. Among the

frequency distributions of the islands, geomorphology, natural habitat, and SLR showed the highest variability in the group means biophysical input vulnerability metrics. The variety of densities of the island populations shows significant differences in the population input metric.

The mean differences and p-value of the ANOVA with Tukey-Kramer test results for each island among their metrics are shown in Table 3.4. The islands are compared in pairs to emphasize the differences with respect to each input vulnerability metric. The *p-values* < 0.001 show significant differences in metric averages with low error, given as a superscript, even lower than the set threshold of 0.05. There is a less than 0.1% chance of obtaining an F-value as large as those presented in Table 3.4, indicating that the results are not random. The compared pairs of islands showed similar results as in Table 3.3 where geomorphology, natural habitat, and SLR effects are significantly different among the islands. The SLR means display the highest variability among the islands, followed by natural habitat. Although the island pairs of Oʻahu and Hawaiʻi and Molokaʻi and Maui exhibit small mean differences, the p-value proves significance in the differences of the mean for natural habitat. The wave exposure effects are similar except for Lanaʻi. Table 4 also displays similar traits between some of the islands. For example, SLR on Kauaʻi and Maui, Kauaʻi and Hawaiʻi and Lanaʻi and Hawaiʻi are not significantly different. In addition to significant mean differences of SLR and natural habitat index metrics among the islands, the largest group of mean differences observed are geomorphology for Oʻahu, Maui, and Hawaiʻi, wave exposure for Lanaʻi, and surge potential for Kahoʻolawe. The results also confirm that Kaho'olawe has the highest significant mean differences in vulnerability metrics, making the island features outliers compared to the others. The most similarities between the islands are found between Kauaʻi and Molokaʻi, except in natural habitat.

With regard to geomorphology, the literature has shown that the resistance to erosion and SLR effects are highly dependent on the type of geomorphologic feature of the shoreline (i.e., Bijlsma et al., 1995; Carter et al., 1993; Griggs and Trenhaile, 1994), which has been observed in the results. Due to rocky coastal cliffs, Kahoʻolawe and Hawaiʻi have more refractory effects for wave action and SLR. Oʻahu's shoreline, which includes pocket and low-lying beaches, and stream mouths (Richmond et al., 2001), is more at risk for inundation due to SLR, waves, and surge actions. The islands have low to moderate vulnerability to geomorphological formation, ranging from 2.0-3.30 (Fig. 3.3).

Relief and wave exposure showed almost equal distributions among each metric for the islands, except for the Maui region, which includes the islands of Molokaʻi, Maui, Lanaʻi, and Kahoʻolawe (Fig. 3.3). The average elevation of the shoreline is greater for shores facing mountainous areas, making them more resistant to SLR effects. The islands are mostly low to moderately vulnerable, except for Kahoʻolawe. The islands are also exposed to four main wave events (Vitousek and Fletcher, 2008) at different times of the year. Kauaʻi, Oʻahu, Molokaʻi, and Maui are primarily influenced by NP swells and trade winds, whereas trade winds have a more significant effect in Hawaiʻi and Lanaʻi. The only significant difference in means is observed between Kauaʻi and Lanaʻi. The formation characteristics of the shoreline (sheltered or exposed) affect the resultant impact. Due to the exposure of the high waves and winds in all directions, the islands show a consistent average of moderate vulnerability, with Lanaʻi ranking as most vulnerable followed by Kauaʻi, Hawaiʻi, and Oʻahu.

Surge potential is highest in areas where the continental shelf (bench) extends further into the ocean, which does not exist in Big Island of Hawaiʻi. The results do not consider the nonlinearity of the surge potential due to tide phase and shelf width, which can significantly change results (Poulose et al., 2017; Zhang et al., 2017). Surge potential varies significantly (Fig. 3.3), with the most variability in Hawaiʻi. Kahoʻolawe also shows a significant difference in mean surge potential compared to all the other islands. The mountainous sides of the islands create shorter continental shelf widths with respect to the shoreline, which reduces the surge potential.

Natural habitats, on the other hand, show a highly clustered formation with low vulnerability scores. This is due to the consistent reef, marsh and forest formations. The natural habitat role in coastal exposure (measured by the difference in the coastal exposure index with and without habitat) is greatest on Lanaʻi and Molokaʻi (Table 3.3). The fringing reef formations surrounding the island seafloor act as an essential defense mechanism for coastal zones to prevent inundation from traveling further inland, demonstrating the importance of adaptation strategies that improve natural habitats. This metric is only ranked high for Oʻahu, where there are industrialized piers for which the natural habitat has been demolished (Fig. 3.3). Natural habitats have a significant role throughout the islands and change the exposure index by the highest average of 0.64 (Table 3.6).

For SLR, hot spot locations are evident north and south-east of Maui and west-northwest of Hawai‘i, which are all highly vulnerable. The highest rates are observed in Hawai‘i and Maui due to the combined effects of SLR and ground subsidence (Fletcher, 2000; Richmond et al., 2001; Romine et al., 2013a). The input vulnerability maps are provided in Onat et al., (2018b).

Among all the input vulnerability metrics, geomorphology and wave exposure most affect coastal exposure in Hawai‘i and is the dominant factor for Kaua‘i and O‘ahu. High wave environments dominate in all islands, although Lana‘i, Hawai‘i, and Maui showed the strongest influences from SLR, while Kaua‘i and O‘ahu were least likely to be affected by SLR. The most dominant effect of surge exposure is on Maui. Moloka‘i, however, shows the highest rate of surge potential among its other ranks. The histograms (Fig. 3.3) also show that climatic forces (SLR, wave exposure, surge exposure) have a strong influence on the biophysical exposure indices for the Hawaiian Islands. In general, the variance of the results is due to differences in shoreline formation, protection, and the potential for exposure to climate stressors.

4.2 Characteristics of Exposure Metrics

4.2.1 Erosion Index (ErI)

Erodible shorelines are evaluated by considering geomorphology, natural habitat, and wave exposure. Although there is not much difference in ErI averages (Table 3.5), the most erodible shorelines exist in O‘ahu, Kaua‘i, and Hawai‘i, however, Maui, and Kaho‘olawe have the average highest ErI. O‘ahu is less prone to measurable erosion due to coastal defense structures (Table 3.5). Moreover, natural habitat effect is strongest at Moloka‘i. The most diverse rank ranges are also in Kaua‘i and O‘ahu, while Moloka‘i has the lowest index rank ranges. The coastal defense structure effects are highest on O‘ahu at 29.47 %. Although these structures provide some protection, there is also damage associated with refraction and disruption of sand budget and natural processes. While coastal defense structures may be needed to protect critical infrastructure and highly urbanized areas, more detailed environmental and coastal assessment are needed before the implementation of protective structures. The probability density functions follow extreme value or Weibull distributions due to multiple identical shoreline segments (Table 3.5 and Fig. 3.4). The shape parameter higher than 2 in Weibull distribution models a steadily increased finite tail that is more like the bell-shaped Rayleigh distribution with skewness. The generalized extreme value distribution

reflects the largest value distributions for Oʻahu. Similarly, the extreme value distribution limits the high peaks, but with an exponentially decreased tail. Because Kauaʻi and Kahoʻolawe exhibit more of a tail distribution with finite ends, their distributions are represented by a generalized Pareto distribution. Moreover, the ErIs of the islands positively correlates with the EIs.

4.2.2 Exposure Index (EI)

Moran's I results for each island showed significant clustering in coastal exposure with $p < 0.0001$ and z-scores between metrics and I index values being close to +1 (Table 3.6). The population effect is misleading when looking only at the means (Table 3.3) of the input vulnerability metric, as Maui shows the highest coastal population rank due to percentile ranges being distributed separately among all the islands. The unbalanced distribution might be the reason why based on input ranks, this metric stood out. This is one of the flaws of the percentile range ranking as relative CVI does not focus on the highest population but rather the density percentile distribution among the shoreline segments evaluated. Using the EI with and without population provides a clearer understanding of the effect of biophysical factors and social factors. Table 3.6 shows EI calculated with and without population. The comparison of mean EI with and without population shows that the exposure means are significantly different from each other for Kauaʻi and Oʻahu (Table 3.6). Not surprisingly, EI with population shows that the most vulnerable shorelines are located on Maui. The islands have a moderate vulnerability percentile (EI $\geq$ 3)—Maui 24.2%, Oʻahu 20.9%, Kauaʻi 17.9%, Hawaiʻi 8.8%, Kahoʻolawe 6.5%, and Molokaʻi 2.6%. The maximum exposure index observed reaches up to 4.05 (high vulnerability) on Maui.

The histograms presented in Fig. 3.5 are plotted with a bin width of 0.01 to reduce the dependency of the empirical probability density function of bin counts and represent the data accurately. The best fit of the probability density function model is shown in Table 3.6 and Fig. 3.5. The histograms that have a regular tail distribution form Generalized Extreme Value (Kauaʻi,Oʻahu, Maui, Lanaʻi), the right-skewed form shows Gamma (Molokaʻi), high peaks in low-moderate index range fit to inverse Gaussian (Hawaiʻi), and a wide range of variety distribution fitted generalized Pareto (Kahoʻolawe) (Fig. 3.5). The more vulnerable shorelines are located from: Lihue to Kapaa in the east and Anahora to Kilauea in the north east of Kauaʻi; Haleiwa to Kahuku in the north and Ewa Beach in south of Oʻahu; west coast and Kamehameha highway in the east of

Moloka‘i;Kahakuloa to Wailua in the north, west coast and Maalaea to Kihei in the south of Maui; Keomuku to Lopa of the north east of Lana‘i; and Kehaka Kai to Kawaihae in the west and Kilauea in the south-east of Hawai‘i (Fig. 3.6). The comparison of the relative EIs showed that O‘ahu, Maui, and Kaua‘i are the top three most vulnerable islands in the island chain (Fig. 3.7). The detailed GIS maps of the EIs are given in Onat et al., (2018b). The InVEST model maps are available online by using the links given in Onat et al., (2018b). The goal is to use these distributions to identify areas that are priorities for immediate action, those that require further study, and those that can be considered low-risk or relatively safe areas.

4.2.3 Model Limitations

Although the CVI maps help visualize vulnerabilities and create social awareness, there are limitations to the method. Limitations of the model originate from the definition of the coastal exposure index, which weighs every contributing layer equally and does not take into account interactions between variables. The number of variables affects the distribution of the exposure index at predictable rates (Cogswell et al., 2018). The model, moreover, does not include storm surge, wave field in nearshore regions, extreme wind and wave events, and sediment transport processes (Sharp et al., 2016). The accuracy is highly dependent on the wave data grid resolution (Sharp et al., 2016). Another limitation is that the model does not consider the quality and functionality of the natural habitat (Sharp et al., 2016) and structures (Arkema et al., 2013b).

Although Hawaii has a significant advantage in the availability and quality of observational data, the CVI model is static and does not include social variables, except for population density and infrastructure. Lack of time dependency and interaction between the effective parameters cannot adopt the CVI applications to future climate change scenarios (Gallina et al., 2016). Including multiple physical and social factors (Maanan et al., 2018) in a comprehensive multi-risk assessment that includes interdisciplinary collaboration (Gallina et al., 2016) would improve the assessment of vulnerability. The index needs to be improved by considering dynamic interactions between human and physical parameters to aid in long-term planning and decision-making. While the maps provide a baseline of the conditions, factors such as frequency and intensity of storms, depth of groundwater, and the location of critical infrastructure affected by environmental change, such as water and wastewater, need to be considered. There is also the potential to integrate more data describing

travel behavior as well as models describing evacuation and sheltering requirements (Kim et al., 2017). Although the model comes with certain limitations, it has been useful to calculate relative vulnerability and project which shoreline segments are highly vulnerable, considering the availability of the data. After identifying the vulnerable locations and hot spots from the InVEST model, a local scale vulnerability assessment can be developed to identify crucial needs and design appropriate adaptation solutions (e.g., Marchant, 2017; Onat et al., 2018a).

5. Conclusion

This study provides insight into the vulnerability of Hawai'i's coastal areas using a GIS-based CVI method to assess the relative influence of biophysical variables of geomorphology, relief (coastal elevation), natural habitats, SLR, wind and wave exposure, and surge potential. In addition to estimated rates of coastal erosion throughout the state, the research also compared islands and shoreline segments. The work resulted in the creation of a visual representation of erosion and vulnerabilities. The contributing factors can be used as tools for increasing public awareness and supporting planning, design, engineering, and implementation of hazard mitigation and climate change adaptation efforts. Key metrics including the frequency distributions, erosion susceptibility, natural habitat conditions, factors associated with changes in the erosion and vulnerability indices, overall exposure, and probability distributions and differences in EI by island and shoreline segment are presented. The approach calculates an EI and evaluates the vulnerability of each island and shoreline segment with various susceptibility metrics, which are ranked from very low (1) to very high (5) vulnerability.

The results confirm that geomorphology and wave exposure have the strongest influences on determining coastal vulnerability in Hawai'i. The geomorphology effect is exceptionally strong on Kaua'i and O'ahu. Although high wave energy affects all of the islands, Lana'i and Kaua'i are most influenced by wave exposure. Sea level rise is most dominant on Maui and Kaho'olawe. Moloka'i is mostly affected by surge potential, among other input vulnerability factors. The shorelines of the island chain are 31.42% exposed to SLR, wave, and surge potential. The formation, position, and location of the islands are crucial to understanding vulnerabilities in Hawaii and variability in the across the state's shorelines to coastal hazards and SLR. Geomorphology, natural habitat, and SLR showed the highest variability among the islands.

The inclusion of population as an input vulnerability metric in calculating EI affect significant differences in EI averages for Kauaʻi and Oʻahu. Oʻahu, Maui and Kauaʻi are the top three most vulnerable islands in the island chain, according to the results from the EI. Although EI averages rank in the low-medium ranges (2.23-2.66), the most vulnerable shoreline ranks moderate-high (4.05) for Maui county. Maui (24.2%) and Oʻahu (20.9%) have the most moderately vulnerable shoreline segments (EI $\geq$ 3). The most common probability distribution observed in EI is a Generalized Extreme Value with a regular tail distribution in low-moderate index ranges. The existing reefs, marshes and coastal forests along the shorelines act as a barrier to the adverse effects of climate change and SLR, and reduce the exposure index by a highest average of 0.64 out of 5. Molokaʻi contains the most erodible shorelines. Coastal defense structures protect against erosion and increase the ErI highest on Oʻahu (29.47%). The most erodible shorelines exist in Oʻahu, Kauaʻi, and Hawaiʻi, however, Maui and Kahoʻolawe have the average highest ErI. Oʻahu is less prone to measurable erosion due to its coastal defense structures. The most commonly observed probability distributions of ErI are extreme value and Weibull.

Although the islands have an average of low to medium exposure when considering climate stressors, bio-geophysical characteristics, and social exposure, the islands' vulnerability reaching high exposure in high energy wave susceptible areas indicates the need for more detailed assessment. Understanding vulnerabilities at each beach can be useful in the planning and design of sustainable adaptation strategies to protect lives and property. The study gives the causes and consequences from input parameters defining vulnerability. The probability density functions provided here help to guide planners in estimating expected erosion and exposure indices. The methods provided in this study can be applied to other island communities around the world that are exposed to high wave energy and varied coastal geomorphology. The work broadens understanding of hazard maps (Richmond et al., 2001) by quantifying the relative vulnerabilities of shorelines with additional measures of vulnerability and exposure. The study considers ecological features unique to the different islands and shoreline segments in Hawaii. The study displays the probability of the event occurring and the impact of that event by reducing quantitative uncertainty (Bolter, 2013) by defining relative risk spatially. The study also improves the spatial resolution that (Arkema et al., 2013b) presented for the coastal hazard index of U.S. coastlines and investigates the complex environmental coastal interactions at a local scale. The approach also resembles the Sendai Framework (UNISDR, 2015) by understanding risk, strengthening hazard governance, and enabling

a platform to investigate risk reduction and preparedness. The study facilitates the use of coastal vulnerability data to support planning and decision-making for hazard mitigation and coastal adaptation. The methods and tools can be used to engage a broad range of stakeholders with diverse backgrounds. While Hawai‘i conjures images of swaying palms and white sandy beaches, it is also an ideal setting for developing, testing, and improving systems of coastal monitoring and evaluating hazards, threats, and mitigation and adaptation efforts. While improvements in the methods and data are needed, there is also need for more attention to integrating these findings into planning, land use, and development of resilient communities. Future research will include consideration of more socio-economic metrics, groundwater, and more advanced hydrodynamic modeling into a dynamic CVI to support the development of comprehensive scenarios and strategies for coastal mitigation and adaptation to climatic and other stressors.

Table 3. 1: Input data layers and their sources. The GIS files are given in Onat et al., (2018b).

Input Variable	Description	Source
Bathymetry & Relief	Fifty meter bathymetry and topography hillshade grids. Projection changed.	(Hawai‘i Mapping Research Group, 2014)
Continental Shelf	The original file is used.	(Natural Capital Project, 2016)
Geomorphology	Modified file by clipping and joining a created table to the attributes of the file. The created table includes descriptions and ranks. 1978-2001	(NOAA Office of Response and Restoration, 2001)
Land Polygon	Modified file by creating a polygon from line shape file	(Charles H. Fletcher et al., 2002)
Sea Level Rise	Created polygons with attributes of sea level trends. The tide gauge measurements are from the Permanent Service for Mean Sea Level (PSMSL) and GPS data from the Nevada Geodetic Laboratory (NGL), which uses the GIPSY/OASIS-II Version 6.1.1 software developed at the Jet Propulsion Laboratory (JPL) to study long-term relative SLR.	(Yang and Francis, 2018)
Climatic Forcing	Compiled wind and wave hindcast data from WAVEWATCH III for 2008-2016 are used.	(Natural Capital Project, 2016)
Natural Habitats	Created polygon to match the Google Earth images of the islands. Created tables to join the modified attribute between 1977-2001.	(NOAA Office of Response and Restoration, 2001)
Population	Modified file by clipping area. The ocean, river, and lake polygon census blocks are deleted. Polygon shapefile was then transformed into a raster file using the attribute of the 2010 population.	(U.S. Census Bureau, 2010)
Structures & Roads	Modified polyline shapefile to the polygon by buffering the area. Area buffer size was taken by the average size of roads to fill line on both ends. Created polygon structures of human-made structures such as buildings. Both files were then merged into one file.	(State of Hawaii Office of Planning, 2015)

Table 3. 2: Natural habitat protective distances. The median of the maximum protective distance along the shoreline for each habitat is measured with ArcGIS.

Habitat Type	*Rank*	*Kaua'i*	*O'ahu*	*Hawai'i*	*Moloka'i/Maui/Kaho'olawe/Lana'i*
Reefs	1	1855	1400	2210	1350
Forests	1	425	401	445	527
Salt Brackish Marshes	2	83			
Freshwater Marshes	2	543			
Freshwater Swamps	2	410			
Mangroves	2	480			
Dunes	3	343			
Vegetative Low Banks	4	68			

Table 3. 3: Ranked input vulnerability metrics. (1: very low vulnerability–5: very high vulnerability). The table gives the average(μ), and standard deviation (σ) of each island ranked shorelines metrics. ANOVA F-values of the each metric compared to different islands are given to indicate the significant differences of the means. The p-value < 0.05 for all metrics.

		Kaua'i		*O'ahu*		*Moloka'i*		*Maui*		*Lana'i*		*Kaho'olawe*		*Hawai'i*	
Shoreline Segments		612		1039		591		866		286		204		1775	
Exposed Shorelines (%)		33.82		19.15		29.44		29.21		46.85		36.94		36.39	
	F-value	μ	σ	μ	σ	μ	σ	μ	σ	μ	σ	μ	σ	μ	σ
Geo.	169.9	3.21	1.28	3.33	1.12	3.03	1.06	2.51	1.25	3.07	1.07	2.09	0.95	2.16	1.05
Relief	32.3	3.0	1.41	3.0	1.41	3.03	1.51	2.71	1.41	2.96	1.07	4.22	0.81	3.0	1.41
Nat. Habitat	144.1	1.55	0.33	1.83	0.69	1.38	0.36	1.53	0.33	1.39	0.28	1.8	0	1.73	0.19
Wave Exp.	6.5	3.02	1.43	3.0	1.41	2.93	1.24	2.88	1.55	3.47	1.23	3.0	1.43	3.0	1.41
Surge Pot.	15.6	3.14	1.33	2.94	1.22	3.14	1.26	3.26	1.46	3.19	1.45	2.43	1.3	3.24	1.47
SLR	1141.	3.0	0	3.53	0.50	1.50	0.5	4.23	1.25	3	0	5	0	2.98	0.72
Population	247.0	2.96	1.41	2.96	1.41	2.86	1.28	3.75	1.21	1.28	0.60	1	0	3.17	1.16

Table 3. 4: The mean differences (μd) and a *p-value* of ANOVA with Tukey-Kramer test results for each island among their metrics. The *p-values* < 0.001 shows significant differences in metric averages, stated superscript (*) and bold.

		Geomorphology	Relief	Natural Habitat	Wave Exp.	Surge Pot.	SLR
Compared Islands		*μd*					
Kaua‘i	Oahu	-0.12	0	-0.28*	0.02	0.2	0.53*
Kaua‘i	Moloka‘i	0.18	-0.03	0.17*	0.09	0	1.5
Kaua‘i	Maui	0.70*	0.29	0.02	0.14	-0.12	-1.24*
Kaua‘i	Lana‘i	0.14	0.05	0.16	-0.45*	-0.05	0
Kaua‘i	Kaho‘olawe	1.12*	-1.21*	-0.25*	-0.03	0.71*	-2*
Kaua‘i	Hawai‘i	1.05*	0	-0.18*	0.02	-0.1	0.02
O‘ahu	Moloka‘i	0.29*	-0.03	0.46*	0.07	-0.2	2.03*
O‘ahu	Maui	0.82*	0.29*	0.30*	0.12	-0.32*	-0.71*
O‘ahu	Lana‘i	0.26	0.04	0.44*	-0.47*	-0.25	0.53*
O‘ahu	Kaho‘olawe	1.24*	-1.22*	0.04	-0.05	0.51*	1.47*
O‘ahu	Hawai‘i	1.16*	0	0.10*	0	-0.30*	-0.54*
Moloka‘i	Maui	0.53*	0.32	-0.15*	0.05	-0.13	2.74*
Moloka‘i	Lana‘i	-0.03	0.07	-0.02	-0.54*	-0.05	-1.50*
Moloka‘i	Kaho‘olawe	0.95*	-1.19*	-0.42*	-0.12	0.71*	-3.50*
Moloka‘i	Hawai‘i	0.87*	0.03	-0.35*	-0.07	-0.1	-1.48*
Maui	Lana‘i	-0.56*	-0.25	0.14*	-0.59*	0.08	1.23*
Maui	Kaho‘olawe	0.42*	-1.51*	-0.27*	-0.17	0.84*	-0.76*
Maui	Hawai‘i	0.34*	-0.29*	-0.20*	-0.12	0.02	1.25*
Lana‘i	Kaho‘olawe	0.98*	-1.26*	-0.40*	0.42	0.76*	-2
Lana‘i	Hawai‘i	0.90*	-0.04	-0.34*	0.47*	-0.05	0.02
Kaho‘olawe	Hawai‘i	-0.08	1.22*	0.07	0.05	-0.81*	2.02*

Table 3. 5: Erosion index (ErI) comparison of the islands. (1: very low–5: very high; the average(μ), and standard deviation (σ). The probability density function equations and their parameters are given in Appendix C.)

	Kaua‘i	O‘ahu	Moloka‘i	Maui	Lana‘i	Kaho‘olawe	Hawai‘i
μ	2.14	2.07	1.93	2.19	2.49	2.62	2.13
σ	0.63	0.62	0.41	0.59	0.37	0.49	0.52
Max	3.41	3.66	2.91	3.87	3.22	3.87	3.46
Min	1	1	1	1	1	1	1
PDF	Generalized Pareto	Generalize extreme value	Weibull	Weibull	Extreme value	Generalized Pareto	Weibull
	k: -0.8277	k: -0.3611	β: 2.0927	β: 2.4190	μ:2.6656	k:-0.6423	β: 2.3399
	σ:1.9970	σ:0.4470	α: 5.3914	α: 4.1072	σ:0.3036	σ:1.3850	α: 4.6701
	θ: 1	μ:2.5467				θ: 1.7320	
ErI w/o structures μ	2.46	2.68	1.96	2.40	2.50	2.62	2.26
ErI w/o structures σ	0.48	0.43	0.38	0.53	0.36	0.49	0.42

Table 3. 6: Coastal Exposure index (EI) comparison of islands (1: very low–5: very high; the average(μ), mean differences (μd) and standard deviation (σ). The probability density function equations and their parameters are given in Appendix C.) *There are no residents on Kaho'olawe. However, because the population input index range is divided according to percentiles, Kaho'olawe's population is classified as 1.

	Kaua'i	O'ahu	Moloka'i	Maui	Lana'i	Kaho'olawe	Hawai'i
μ	2.55	2.66	2.23	2.61	2.33	2.36	2.48
σ	0.44	0.40	0.35	0.56	0.37	0.41	0.36
Max	3.77	3.77	3.22	4.05	2.97	3.19	3.77
Min	1.50	1.77	1.28	1.25	1.49	1.60	1.55
Range	2.265	2.003	1.944	2.804	1.478	1.591	2.218
PDF	Generalized extreme value	Generalized extreme value	Gamma	Generalized extreme value	Generalized extreme value	Generalized Pareto	Inverse Gaussian
	k:-0.2855	k:-0.2166	α:41.6862	k: -0.2885	k: -0.5552	k:-0.8273	μ: 2.4776
	σ: 0.4358	σ: 0.3831	β:0.0535	σ:0.5572	σ 0.4056	σ: 1.3176	λ:113.4271
	μ: 2.3962	μ: 2.5040		μ:2.4113	μ:2.2501	θ:1.6013	
Moran's index	0.7955	0.7752	0.7733	0.7868	0.9315	0.7867	0.5828
z-score	22.593	25.8514	18.9048	23.4627	15.6677	11.4997	27.3917
Nat. Habitat Role μ	0.562	0.504	0.531	0.554	0.644	0.508	0.470
Nat. Habitat Role σ	0.156	0.138	0.108	0.172	0.197	0.103	0.103
EI w/o population μ	2.54	2.67	2.18	2.48	2.62	2.74	2.40
EI w/o population σ	0.43	0.42	0.34	0.55	0.54	0.55	0.38
EI w/o population Max	3.73	3.73	2.99	3.91	3.57	3.87	3.59
EI w/o population Min	1.49	1.48	1.30	1.03	1.59	1.73	1.49
EI w/o population F-value	0.13	0.66	5.07	21.36	371.37	*	29.95
EI w/o population *p-value*	0.717	0.415	0.024	<0.05	<0.05	*	<0.05

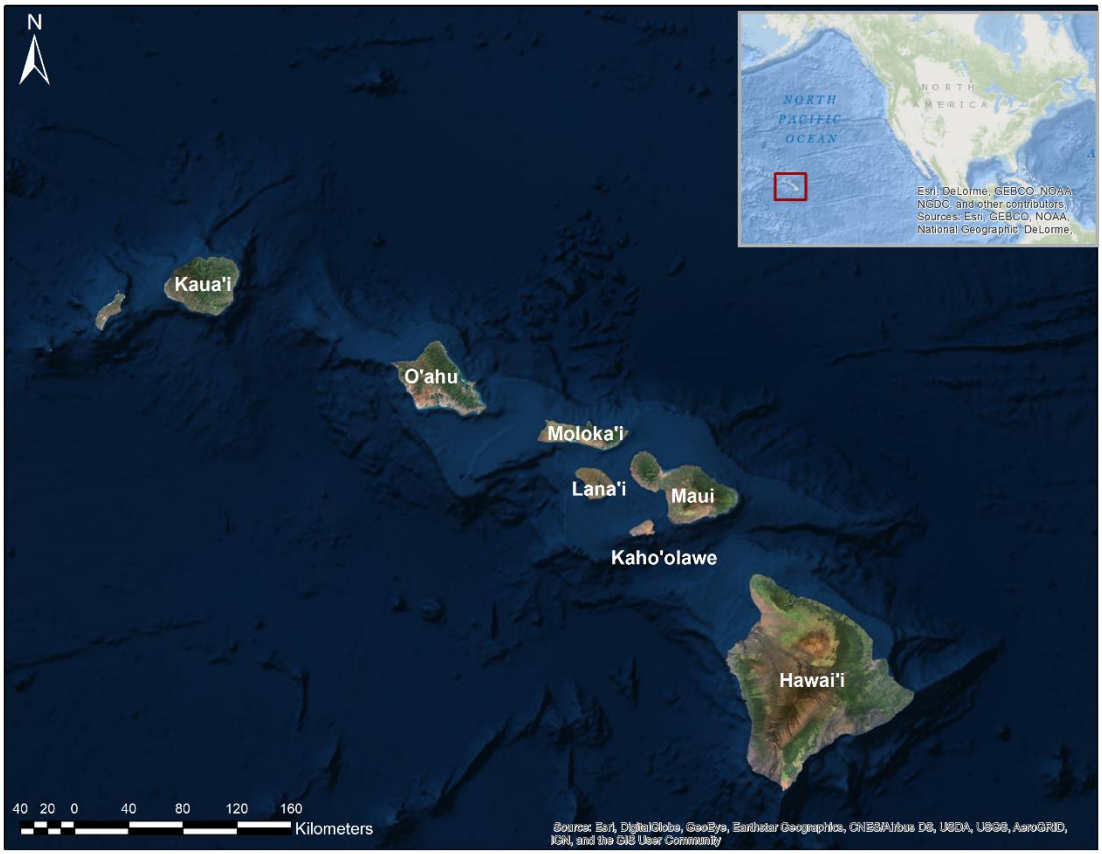

Figure 3. 1: The study area covers the shorelines of the main Hawaiian Islands—Kauaʻi, Oʻahu, Molokaʻi, Lanaʻi, Maui, Kahoʻolawe and Hawaiʻi (Big Island)—located in North Pacific. The red square on the insert shows the location of the islands on a world map.

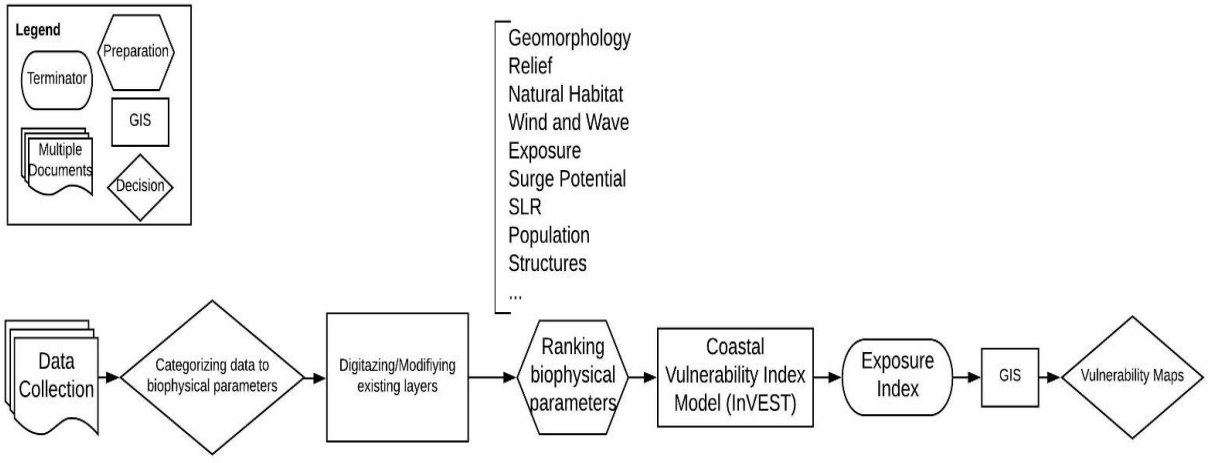

Figure 3. 2: The hierarchical procedure for CVI map generation via InVEST Coastal Vulnerability Model.

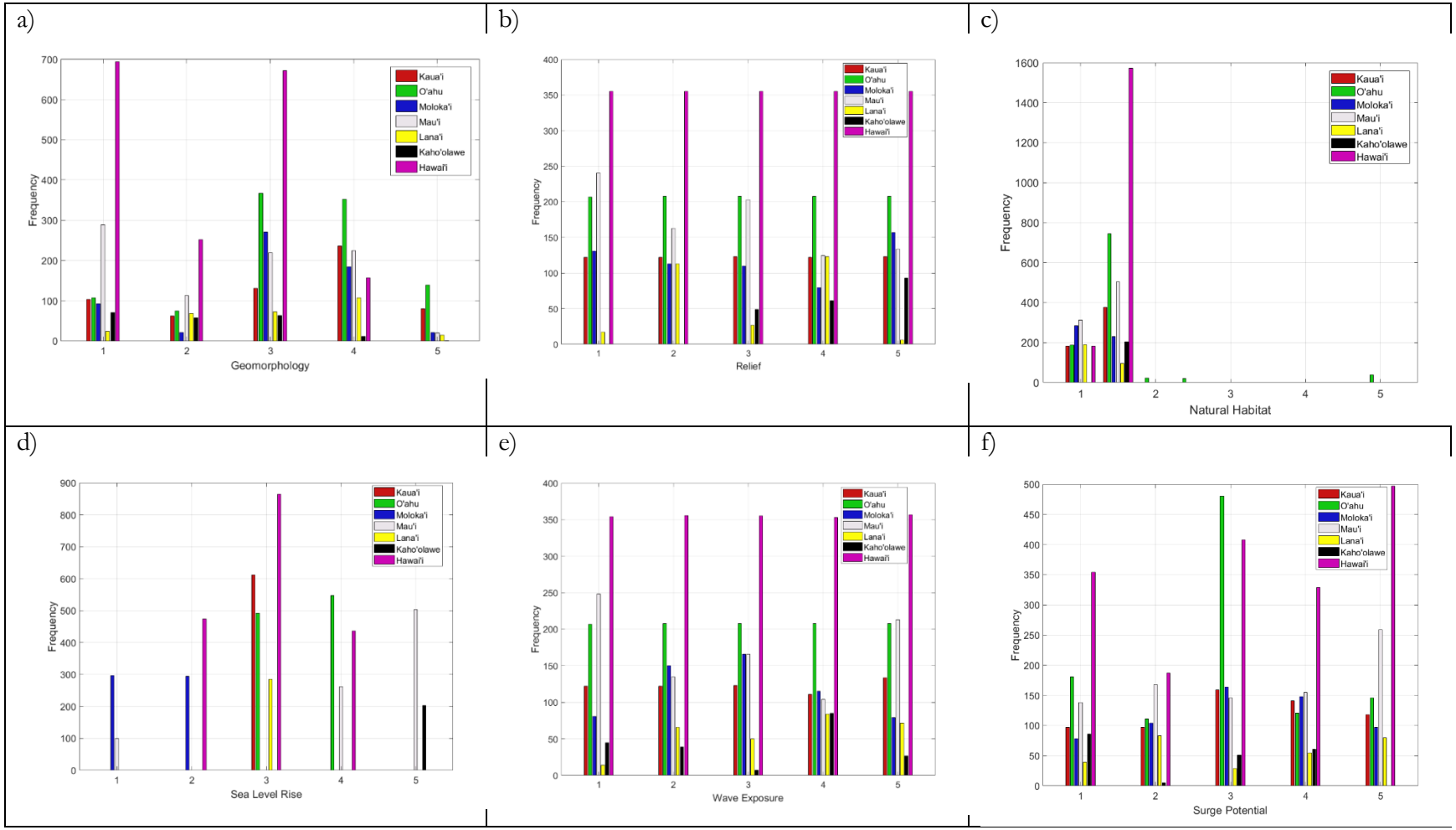

Figure 3. 3: Histograms of each island's ranked input vulnerability variables (1: very low vulnerability–5: very high vulnerability). The y-axis shows the frequency number while x-axis shows the index numbers for each input variable. The bar colors for the islands: red for Kauaʻi; green for Oʻahu; dark blue for Molokaʻi; grey for Maui; yellow for Lanaʻi; black for Kahoʻolawe; and pink for Hawaiʻi.

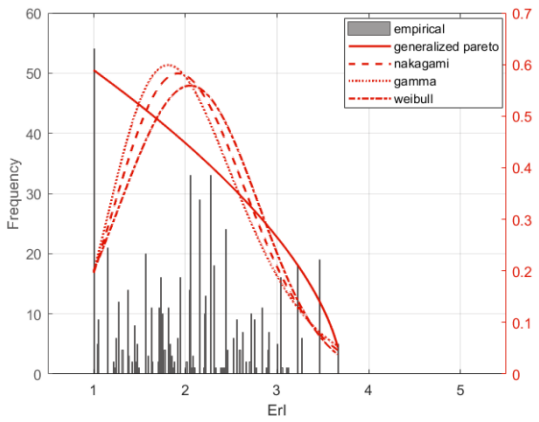

Kauaʻi

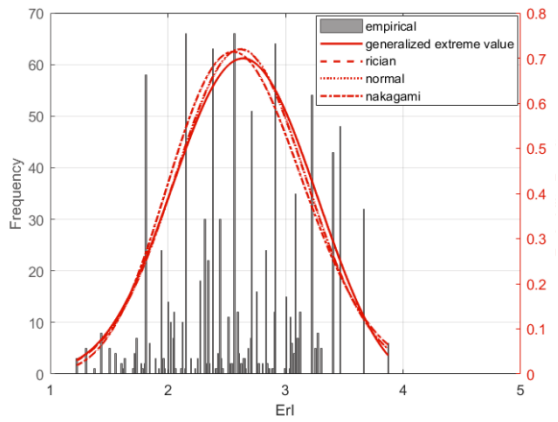

Oʻahu

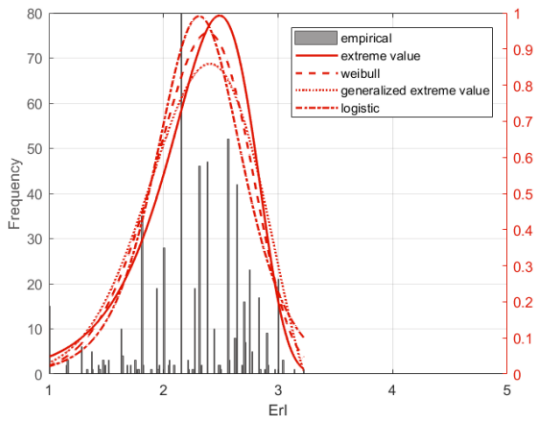

Molokaʻi

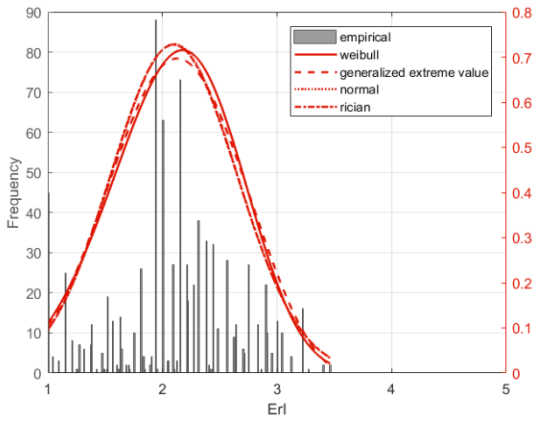

Maui

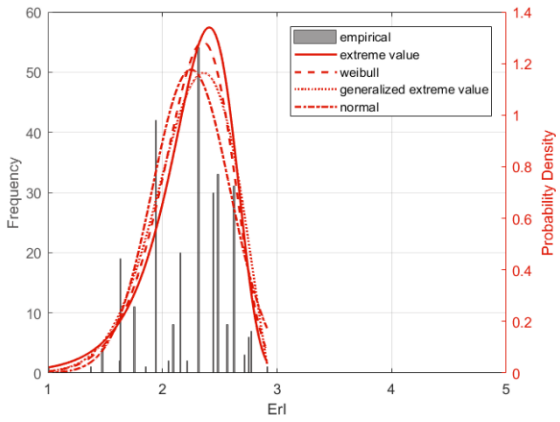

Lanaʻi

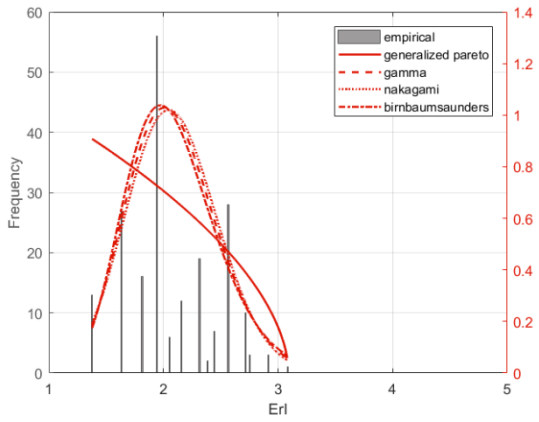

Kahoʻolawe

Figure 3.4 continues

Figure 3.4 continues

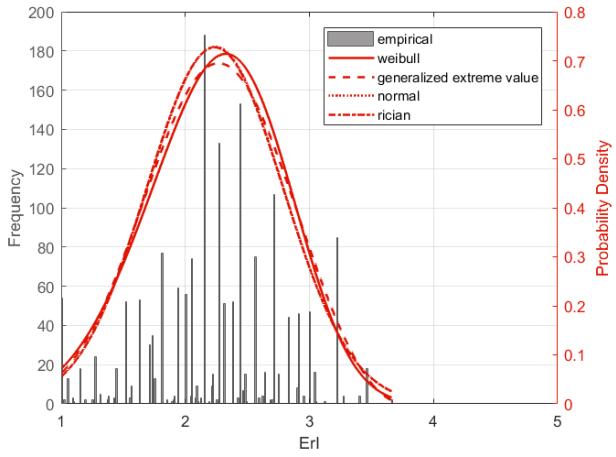

Hawai'i

Figure 3. 4: ErI histogram and the probability distribution of the islands.

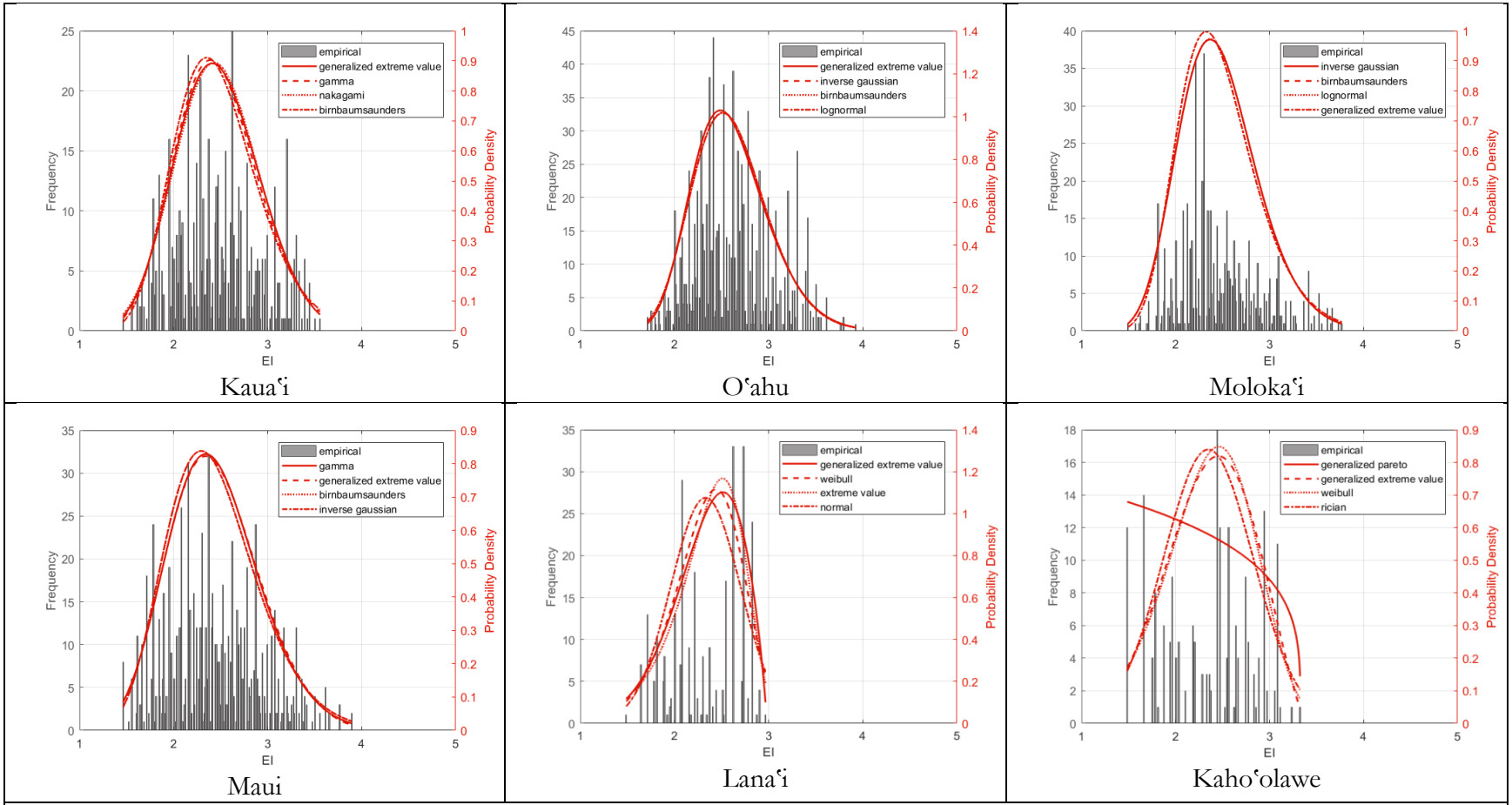

Figure 3.5 continues

Figure 3.5 continues

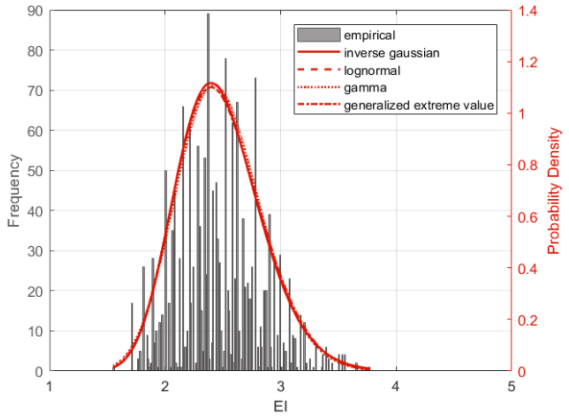

Hawai'i

Figure 3. 5: Probability density distribution of EI of the Hawaiian Islands.

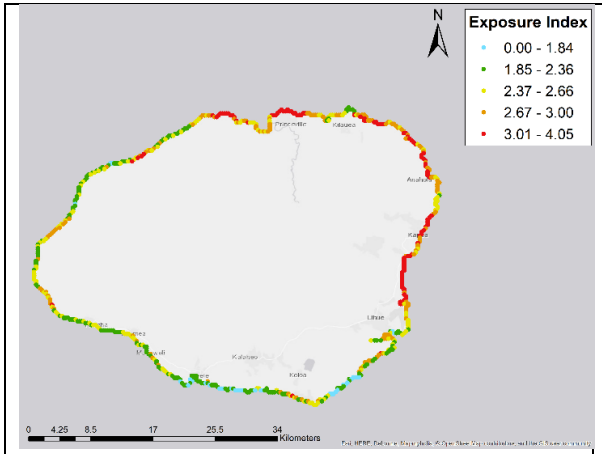

Kauaʻi

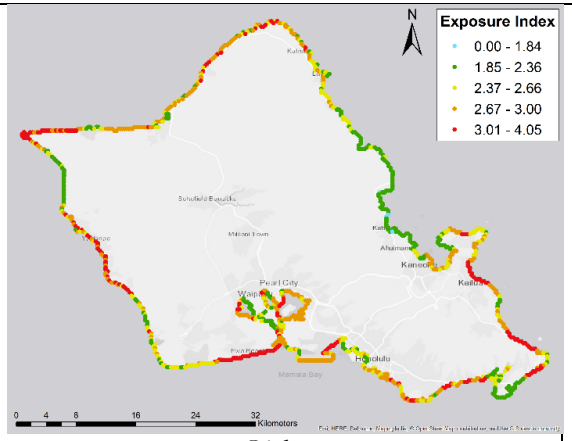

Oʻahu

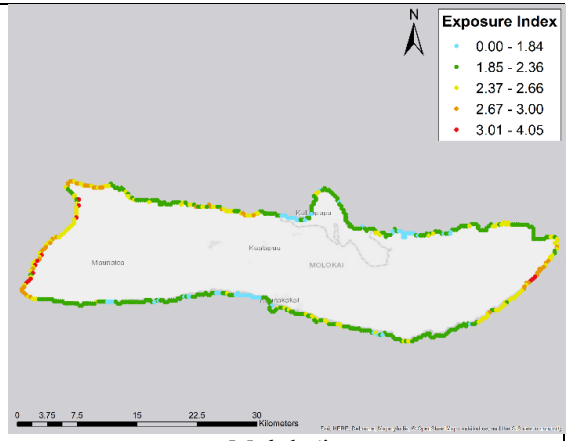

Molokaʻi

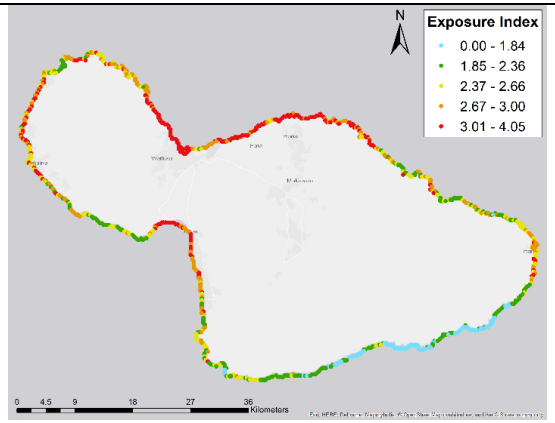

Maui

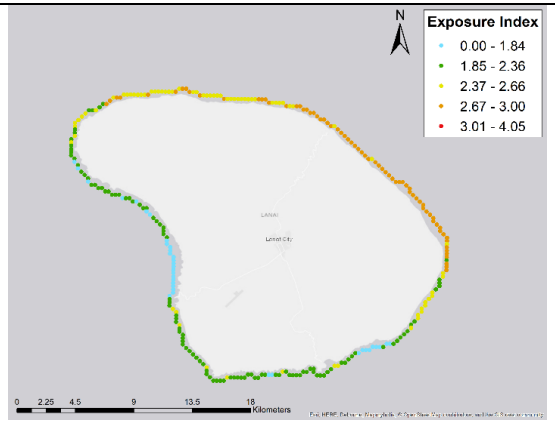

Lanaʻi

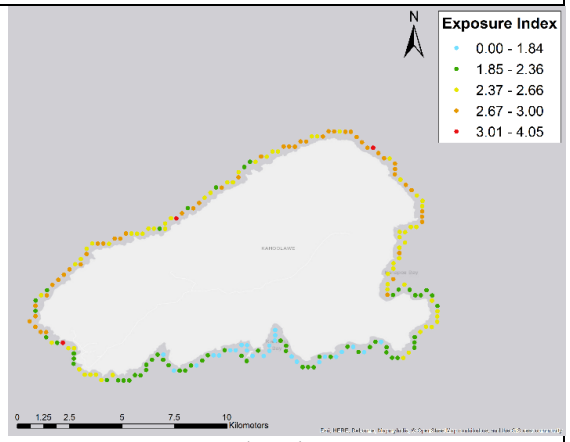

Kahoʻolawe

Figure 3.6 continues

Figure 3.6 continues

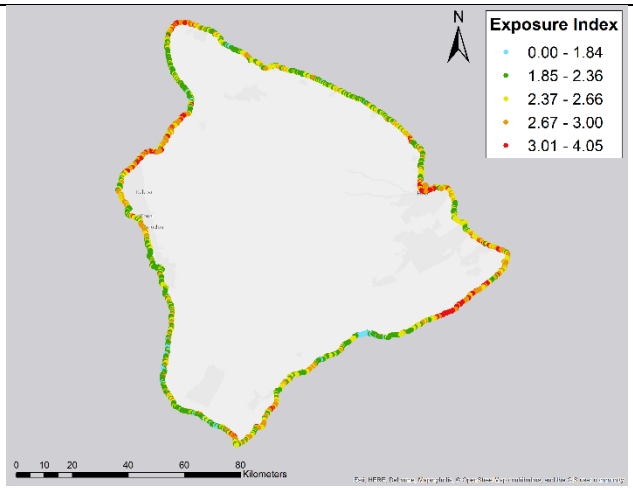

Hawai'i

Figure 3. 6: Coastal EI maps of the islands (1: very low vulnerability–5: very high (extreme) vulnerability).

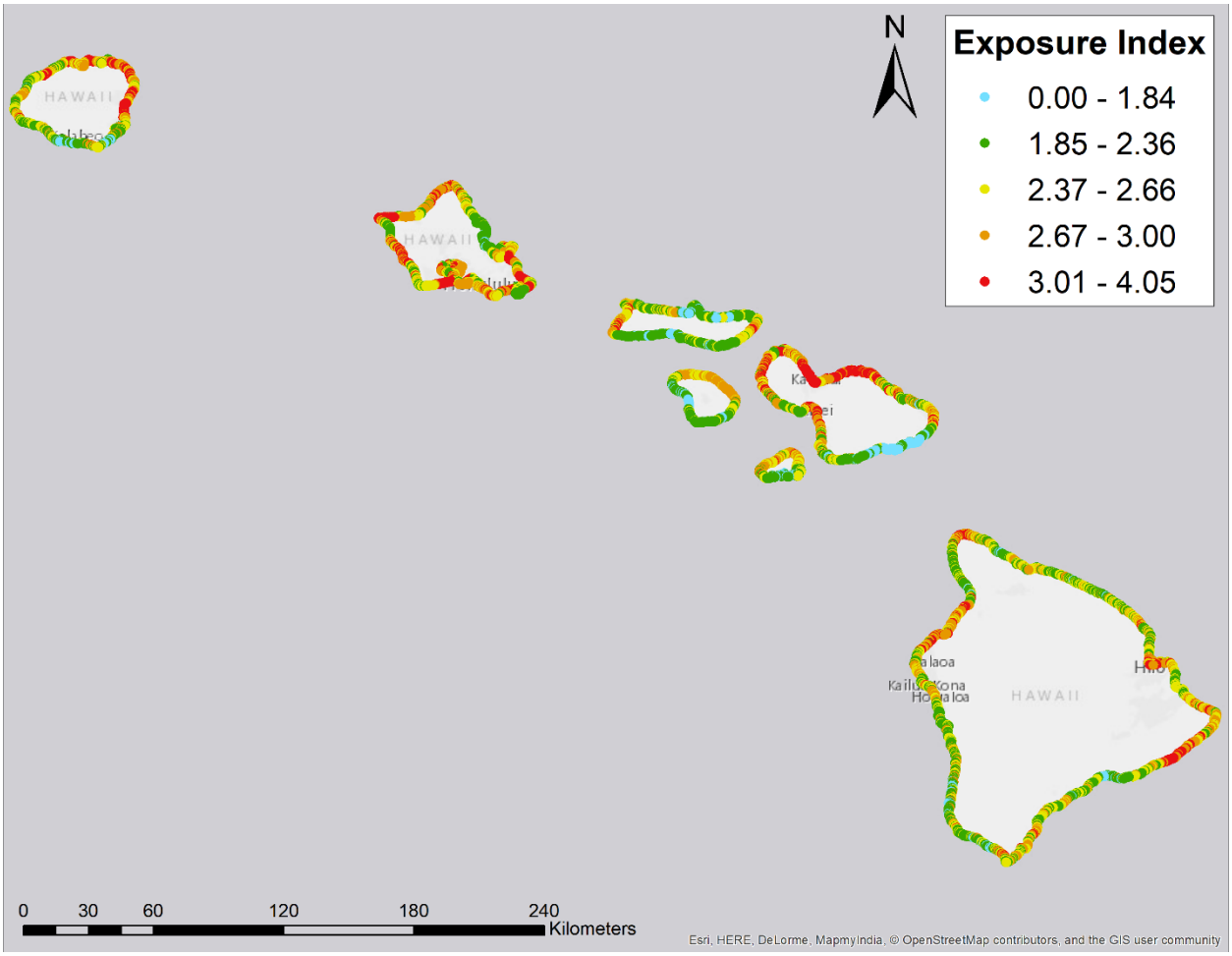

Figure 3. 7: Coastal EI map of the islands (1: very low vulnerability–5: very high (extreme) vulnerability).

CHAPTER 4. Vulnerability Assessment and Adaptation to Sea Level Rise in High-Wave Environments: A Case Study on O‘ahu, Hawai‘i

The material presented here is a version of published article in Ocean and Coastal Management by Yaprak Onat, Oceana Francis and Karl Kim.

High-energy waves intensify the impacts of sea level rise and threaten coastal communities, requiring measures to prevent harmful consequences. Vulnerability assessments using NOAA's assessment guide were performed in a high wave environment, accounting for the impacts of sea level rise on coastal inundation, longshore transport, benthic habitat as well as on beach users and homeowners. This case study of the North Shore region of Oahu, Hawai'i' uses multi-criteria evaluation and cost-benefit analysis based on vulnerabilities, impacts, and protective actions such as shoreline hardening, beach nourishment and dunes, vegetative cover, and elevation or relocation of structures. Geomorphology and natural habitats dramatically affect coastal exposure in high-energy wave environments. The most viable adaptation strategies include expansion of artificial reefs in benthic habitat dominated areas, while vegetative cover and beach nourishment are most appropriate in developed locations and surf tourism areas. Suitable adaptation strategies were determined based on differences in the biophysical environment and community perceptions. The value of this approach lies in both a generalized method for compiling and analyzing large amounts of data as well as customizing the proposed framework to identify crucial elements necessary for effective adaptation to sea level rise in high-energy wave environments.

1. Introduction

Both increased atmospheric heating due to greenhouse gas concentrations (Meehl et al., 2005; Solomon et al., 2009; Widley, 2005), and rises in ocean temperatures with thermal expansion of ocean waters, contribute to sea level rise (SLR), generating primary climate stressors for coastal communities (Domingues et al., 2008). Over the past century, global mean sea level has risen dramatically after approximately 2,000 years of little change. The Intergovernmental Panel on Climate Change Fifth Assessment Report (IPCC 2014) found that the projected global mean sea level is estimated to be approximately 60 cm by 2100, making it a significant stressor on coastal communities.

Gornitz (1991); Klein et al.(1999); Adger et al. (2003) found that with SLR, flooding due to storm surges can penetrate further inland and escalate coastal erosion. Saltwater intrusion can also contaminate water supply systems. With SLR, the quantity and quality of marine life may also decrease. These biophysical risks and the responses of communities determine potential coastal vulnerabilities. Since coastal systems often have unique characteristics, site-specific research is needed to prepare for probable scenarios triggered by climate change. Managing risks of climate stressors to exposed zones can be supported with vulnerability assessments coupled with the design and implementation of appropriate adaptation strategies.

It has been challenging for policymakers to devise effective responses to climate change (Kelly et al., 1994). The vulnerability is often used as a broad term describing the risk assessment of a community often ends up focused on specific impacts. These include whether the vulnerability is the starting point, end point, or another part of the assessment, its relationship to external factors, whether it is inherent to a scenario or system, and whether it is static or dynamic (Fussel and Klein, 2006). If a vulnerability model can quantify the impacts of probable scenarios associated with climate change, the exposure and sensitivity of the region to future climate events can also be better estimated. Assessing the vulnerability of a region due to SLR and estimating the effects of strategies such as accommodation, protection or retreat can also increase adaptive capacity. Vulnerability assessments, therefore, serve as a tool to navigate feasible adaptation solutions for communities (Smit and Wandel, 2006). The coastal vulnerability index (CVI) is used with vulnerability assessment to identify regions with relatively high risks. The resulting CVI provides a simple numerical basis for ranking sections of coastline regarding their potential for change. Lack of preventive measures can increase the damage caused by SLR (Nicholls et al., 1999). Nicholls and Cazenave (2010) point out that adaptation strategies should include determination of the impacts of climate stressors. Technically efficient, compatible, easily implemented and optimally funded adaptation solutions will likely be mostly to be executed and enhance adaptive capacity (Fatorić and Chelleri, 2012). Communities like Hawai‘i rely on coastal areas exposed to high waves for much of their livelihoods. Raising public awareness, determining vulnerabilities and using information for planning and decision-making are needed. Integrating ecological and social factors in the implementation of ecosystem-based management supports long-term sustainable development (Mangubhai et al., 2015).

This research identifies factors that increase the vulnerability of high-wave energy environments to SLR by evaluating the relative contributions of vulnerability indices. The exposure of coastal environments to high wave energy and SLR are evaluated using NOAA's assessment framework (NOAA Needs Assessment Guide, 2016). Based on input from the public and policymakers, interactions in the coastal zone and support for vulnerability reduction and adaptation strategies are identified. Quantitative evaluation of adaptation strategies is presented to support planning, engineering, and decision-making in coastal areas.

2. The Case Study Area – Waimea to Rocky Point, O'ahu

The case study area is from Waimea Bay to Rocky Point, a high wave environment, as shown in Figure 4.1. It is bordered by Kamehameha Highway and a residential neighborhood. Houses are located on much of the 7-mile coast from Haleiwa to Kahuku. The area includes a Marine Life Conservation District (MLCD) (Pupukea-Waimea) located from the southern islets of Waimea Bay to the northern end of Shark's Cove and from Kaunala Stream at Sunset Point to Rocky Point to the west and from the shoreline to Kamehameha Highway (HNL C&C., 2016). Waimea Bay Park, located across from Waimea Falls Park, Pu'u o Mahuka Heiau State Monument and Sunset Beach Park contain recreational areas, a lifeguard tower, and parking areas. The region experiences four dominant swells including North Pacific, trade winds, southern swells, and Kona storm waves as well as distant storms and tropical cyclones from the northern and southern hemispheres (Moberly and Chamberlain, 1964). Tradewinds generate swells with wave heights of 1–3 m with 6–8 s periods (Bodge and Sullivan, 1999), (Vitousek and Fletcher, 2008). Aucan (2006) documents the dominance of North Pacific swells from the northwest in winter months, while trade wind swells persist throughout the year but are most common during the summer. The area is famous for international surfing competitions from December through February, when wave heights can reach over 10 m. Caldwell (2005) calculated annually recurring significant wave heights in deep water from NOAA Buoy 51001, with North Pacific swells which hit the North Shore with the highest wave heights of 7.7 m high with long wave periods of 14-18 s (Vitousek and Fletcher, 2008).

Due to large swells, the area has dealt with coastal flooding and erosion for decades. Dail et al. (2000) emphasize that the difference between the summer and winter shoreline profiles results from high-energy waves washing up on the shore at Sunset Beach. According to Cocke (2014), several

Sunset Beach homes were destroyed in 1969 by a powerful storm and then rebuilt in the 1980s, at a further distance inland. The state land use law was modified (State Land Use Law Hawai'i Revised Statutes (HRS) Chapter 205 to the State CZM Law, HRS Chapter 205A) in 1986 to restrict new construction of homes 6 m from the certified shoreline. Structures built before the rules were modified in the hazard zone are often damaged by high waves and then repaired, allowing the problem to persist and worsen over time. On January 27, 2016, large north swells off Pupukea reached the roadway and damaged several properties (Now, 2016). With the land movement being consistent, tide gauge measurements from 1905 to 2006 display the mean sea level at 1.44 ± 0.21 mm/year for Honolulu (NOAA Tides and Currents, 2013). Hawai'i is expected to experience SLR of 0.3 m by 2050, and 0.91 m by the end of the century (NOAA Tides and Currents, 2013) which will only serve to increase the risks of coastal flooding.

The area is used for residential and recreational activities and as a natural habitat for different marine and terrestrial species, forming a complex system of vulnerabilities. Adaptation strategies, therefore, must address multiple interwoven needs, requirements, and dependencies.

3. Methods

3.1 NOAA Assessment to Find the Degree of Vulnerabilities

This study uses the NOAA Needs Assessment Guide (NOAA, 2011; "NOAA Needs Assessment Guide," 2016) to determine the vulnerability of the coastal area and then to develop policies that reduce risks associated with SLR and climate change. The goal of the needs assessment is to identify information gaps and develop priorities for new climate-related products and services.

The NOAA Needs Assessment Guide (NOAA, 2011; "NOAA Needs Assessment Guide," 2016) was chosen since it particularly focuses on the vulnerability from physical processes driving sea-level rise and coastal inundation to society, from local to national level, while providing the best available information to decision makers on sea-level change impacts and adaptive management strategies.

It is the priority of NOAA to ensure that coastal decision makers have a working coastal management framework which can be applied to many different scenarios. Coastal decision makers' needs for addressing the impacts of sea level changes include:

1) Improved ability to predict sea-level change
2) Assessment and predictions of sea-level change impacts to coastal communities
3) Science-based assessment and predictions of sea-level change impacts to coastal ecosystems
4) Adaptation strategies for coastal decision makers
5) Engagement, education, and outreach to stakeholders on sea-level change science and adaptation strategies.

In our paper, we mainly focus on Items 3 and 4 considering IPCC (2014) Representative Concentration Pathway 4.5 scenario is considered.

Understanding science-based assessments and predictions of sea-level change impacts under the influence of different coastal environments includes having a better understanding of marine resources and ocean dynamics, shoreline stability and erosion; biological and physiological tolerances to SLR; understanding the human connection and our dependence on healthy ecosystems; prioritization of adaptations given sea-level and climate change predictions; natural resource mapping and identification of high-priority areas and the impacts of sea-level rise; and use of tools to predict impacts on habitats.

Adaptation strategies for coastal decision makers include understanding the likely changes to human communities or local ecosystem; develop local capacity; develop strategies towards sustainability; performing vulnerability assessments; adaptive management planning; strategies for incorporation of the outputs of sea-level rise research and modeling into planning, policies, and regulations. In addition, there is a need for an economic assessment and cost-benefit analysis of adaptation strategies.

The results of the needs assessment serve as one input to help frame national and international climate science assessments. This effort will help NOAA understand the nation's vulnerability to climate variability and change, and inform climate adaptation strategies at all levels.

The approach includes twelve steps that include: 1) defining the issue and target population, 2) establishing a planning team, 3) gathering existing data and information, 4) characterizing the target population, 5) identifying the data collected, 6) selecting data collection methods, 7) determining an appropriate sampling strategy, 8) designing and plotting the data collection instruments, 9) gathering and recording the data, 10) analyzing and 11) managing the data and 12) finally synthesizing and

reporting the information. The process starts with identifying information about the project area and collecting data on the target population using a checklist, which helps to narrow the range of questions for the target audience. After the public has been identified, the unknown information must be determined, collected, and analyzed. From the known information, different methods to obtain inputs are formalized. Input on potential solutions is gathered. After both known and unknown elements are compiled, the information is synthesized and shared with the public so that the data on the project area and potential actions can be expanded for use by others in the future.

The method requires much information to be synthesized from many sources including online resources, archives, and interviews with the public and professionals. Interviews were held with five experts representing six agencies (Department of Land and Natural Resources - Office of Conservation and Coastal Lands (DLNR-OCCL); City and County Department of Parks & Recreation (DPR); State Hawai'i Department of Transportation (DOT); City and County Department of Planning and Permitting (DPP); State Coastal Zone Management Program (CZM); and Sea Grant College Program), eight residents in Ke Nui Road and 20 beachgoers in February 2015. The interviewees were asked about their knowledge of SLR, their experiences, what has been done to improve the condition, drawbacks, and conditions for the vulnerability and adaptation of the study area. The research team agreed to maintain the anonymity of the interviewees. The assessments included wave inundation, beach erosion, impacts to benthic habitat, and impacts to the community. The framework of the evaluation is given in Figure 4.2. The framework starts with deciding on the climate stressor and gathering data that will be used in GIS-based vulnerability index calculations and NOAA assessment tool to obtain a vulnerability assessment. The biophysical parameters obtained from each shoreline segment are ranked for CVI calculations. This process provides vulnerability maps relative to the climate stressor. The climate stressors considered in this study are wind and wave exposure, surge potential and SLR. The coastal storm effects considered in this study are examined under wave and wind exposure and surge potential. On the other hand, classifying influential factors into the ecosystem and community will include societal norms as well as physical impacts in preparing the vulnerability assessment. The potential impacts will be decided on using the vulnerability assessment and maps, which will lead towards understanding the vulnerability of the region. Once the vulnerability is assessed, adaptation measures can be chosen.

3.2 Coastal Exposure of the Area

One of the most established and direct methods to assess coastal vulnerability is with the CVI, to generate an interactive vulnerability map. The model includes the contribution of each factor and climate stressor. The GIS-based model known as InVEST Coastal Vulnerability Model, (2016) defines exposure with ranked scores for geomorphology, relief (elevation), natural habitats, sea level change, wave exposure and potential surge categories using a system created by Gornitz (1990) and Thieler and Hammar-Klose (1999) to calculate exposure indices for each shoreline segment. (InVEST 2016) model requires nine GIS input layers including bathymetry (from Hawai'i Mapping Research Group, 2014), geomorphology (from NOAA Office of Response and Restoration 2001), land polygon (from Fletcher et al., 2002), SLR (from NOAA Tides and Currents, 2013; and Romine et al., 2013), natural habitats (from NOAA Office of Response and Restoration 2001) and continental shelf and climatic forcing (from Natural Capital Project, 2016). These layers create geomorphology, relief (elevation), sea level rise, wave and wind exposure, surge potential, and natural habitats input categories by ranking the percentile ranges stated in Sharp et al. (2016). The exposure index is calculated by taking the geometric mean of the categories in the ranking system (for detailed information on the procedure please see in Sharp et al. (2016).The overall vulnerability score ranges from 1 (very low) to 5 (very high), according to the severity of the risk for each 250 m shoreline segment. The relative coastal exposure index (EI) for each 250 m shoreline segment is calculated by Eq. (3.1) where R is the rank of the variable and n is the number of variables. The model reflects a general overview of the survey area and depends on the quality and the quantity of the available data. The procedure enables overlapping CVI variables to visualize overlaying spatial distributions, illustrating impacts of SLR. A more detailed CVI model is required to explain the complex interaction of island communities to the region. Nonetheless, being easily buildable allows the (InVEST 2016) model to be improved by multiple parties in the future while offering the integrated analysis that is crucial in the coastal vulnerability assessment.

3.3 Methods for Identifying and Assessing Adaptation Options

Although the coastal vulnerability index shows high vulnerability for the study area, the differences between residential uses and natural areas lead to different adaptation strategies. In residential areas, minimizing structural losses and preventing harm to residents in the Sunset Beach

community emerge as key goals and priorities for adaptation, whereas preventing harmful effects to the ecosystem and improving the benthic habitat in Pupukea-Waimea area are the most promising adaptation goals. As the costs of implementing adaptation options are high, comparisons of the benefits and costs of the adaptation methods are presented by the use of multi-criteria analysis. The adaptation options are analyzed in two parts: i) identifying the adaptation option in multi-criteria analysis and ii) assessing the most balanced adaptation option via cost-benefit analysis.

Multi-criteria analysis determines the adaptation option through whether the adaptation delivers action or builds adaptive capacity is also considered. Reducing damage to the assets and services and exploiting opportunities are considered as delivery of adaptation action. Creating information through research, monitoring the site, raising awareness, and supporting governance through new legislation and regulation is evidence of increased adaptive capacity. Adaptation options are assessed in terms of implementation mechanisms, application party, resources required, and level of effort, acceptance, and urgency. The primary instrument for application, the condition of the device, the primary entity responsible for implementation, ownership of the assets, existing and additional need for technical and funding resources for the implementation, time period and ease of implementation, the social resistance to the method and political support behind it and robustness to the future scenarios are all considered for choosing the possible adaptation options. This evaluation framework for the multi-criteria adaptation options is given in Table 4.1, which can be applied to all the possible adaptation option candidates to choose suitable adaptation options.

Potential migration or adaptation actions defined in the multi-criteria analysis are assessed regarding costs, benefits, equity, efficiency, urgency and implementability (Smit et al., 1999). The Eastern Research Group (2013) demonstrates how adaptation options can improve social and natural environments exposed to SLR by use of simple benefit-cost analysis. The multi-criteria consideration is also included in cost-benefit analysis as it includes social, technical, administrative, political, economic and environmental aspects while defining benefits and costs affecting vulnerabilities created by SLR and high wave events. These six aspects are clarified by expending via questions to allow user to rank the adaptation options easily. The costs and benefits include: monetary (operating and investment costs), personnel (training, knowledge, morale, employee retention, health and safety, absenteeism), production (re-tooling, efficiency, inventory, equipment, input costs), environmental (toxic emissions, waste management fees, legal liability, fines), and

product (durability, energy requirements, serviceability, user operating expenses). In the cost-benefit analysis (Table 4.4 and 4.5), the benefits and costs are ranked from 1 to 5, with 1 as low and 5 as high. While considering the benefits of an adaptation option within the related aspect, the option that may provide the most favorable benefit or advantage to the region compared to its alternatives is ranked the highest (5), whereas the least favorable is ranked lowest (1). While the user cannot use the same ranking score in the same row for the same aspect, benefits and costs of the option may take same ranking scores. Oppositely, while ranking aspects in cost, the option that creates the least possible monetary and effort expenditures are considered the most favorable to the region and is ranked with the lowest score (1), whereas the most expensive/least favorable is ranked highest (5).

The resulting benefit to cost ratios are used to determine which options provide optimal solutions. The multi-criteria categories are not weighted according to their importance. As such, the cost-benefit analysis provides a starting point that can be regularly updated with additional information. Adaptation actions with a benefit-cost ratio greater than 1 are examined more closely and then prioritized.

4. Results and Discussion

4.1 Vulnerability Assessment for Waimea to Rocky, Point, Oʻahu

4.1.1 Inundation

Increased SLR produces inundation of low-lying coastal areas causing property losses, especially in dense residential areas. The U.S. Global Research Program estimates $23 to $170 billion in property damage due to a 0.5 m increase in sea level which demonstrates the need for determining inundation vulnerabilities at specific locations (Karl et al., 2009). In addition to being in a high wave environment, rivers, larger tide ranges, and high storm frequencies contribute to inundation of the area.

Rivers in the region increase the risk of inundation. Waimea River Valley is especially prone to flash floods and historically has had significant stream flooding. This is due to the high number of stream mouths in the area, which increases inundation risk by high waves, SLR and storm surge.

Another contributor to inundation is tidal fluctuations. Firing and Merrifield (2004) identify drainage problems due to high tides, which intensify storm runoff, especially with SLR. High tides can also raise the elevation of the water table up by 0.5 m depending on seepage, sand permeability and beach slope (Nielsen, 1990). The mean higher high water and mean lower low water level of Hawai'i range between 0.58 and 1 m (Dail et al., 2000). Although the tidal range is small, high tides combined with a high wave and storm event may raise the water table, contributing to flooding in residential areas.

By far, the greatest contributor to coastal flooding is from storm surge. During hurricane season, from June to November, the North Shore is already at high risk of coastal flooding. Fletcher et al., (2011) analyze storms that originate from lower latitudes that generate large swells during the winter months for 1 to 1.5 weeks (with 5 to 7 m wave heights), 2 to 3 weeks (with 7 to9 m wave heights) and one month (with wave heights of 9 m or greater). As SLR increases, wave heights increase as the depth increases due to lessened bottom dissipation effect. During 1957-1995, total hurricane losses surpassed $2.7 billion. Hurricane Iniki, the strongest hurricane to Hawaii, resulted in seven deaths, 2 billion dollars in damage, and $295 million in FEMA disaster relief in 1992 (Ruth et al., 2007). According to (FEMA, 2011), a 3 m increase in SLR will result in an 18% loss of beach, while a 4.5 m increase will result in a 25% loss from current levels due to conditions such as storm surge, wave run-up, and tides. SLR increases wave effects and inundation, resulting in greater damages and property losses.

4.1.2 Beach Erosion

Waves, currents, sedimentation, abrasion, cementation of beach rock and storms are the main mechanisms that contribute to the sand loss in deep water in the Hawaiian Islands (Moberly, 1968). At the near shore, Fletcher et al., (2012) found that aggressive wave conditions, coastal geomorphology, sediment characteristics, seasonal coastal line drift and human activities are the main factors contributing to erosion. Although it is difficult to isolate the contribution of individual factors to erosion including SLR (Romine et al., 2013), many studies have helped to increase understanding of sediment transport in the area.

The shallow slope of beaches on the North Shore tends to become deeper quickly due to the formation of the islands. Sand deposits are highly porous (Stearns and Vaksvik, 1935) and change

the water table, making these areas more vulnerable to beach erosion and saltwater and brackish water intrusion. Reefs in the Pupukea area also affect sediment production (Anderson et al., 2015). Sandy beaches also protect against wave action and intrusion.

Studies by Fletcher et al. (2011) and Romine et al. (2013) show that long-term erosion has resulted in the loss of 60% of Oahu's with greater losses of 73% in the North Shore. Romine et al., (2013) and Romine and Fletcher (2012) find, moreover that Oahu's overall average shoreline change rate of −0.03 ± 0.03 m/yr (median rate = −0.03 m/yr) is slower than the North Shore's -0.09 ± 0.06 m/yr (—0.11 ± 0.01 m/y long term; -0.07 ± 0.01 m/y short-term) rate. Fletcher et al., (2011) also find that due to seasonal variability, the maximum long-term accretion rate is 0.8 ± 0.8 m/yr at Rocky Point in the Sunset sub-region, and it is -0.8 ± 0.4 m/yr at Waimea. Fletcher et al., (2012) also point out the Sunset Beach Park shoreline is receding at a rate of 0.3m/yr while Sunset Point is retreating 0.15 m/year. These rates of erosion threaten coastal houses and roadways including Kamehameha highway, which could be flooded within 30 years (Fletcher et al., 2010). The rocky cliff at Waimea protects the bay from longshore transport (Moberly and Chamberlain, 1964) and making the risk in the area moderately low, whereas, for the rest of the shoreline, the risk is moderately high to high (C H Fletcher et al., 2002). Anderson et al. (2015) produced probabilistic estimates of coastal erosion due to SLR and found that in 2050 and 2100, estimated erosion rates are 2 and 2.5 times, respectively, higher than historical extrapolation. In addition to the potential loss of infrastructure and homes, erosion threatens culturally significant resources including iwi kupuna (burials), historical artifacts and ancient home sites (Kane et al., 2012).

4.1.3 Benthic Habitat

Fluctuations in water depth, wave actions, sedimentation, and water temperature due to climate change can affect the quality and quantity of coral cover. The response of the natural benthos in the intertidal or eulittoral zone, which extends from the shoreline downward along the surface of the continental shelf out to sea, requires further examination. SLR is likely to steepen beach slopes, increasing sedimentation and wave effects (Yamanaka et al., 2013), which may lead to a decline in aquatic populations due to interference with their life cycles. According to Brown et al. (2004), SLR can also contribute to increased turbidity on fringing reefs due to the accumulation of finer grain

sized particles and increased sedimentation. It also has been noted that wave energy is one of the primary factors affecting benthic communities in Hawai'i (Dollar, 1982; Grigg, 1983).

The Pupukea-Waimea region, which was designated as a MLCD by the DLNR (Department of Land and Natural Resources, State of Hawaii) in 1983 to protect the benthic and pelagic species, needs to be monitored to record the effects of SLR. The coral cover facing the north side is poorly developed and consists mostly of wave resistant species which have adapted over time to large swells. The Coral Reef Assessment and Monitoring Program (CRAMP) established in 1997, over a three year period, found decreases in coral cover at 4 m depths but increases in cover at 8 m. These changes could be the result of anthropogenic stressors. Jokiel et al. (2004) have suggested that constant human interference over the past 30 years is the primary reason for degradation. The decline could also be due to high wave energy damaging or interfering with the accretion of coral. SLR might not be the direct cause of coral reduction, but other processes coupled with SLR could have contributed to the decline.

4.1.4 Impacts on Communities

4.1.4.1 Impact on Homeowners/Residents

Clark (2005) reports that the land from Sunset Point to Pupukea Beach Park was subdivided in the 1920's. The community has existed and grown for almost a hundred years complicating growth, development, planning, and management of change. Some residents have lived there since they were born, while others have lived there since the 60's. Other residents have moved into the community more recently. The area has long been famous for beaches, waves, surfing, and other recreational activities. The value of homes has grown from five to ten thousand dollars in the 1960's to millions today. The diversity of the community including long-term residents, recent arrivals, resident homeowners, outside investors, absentee landlords, renters, and other stakeholders , including beach users complicates planning and implementation of adaptation strategies including elevating or relocating homes.

The principal land use is residential with 200 homes in Sunset Beach and 66 in Rocky Point. The interviewees in this study have been broken up into three categories: 1) long-term residents (residents that have resided in the area for over 10 years); 2) recent residents (residents that have

resided less than 10 years in the area); and 3) investors (owners who visit seasonally and/or rent out their property as vacation homes).

Based on interviews (Anonymous. 2015. Interview with residents by authors. Feb 27) held with the residents, the perception is that erosion from sea level rise, although the impact varies every year, is getting worse. Those interviewed observed erosion occurring largely during winter months when strong Northwest winds cause high swells that wash away much of the sand from the beaches. Long-term residents stated that they also observed minor erosion threats -- such as foundation cracks, cracks in the home, or flooding – occur one to two times a year, while major threats -- loss of land, homes being pushed off a foundation, or homes being pulled into the water -- occur approximately once every decade.

4.1.4.2 Impact on Beach Users

The area from Sunset Beach to Rocky Point attracts local residents and out-of-town visitors every day. Data were gathered by asking beach users to answer a series of questions (Anonymous, 23 Feb. 2015 with beachgoers by authors. Feb 23) about how SLR was affecting beach use and what they thought of proposed adaptation options. Based on interviews with beach users, it was difficult to find those who had in-depth knowledge of SLR and its annual and long-term effects, except for those few who were in a related industry or had an interest in the topic. Many of the people interviewed only visited the area between a few times a month to a few times a year, so their opinions were based on limited experience or guesses. Local groups and beachgoers agreed on seasonal beach movement due to high waves and currents and steadily declining sand supply over the entire area. They concluded that high waves reduce public access and the available space for beach users.

4.1.4.3 Impact on State and Local Government

In addition to residents, investors and the public, state and local government are also relevant stakeholders, since they regulate land use and construction in the coastal zone and approve permits needed by property owners as well as others involved in coastal protection, elevation of structures, relocation, and other adaptation strategies. For the region between Sunset Beach Park and Rocky Point, there are eight agencies involved in planning and permitting of coastal activities including

DLNR-OCCL; DPR; DOT; DPP; Department of Health (DOH); U.S. Army Corps of Engineers (USACE); CZM; and Sea Grant College Program. Each agency was aware of concerns of the residents about the effects of SLR in the area. A common point that all the interviews conducted (Anonymous, 25-26-27 Feb. 2015 Interview with residents and agency representatives by authors.) focused on the "soft" solutions implemented in the past such as beach and dune restoration over shoreline armoring. The different agencies have tried to initiate various plans, but not all have worked out in the long run. Anonymous, 25-26-27 Feb. 2015 (Interview with agencies by authors) also emphasized that one of the major difficulties that prevent the implementation of initiatives is that many of the agencies have overlapping jurisdictions, which require cooperation and coordination, as well as shared financial responsibilities.

4.2 Coastal Exposure of the area and contributing factors

The coastal stressors (wave exposure, surge potential, and mean sea level change) in the high wave energy area of Pupukea-Waimea and Sunset Beach are shown in Figures 3 and 4. The 7 km coast of Waimea to Rocky point consists of 43% moderately vulnerable and 57% high vulnerable zones.

The Sunset Beach coast (Figure 4.3) is most highly susceptible and under similar threats of SLR, wave and surge exposure. The overall exposure score varies from 2.88 (moderate exposure) to 3.92 (high exposure). The area is characterized by low-lying beaches fronting residential development. Coral reefs reduce exposure effects by a factor of 0.65.

The Pupukea-Waimea area (Figure 4.4) has a more varied coastline, consisting of bays and headlands. The area is more likely to be affected by SLR and storm surge rather than wave exposure due to the sheltering provided by its geomorphology. Overall exposure ranges between 2.47 (low-moderate exposure) to 3.36 (high exposure). This area has less residential development compared to Sunset Beach, with more land at higher elevations. Natural habitats such as reefs protect the shoreline except for Waimea Bay. Pupukea-Waimea area also has the densest reef formations complicating the effects of SLR. Coral reefs reduce exposure effects, which range between of 0.46- to 0.62.

The results indicate that the geomorphology and the natural habitat change the exposure of the coastlines to the SLR in high wave environments. Sand and cobble beaches, delta areas, estuaries are common geomorphologic features in Hawai'i that increase the vulnerability of the region due to being more prone to inundation and erosion than rocky cliffs. Coral and fringing reefs and coastal forests reduce the energy of high-wave environments. Highly vulnerable environments are also affected by elevation and the existence of residential developments. Additional work on vulnerability assessment was conducted to minimize adverse impacts on exposure to protect shorelines.

The high energy swells in the northern Pacific are generally due to extratropical cyclones during the winter season. Conserving their energy while traveling long distances, strong swells increase the susceptibility of coastal zones of remote islands by increasing their vulnerability. The approach here is to quantify how extratropical storm generated swells affect the vulnerability of remotely located tropical islands. The atmospheric conditions needed to create strong swells that can reach the remote island of O'ahu, Hawaii are analyzed and the swells formed by these cyclone conditions in the Northern Hemisphere from 2008-2016 hindcasted. The model integrates NP swells and compares the scenarios without climatic forcing to emphasize the effect of swells in vulnerability modeling. ANOVA and Tukey-Kramer between the scenarios quantify the significance of swell exposure. The InVEST model is used to calculate four exposure index scenarios: i) multi-modal state wave climate (multi-EI); ii) swell as wave climate (swell-EI); iii) wind-waves as wave climate (windWave-EI). The other factors—geomorphology, relief (elevation), sea level rise, natural habitats, population, and structures—remain the same for all EIs. The average top 10% of wave height and period, wave power, and proportion of wave power around the islands are given at every 0.05 arc degree grid space in 16 equiangular sectors.

Swells affect 18.96% of the all shorelines of O'ahu. The 21.91% of the northwest, north and northeast shores are predominantly exposed to EX-storm generated swells (from Waianae to Waimanalo on the north side). The mean wave exposure index values are very high for swells (4.99) and moderate (3.01) for wind waves. The two sample t-test results of only swell and only wind wave exposure of north side of O'ahu showed that the two wave exposures' effects are significantly different on general coastal exposure.

The equal group means are compared using the ANOVA test on exposure indices of all scenarios (Table 4.3). The results show the group means are significantly different and that the swell exposure on coastal vulnerability is higher.

4.3 Cost-benefit Analysis

To select the most suitable adaptation strategy for a high wave environment in the Sunset and Waimea-Pupukea region, we used multi-criteria analysis coupled with cost-benefit analysis. The multi-criteria evaluation of adaptation options is given in Table 4.1. Artificial reefs, vegetative cover, beach nourishment, shore protection and elevation of homes were identified as the best adaptation options for Sunset Beach while breakwaters, groins and artificial reefs selected for the Pupukea-Waimea region. The simple cost-benefit analyses for Sunset Beach and for Pupukea-Waimea are given in Table 4.4 and Table 4.5, respectively. The numerical ranking in the tables refers to high (5), medium (3) and low (1) to describe action's total benefits (B) and costs (C). The weights among the social, technical, administrative, political, economic and environmental aspects are considered the same.

The ranking of the costs and benefits (Eastern Research Group, 2013) are done according to multi-criteria evaluation results, and interviews with government officials and citizens. Each ranking score can be used once in a row for benefits and costs. For example, vegetative cover has the highest support from the majority of the community, so it was ranked 5 for the question "will the citizens be behind this effort?" based on completed interviews. The rank went down with beach nourishment, shore protection structures, and artificial reefs. Elevation of homes is ranked the lowest. On the other hand, when the same question is considered under the cost column, the question can be interpreted as "will the citizens be behind having the monetary actions of this effort?". The highest monetary cost is ranked highest for elevated homes since the public is not in favor of this method (5 is considered the high cost/least favorable), whereas vegetative cover costs less and receives public support when needed, therefore it is ranked as 1. Another example of ranking can be given for "Can the action be implemented from a technical point of view?" in a technical perspective. Periodic application of beach nourishment and previous implementation of artificial reefs in different regions of Hawai'i satisfies the high expertise needed from a technical point of view, which makes ranking highest for benefits. Whereas, the elevation of homes are not organized by government agencies and

have not had much application on the island, which creates the least expertise in dealing with implementation and high-cost ranking.

Table 4.4 shows that the community supports vegetative cover over the construction of seawalls or hard structures on the coastline. Conserving nature is a priority for the North Shore community. Hence, choosing an adaptation method cannot be only considered with protective needs. From a technical point of view, the implementation of artificial reefs is ranked highest for B/C compared to the other adaptation options. The reason why artificial reefs are ranked highest for B/C is that they can dampen waves as waves propagate along the reef and create a benthic habitat environment which sustains wildlife. From an administrative and political perspective, beach nourishment has a higher rank because it is a common practice implemented in Hawaii. Although beach nourishment maintenance is high and does not offer the same protection as hardening, elevating, or relocating, Hawaii's main economy depends on tourism so maintaining pristine beaches is key to attracting a thriving tourism industry for Hawaii. Another reason beach nourishment has a higher rank is due to erosion and scour that undermine foundations causing structures or posts to fail. In terms of economics, with its natural habitat and funding options (how much, who pays and maintenance issues) , vegetative cover is very efficient to implement in the region. On the other hand, artificial reefs are important for building resilience to natural habitat and creating a new coral environment, which would be especially beneficial to a conservation area like Pupukea-Waimea. However in a popular surf area, like Sunset Beach, artificial reefs do not have support from the surf community since they dampen wave action and affect the sand budget. Based on this analysis, it was determined that vegetative cover brings the greatest benefits to Sunset Beach.

Considering that the Pupukea-Waimea area is not a surf spot and has a MLCD, the community is more supportive of artificial reefs, see Table 4.5. As its implementation will cost less and the agencies have experience with implementing them, artificial reefs are more favorable from a technical, administrative and economic perspective. Artificial reefs are a better alternative for the Pupukea-Waimea region.

There are uncertainties associated with future climate scenarios and impacts associated with coastal flooding (Wang et al., 2015b) as well as public support for different interventions (Wang et al., 2015a). If an adaptation option provides a high benefit-to-cost ratio, severe future SLR scenarios

are likely to generate more substantial net adaptation benefits in the long term (Wang et al., 2015a). Conservative interpretation of uniformly applied multi-criteria across all locations supports the selection of adaptions with lasting benefits (Wang et al., 2015a).

4.4 Multi-Criteria Evaluation of Adaptation Options

Understanding of ecological, social, political and economic constraints enhance the adaptive capacity of the ecosystems and communities to react to climate impacts. Maintenance, expertise, data availability, funding, technological developments, existing infrastructure, and politics are influential factors affecting adaptation at the local level (Handmer et al., 1999; Kelly and Adger, 2000; Smit and Pilifosova, 2003). Adger et al., (2005) success of the adaptation depends on how definite the adjustment option overcomes the uncertainty of the future event. This flexibility of the implementation and coping mechanism for future scenarios is the primary concern for suggesting adaptation choices.

This study includes observations, analysis and *a priori* reasoning with the given data to create adjustment options. It undertakes certain assumptions in modeling and ranking of the advantages and disadvantages of each adaptation option to cope with the SLR of the region. The approach taken, which includes the contexts of socioeconomic, cultural and legislation (Mangubhai et al., 2015), supports future planning and implementation of coastal zoning and land use controls. The methods can be improved with additional participation and further interviews to refine both assessments of physical and social conditions as well as support (or opposition) to various adaptation strategies.

Vulnerability assessment indicated that beach erosion at Sunset Beach and protection of the benthic habitat in Pupukea-Waimea are major problems to be considered. As described in Table 4.1, we investigated artificial reefs, vegetative cover, soft shore protection (i.e., beach nourishment), hardened shore protection, and the elevation of homes for Sunset Beach and artificial reefs and hardened shore protection structures for Pupukea-Waimea region, respectively.

The proposed adaptation options build adaptive capacity by raising awareness with media coverage and sharing information through research, data collection, and monitoring. Hardened structures and the elevation of homes can reduce damage to assets, but may lead to beach/dune loss.

The application procedures for all options include setting up regulations, legislation, planning processes, and programs through existing agencies. The permit process can be affected by many organizations, as well as the regulations to revert the coastline to the natural state, which causes an exploitation of most shoreline protection options. Except for the elevation of buildings, state and local government and private contractors play an active role in the implementation of adaptation options. The state has much experience in implementing artificial reefs, beach nourishment, and shore-hardening structures. Elevation of houses and the use of vegetative cover have not been actively pursued. Elevation of structures creates problems in communities where coastal views are valued, and the introduction of new vegetation may cause problems with the determination of private property lines, shorelines, and public beaches. Solutions such as beach nourishment require continued maintenance and ongoing sources of funding. While the first implementation requires research and technical expertise, vegetative cover, artificial reefs, and shore-hardening structures typically are implemented as one-time or long-term efforts. The increased biomass and the diversity of benthic and pelagic species due to the implementation of artificial reefs and vegetative cover applications will raise public acceptance. Political support for vegetation and beach nourishment is strong because it is less expensive than shore-hardening structures, preserves the recreational beach and promotes Hawaii's natural environment. The results of the multi-criteria evaluation are then used to perform a cost-benefit analysis under different aspects (Table 4.4 and 4.5). The aspects provide a relative comparison of the proposed adaptation methods. Since the evaluation is based on the highest benefit to cost (B/C) ratio, the values assigned to benefit (B) and cost (C) were adjusted, as discussed in Section 4.3. The cost-benefit analysis results might be biased in assigning benefit and costs relative to each other, which can be reduced by the contribution of multiple experts from multi-disciplinary backgrounds.

Since the community needs are more pronounced in Sunset Beach, a variety of adaptation options, including soft and hard approaches, are considered. If there are more than five proposed adaptation options, the ranking range can be increased to reduce repetition of the same ranked numbers.

Vegetative cover with beach nourishment for Sunset Beach and artificial reefs for Pupukea-Waimea are optimal adaptation methods based the cost-benefit analysis. Vegetative cover is most favorable, considering the societal and political acceptance, easy administrative implementation, and

favorable economic and environmental impacts on Sunset Beach. The results show that evaluation of an adaptation method may not be favored in all categories, but an overall higher B/C ratio is considered for the adaptation option to be approved or ranked higher. Due to the complexity of ongoing impacts of climate stressors, SLR, a combination of top-ranked adaptation options can lead to long-term solutions. For instance, the combination of vegetative cover with beach nourishment may stabilize the beach erosion problems in Sunset Beach and provide a longer-term solution than just a simple vegetative cover application.

In Table 4.5 for Pupukea-Waimea, artificial reefs are considered most favorable in all aspects, except for political. However, this conclusion is not supported by any coastal modeling results, which may change the society or ecosystem perspective on it.

All options will need an environmental impact assessment triggered by proposed actions in the conservation district as well as by the expenditure of public resources unless on private property. Pre-permitting and construction surveys, permit processing fees, material purchasing/cleaning/preparation, transportation, liability insurance, compliance monitoring and maintenance, employees and personnel, operating expenses, data management and performance monitoring (Lindberg and Seaman, 2011) should be taken into account. Any delays to the implementation likely increase the already high costs due to research, management, and the cost of materials.

5. Conclusion

The study examines high-wave coasts and identifies contributing factors that worsen the effects of SLR on shorelines. Geomorphology and habitat conditions influence coastal vulnerabilities and should be incorporated into the design and implementation of appropriate adaptation strategies. A multi-criteria benefit-cost analysis is presented as a tool for comparing and evaluating different adaptation strategies. The approach is applied to two different coastal environments to better understand and account for varying coastal conditions, needs, requirements, and alternative adaptation strategies.

The vulnerability assessments are based on available data with somewhat uneven quality, accuracy, and timeliness contributing to uncertainties in the analysis. There is a need for additional

resources to better monitor the effectiveness of strategies as well as capturing benefits and costs and the return on investments over time. Such efforts also provide opportunities to raise public awareness and promote increased dialogue, deliberation and planning for adaptation to sea level rise. Comprehensive, quantitative research on SLR and the creation of local knowledge and information base will also help to foster stronger understanding and design of adaptation strategies.

The adaptation methods for high-wave energy environments are examined using multi-criteria evaluation combined with cost-benefit analysis. Community needs, in addition to the ecological conditions of the coast, determine requirements and approaches to adaptation. The combined approaches of beach nourishment and vegetative cover provide long and short-term protection to a developed shoreline like Sunset Beach where there are both residential and recreational uses. While vegetative cover has low maintenance and allows for relatively easy and inexpensive implementation, beach nourishment could also be implemented to lessen potential disruptions of access and use of beach areas due to coastal flooding.

In high-wave environments with healthy benthic habitats such as the Pupukea-Waimea area, the proposed optimal solution is the introduction of artificial reefs. This adaptation strategy has social and political support because of its ability to enhance environmental and aesthetic values of the MLCD, which in turn serves to benefit residents and the tourism industry. Implementation of artificial reefs may be the optimal solution considering technical knowledge, experience and ability to be deployed in a timely and cost-efficient manner. Multi-criteria evaluation combined with cost-benefit analysis supports the understanding and evaluation of suitable coastal adaptation options. Additional detailed coastal modeling and environmental assessment are needed to support this decision making, as well as design and construction of selected adaptation options.

Risk management and decision-making for property owners in these high-susceptible areas are affected by the potential loss of natural, social, and cultural assets threatened by SLR and high wave environments. This includes the loss of land, a subsidence way of life (due to the change in the benthic habitat), and recreational activities (public beach users) are affected.

Across the research community to decision makers, the most prevalent trend is the need for more data, and better methods and analyses. While location affects specific needs for data, the common needs that are shared with sea-level change were identified concerning data accessibility,

utility, interoperability, and reliability. This analysis supports a new understanding of the phenomena of SLR in high wave environments. Further data, methods and analyses improvement would include: covering broader specific geographic regions; applying more parameters; using higher resolution; proper scaling; validating results from in situ observations; stating assumptions and uncertainties; compatibility with other data being collected; readily accessible to the public; and provide an easy-to-use format.

Finally, it comes down to three choices: accommodate, protect or retreat. The two most supported by this analysis in these regions are to protect and accommodate. Beach nourishment protects, while vegetative cover protects from erosion and accommodates SLR. Both offer the living shoreline approach, which is highly sought after in this area. Artificial reefs protect by dampening wave action while offering new benthic habitat environments. These solutions needed to satisfy government official, homeowners, public users, while offering protection from SLR and high wave conditions in a highly non-cohesive sand environment yet keeping pristine beaches and the desire to promote living shorelines, presented challenges, but offered the best solution.

This study provides a framework to analyze the effects of SLR and adaptation strategies in a high-energy wave zone in Hawaii. Ecological, as well as social, political, and economic factors and conditions, are considered. While the research focuses on one particular area on Oahu, efforts will be undertaken to examine other parts of the state and other Pacific island communities to increase opportunities for comparative analysis. The limitations of the work comes from considering only one SLR sceanario (IPCC RCP 4.5 scenario), InVEST Coastal Vulnerability model limitations and using same weight rankings in the coastal EI and cost-benefit analysis. Further work is recommended to include the effects of saltwater intrusion on both vulnerability assessment and adaptation solutions.

Table 4. 1: Multi-criteria evaluation of adaptation options.

Climate Stressor: Sea level rise

Part 1 - Identifying Adaptation Options		Part 2 - Assessing Adaptation Options					
Adaptation option	Adaptation Type: Select either A and/or B	Implementation Mechanism	Implementation Agent	Resources Required	Level of Effort	Acceptance	Urgency
	A) Delivers adaptation action:	What is the primary instrument for implementation?	Who is the primary entity responsible?	What resources might be needed for implementation?	What is the level of effort required?	To what degree is the public likely to accept the adaptation option?	What is the appropriate timeline for implementation?
	* Reduces damage to assets * Reduces service or network disruptions * Exploits opportunities	* Regulations * Legislation * Incentives * Planning processes * Programs	* State government * Local government *Landowner *Private organization	* Staff time * Technical expertise * Funding	* Continuous * Periodic * One-time	* Poor * Fair * Good * Excellent	* Immediately * Short term * Long term
	B) Builds adaptive capacity	Are these instruments:	Is this different than who has ownership of assets?	Needs can be met with:	How easy is the option to implement?	To what degree is their political support the adaptation option?	If the implementation is delayed, will the cost likely be higher?
	*Creates information through research, data collecting & monitoring *Raises awareness through dissemination of information *Supports social structures through organizational development, working in partnership, strengthening institutions *Supports governance through regulations, legislation, & guidance	*New *Existing *Existing but modified	*Yes *No	*Existing resources *Additional resources needed	*Easy *Moderate *Difficult	*Poor *Fair *Good *Excellent	*Yes *No

Table 4. 2: Exposure index of only swell and wind wave scenarios, t-test results.

Sample	Mean	StDev	SE Mean	*t-value*	*p-value*
EI-swell	2.547	0.505	0.023	1.22	0.223
EI-windWave	2.511	0.405	0.018		

Table 4. 3: The ANOVA results of the three wave scenarios on exposure show the group means are statistically different.

Factor	N	Mean	StDev	95% CI	Model Summary
EI-swell	502	2.5467	0.5053	(2.5074, 2.5859)	F-value:2.58
EI-windWave	502	2.5114	0.4054	(2.4721, 2.5507)	p-value:0.076
multi-EI	502	2.5756	0.4290	(2.5363, 2.6149)	Pooled stDev: 0.448

Table 4. 4: Cost-Benefit analysis for Sunset Beach (B: Benefit, C: Cost, B/C: Benefit to Cost ratio, the ranking goes as 1 (lowest) to 5 (highest).

Cost-Benefit analysis for Sunset Beach		**Artificial Reef**			**Vegetative Cover**			**Beach Nourishment**			**Shore Protection**			**Elevated Homes**		
		B	C	B/C	B	C	B/C	B	C	B/C	B	C	B/C	B	C	B/C
Social	Will the citizens be behind this effort?	2	3	0.67	5	2	2.50	4	1	4.00	3	4	0.75	1	5	0.20
	Will the action lead to an increase in social resilience?	3	4	0.75	5	2	2.50	4	1	4.00	2	3	0.67	1	5	0.20
	Is the action equitable?	2	2	1.00	5	5	1.00	4	4	1.00	3	3	1.00	1	1	1.00
Technical	Can the action be implemented from a technical point of view?	4	2	2.00	3	3	1.00	5	1	5.00	2	4	0.50	1	5	0.20
	Can the action handle a range of climate change impacts?	4	1	4.00	3	2	1.50	2	4	0.50	5	3	1.67	1	5	0.20
Administrative	Does your agency/organization have the operational control to implement this action?	2	3	0.67	4	1	4.00	5	2	2.50	3	4	0.75	1	5	0.20
	Table 4.4 continues															

	Table 4.4 continues															
	Can this action be implemented in a timely manner?	3	3	1.00	5	1	5.00	4	2	2.00	2	4	0.50	1	5	0.20
Political	Does this action have political support?	1	3	0.33	4	2	2.00	5	1	5.00	2	4	0.50	3	5	0.60
Economic	Is it cost effective? Does the benefit exceed the cost?	3	2	1.50	5	1	5.00	4	3	1.33	2	4	0.50	1	5	0.20
	Does funding exist or can it be acquired to finance the action?	2	3	0.67	4	2	2.00	5	1	5.00	3	4	0.75	1	5	0.20
Environmental	Will the action increase the resilience of the natural environment?	4	1	4.00	5	2	2.50	2	4	0.50	3	3	1.00	1	5	0.20
	Are there any positive side effects on the environment of the action?	4	2	2.00	5	1	5.00	3	5	0.60	2	4	0.50	1	3	0.33
	Rank			3			**1**			2			4			5

Table 4. 5: Cost-benefit analysis for Pupukea-Waimea (B: Benefit, C: Cost, B/C: Benefit to Cost ratio, the ranking goes as 1 (lowest) to 5 (highest).

Cost-benefit analysis for Pupukea-Waimea		Breakwaters			Groins			Artificial Reef		
		B	C	B/C	B	C	B/C	B	C	B/C
Social	Will the citizens be behind this effort?	3	3	1.00	1	5	0.20	5	1	5.00
	Will the action lead to an increase in social resilience?	1	3	0.33	3	5	0.60	5	1	5.00
	Is the action equitable?	3	3	1.00	1	5	0.20	5	1	5.00
Technical	Can the action be implemented from a technical point of view?	1	1	1.00	3	5	0.60	5	3	1.67
	Can the action handle a range of climate change impacts?	3	3	1.00	1	5	0.20	5	1	5.00
Administrative	Does your agency/organization have the operational control to implement this action?	1	3	0.33	3	5	0.60	5	1	5.00
	Can this action be implemented in a timely manner?	1	3	0.33	3	5	0.60	5	1	5.00
Political	Does this action have political support?	3	1	3.00	1	5	0.20	5	3	1.67

Table 4.5 continues

Table 4.5 continues										
Economic	Is it cost effective? Does the benefit exceed the cost?	3	3	1.00	1	5	0.20	5	1	5.00
	Does funding exist or can it be acquired to finance the action?	3	3	1.00	1	5	0.20	5	1	5.00
Environmental	Will the action increase the resilience of the natural environment?	3	3	1.00	1	5	0.20	5	1	5.00
	Are there any positive side effects on the environment of the action?	3	3	1.00	1	5	0.20	5	1	5.00
	Rank			3			2			**1**

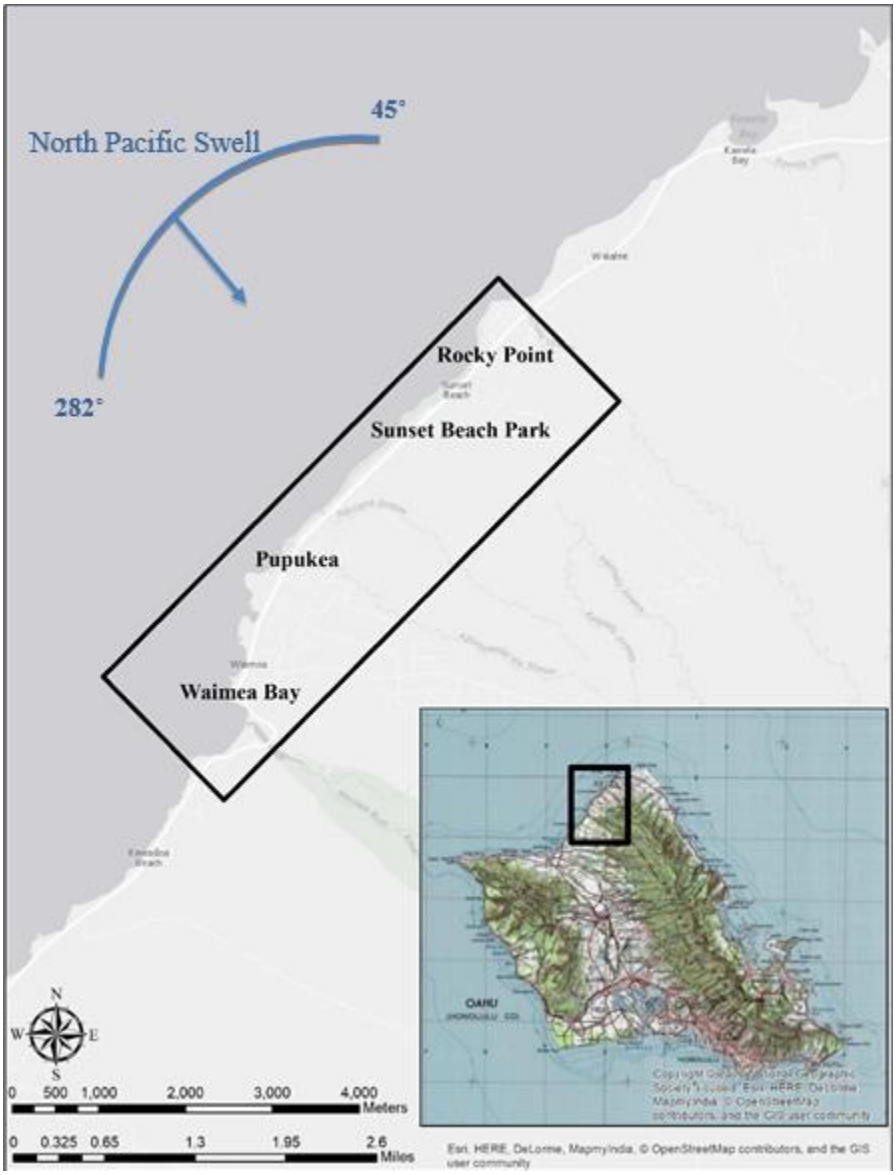

Figure 4. 1: High-wave energy environment, case study area. The black border contains the study area of the North Shore including Waimea Bay, Pupukea, Sunset Beach and Rocky Point. The blue arrow and arc represent the North Pacific swell directions between 282˚ to 45˚ (Moberly and Chamberlain, 1964; Vitousek and Fletcher, 2008).

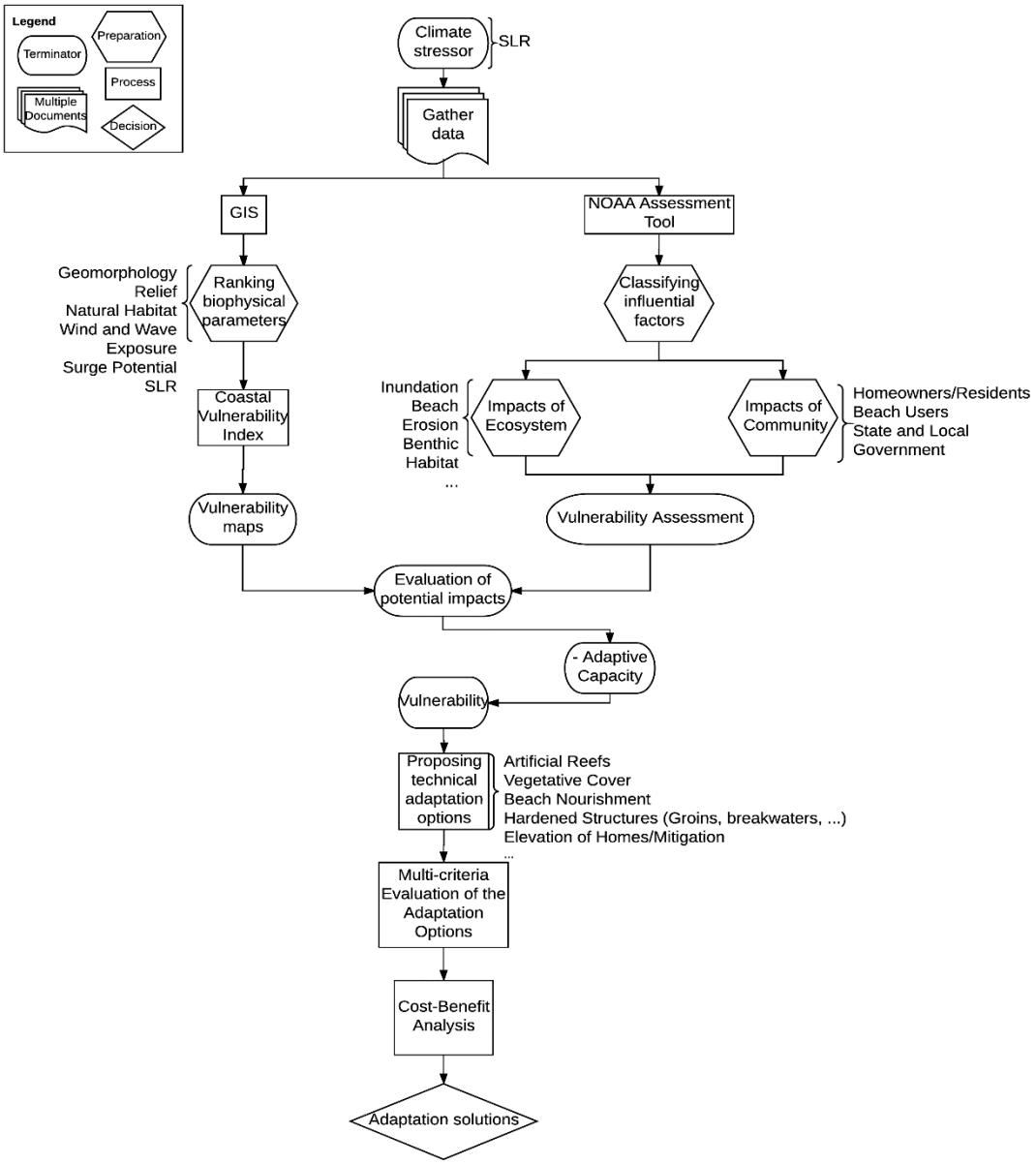

Figure 4. 2: Framework for understanding vulnerabilities and adaptation measures.

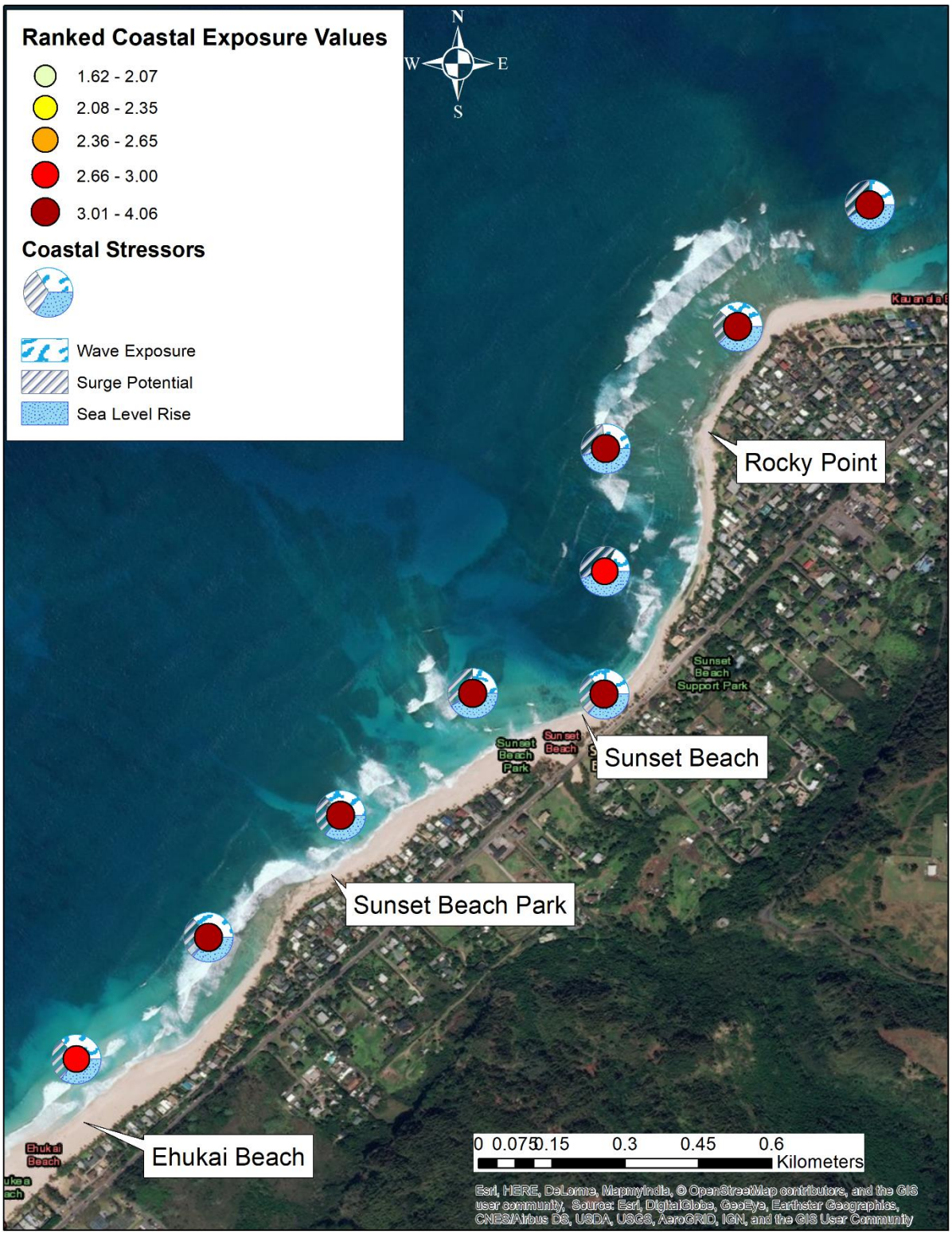

Figure 4. 3: Coastal exposure of Sunset Beach to coastal stressors, geomorphology, elevation, and natural habitat. The SLR and wave exposure impacts on the beach are higher than surge potential.

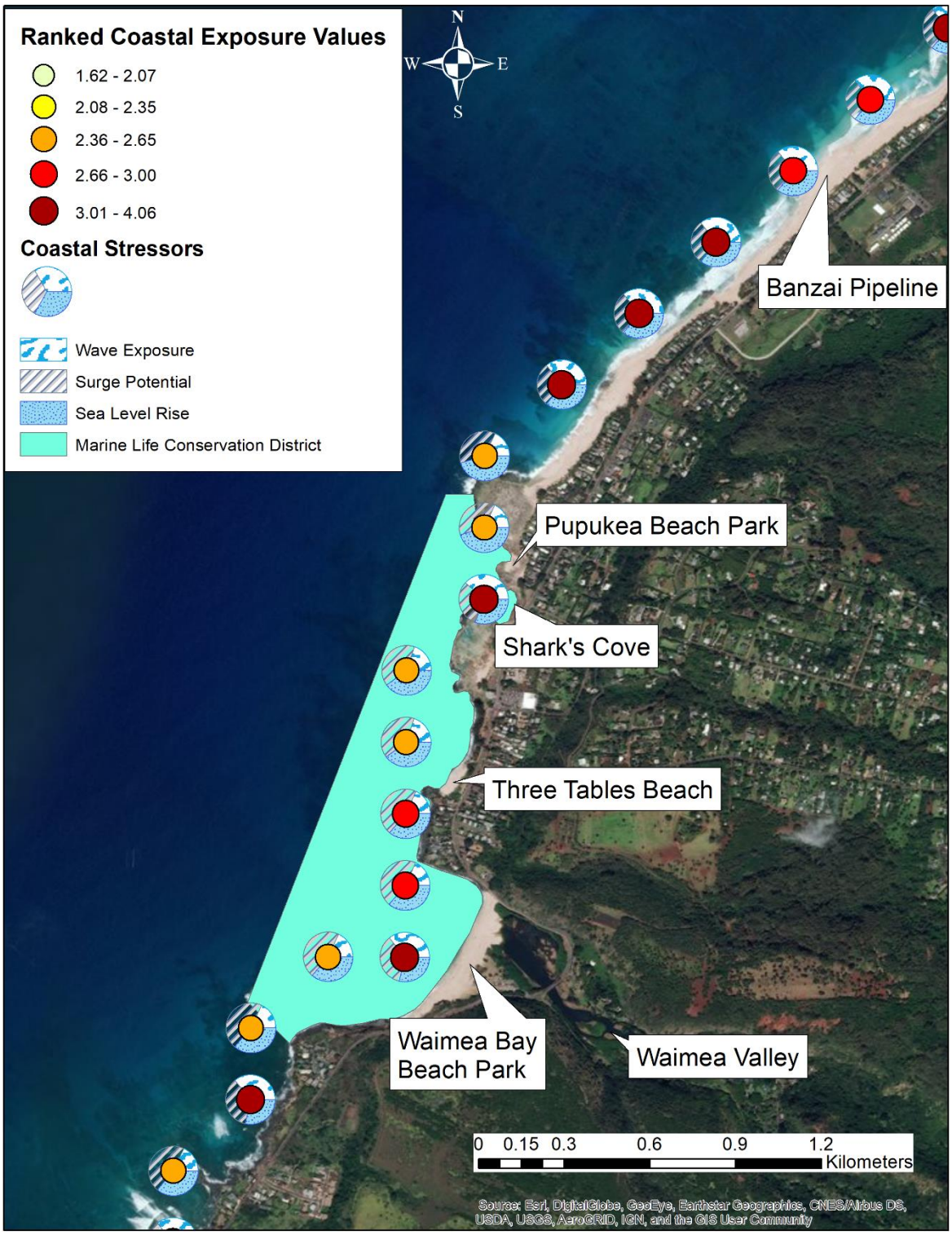

Figure 4. 4: Coastal exposure of Pupukea-Waimea based on coastal stressors, geomorphology, elevation, and natural habitat. While the surge potential is higher in the MLCD, SLR and wave exposure are dominant in the Pupukea area.

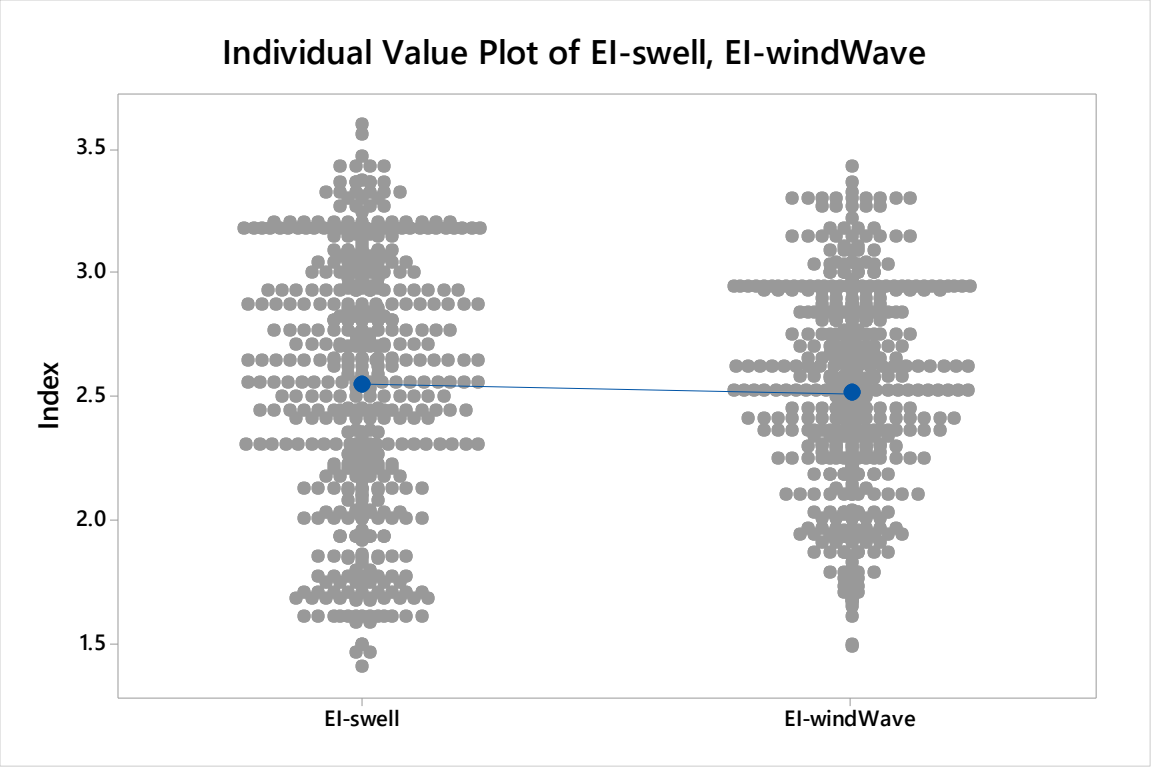

Figure 4. 5: The exposure index distribution on the north side of O'ahu. The two wave exposures have different effects on the overall exposure.

CHAPTER 5. Concluding Remarks

1. Summary

Defining the vulnerability of small islands like Hawai'i is crucial to reducing the risk potential for the exposure of coastal infrastructure. The Pacific islands are exposed to remote source generated swells, which reveals a need to define the effect of wave exposure generated by strong EX storms. The strong EX cyclones are identified using minimum MSLP, geopotential height, and maximum vorticity from CFSR reanalysis dataset between 2007–2017, and are modelled to hindcast associated swells. The study supports the hypothesis by finding the swell trends for the Hawaiian Islands by using wave modeling of strong EX cyclones throughout the decades and validating results with buoy measurements. The three research questions answered in the dissertation are as follows.

- What is the relation between strong EX cyclones and swell characteristics around the Hawaiian Islands?

There is a correlation between the strong EX cyclones generated in the NP and associated swells. The strong EX cyclone trends showed that increased cyclone activity increased the number of incoming swells. The MSLP and geopotential height values showed that there was a decrease in the trends, which become stronger during 2007–2017. The MSLP and geopotential height change over 2007–2017 are 3.34 hPa and 23.85 m, respectively. There is a northward 2.7° and westward 4.65° shift in the cyclone locations. The strong EX cyclones are located mostly around northeast Pacific and the Aleutian Islands. The analysis also showed that the high range of swells is mostly observed during December-January-February. ENSO events were also observed to have an effect on EX cyclones and associated swells. The location of the most dominant swells generated from the EX events are detected around the Kuril and Aleutian Islands. The maximum value of the significant wave height de-seasonalized trend of the swells shows a most of the maximum changes observed around 0.40–0.45 m except for the January and February, where the maximum trend difference reaches up to 0.65 m. Low trend differences for EX storms behind the north of the Hawaiian Islands indicates the sheltered zones from the north swell effects.

The swell characteristics in the northwest location of O'ahu (21.75° N 158.42° W) were obtained by taking a de-seasonalized average of the mean and maximum values. The mean trend

showed an average of 1.26 m significant wave height and 13.41 s peak period mostly coming from 320-330°. The average of the maximum values of significant wave height and peak period trends are 2.18 m and 17.68 s, respectively. During intense ENSO years, the swell characteristics reach an extremely high, significant wave height of 7 m and 17.1 s coming from 320° when the geopotential height drops up to 329.6 m.

- What is the trend of the strong EX-generated swells affecting the Hawaiian Islands?

The swell systems generated by strong EX cyclones represent 24.18% of the swells generated during the modeling period. The average series trend in the northwest point of O‘ahu showed a difference of increase of 0.36 m in significant wave height and 1.43 s during 2007–2017. The difference in the maximum value trend is 0.51 m significant wave height and 1.74 s of peak period over the record period. There is a significant increase in wave heights and periods during September, October, January, February, and March. The trend maps of the islands show slight trend difference in the sheltered areas. The maximum value of de-seasonalized trend maps of swells show more strong EX storms in October. The strong EX storm belt moves toward the equator during the winter, making the trend slope differences smaller as the swells travel shorter distances than in the fall for the peak period. The EX storm belt is closest to the Hawaiian Islands during February. The strong EX storm generated swells have higher wave height and peak period trends than the overall trend of the swells north shore of O‘ahu, implying that strong EX storms are moving northward and getting stronger.

- What is the impact of the swells generated by EX storms on the vulnerability of the Hawaiian Islands?

The vulnerability of the Hawaiian Islands is visualized using a GIS-based CVI method that assesses the relative influences of the biophysical variables of geomorphology, relief (coastal elevation), natural habitats, SLR, wind and wave exposure, and surge potential. The results showed the strong influence of geomorphology and wave exposure layers in determining the coastal vulnerability in Hawai‘i. The study found that 31.42% of the Hawaiian Islands’ shorelines are exposed to SLR, wave and surge potential. The vulnerability of the coasts facing the NP swells is high. The strong EX-generated swell exposure is found to influence the total exposure of the north shore of O‘ahu by 22%. The wave exposure index calculations showed a significant influence of 18% for swells on the northwest side of O‘ahu.

A generalized approach to define the vulnerability and possible adaptation measures in the high wave energy environments was developed using multi-criteria evaluation and cost-benefit analysis based on vulnerabilities, impacts, and protective actions. The case study of the North Shore region of O'ahu showed geomorphology and natural habitats dramatically affect coastal exposure in high-energy wave environments. The most viable adaptation strategies include expansion of artificial reefs in benthic habitat dominated areas, while the vegetative cover and beach nourishment are most appropriate in developed locations and surf tourism areas. Suitable adaptation strategies were determined based on differences in the biophysical environment and community perceptions.

This research reduces uncertainty on the effect of the strong EX storm trends and associated swell impacts on the Hawaiian Islands. The maps provided enable prioritization of vulnerable coastal systems and dominant factors affecting the susceptibility of the shores. The methods shown here are aim to be a guide to use on other tropical islands and reduce the vulnerability in local and regional scale due to high energy swells.

2. Future Recommendations

The limitations of the hindcast model can be improved by developing the attenuation rate of swell energy with frequency dispersion and angular spreading. The CVI model is limited because it does not include the dynamic interactions between elements that affect vulnerability and uses the same weight rankings in the coastal EI and cost-benefit analysis. However, the research provides an initial stage towards building a dynamically complex susceptibility map in a high energy swell environment.

Future research includes expanding the strong EX storm analysis region, estimating the probability of the associated swells, considering more elements in defining the vulnerability, and improving an automated logic statement for CVI calculations.

Appendices

Appendix A. Input Exposure Index Ranking

The input variables are ranked by a ranking matrix (Table A.1) developed from (Gornitz 1990; Thieler and Hammar-Klose 1999) to calculate the coastal exposure index (EI) for each shoreline segment.

Table A. 1: The ranking system for coastal exposure (Sharp et al. 2016).

Rank	**Very Low**	**Low**	**Moderate**	**High**	**Very High**
Variable	1	2	3	4	5
Geomorphology	Rocky; high cliffs; fjord; fiord, seawalls	Medium cliff; indented coast, bulkheads and small seawalls	Low cliff; glacial drift; alluvial plain, revetments, rip-rap walls	Cobble beach; estuary; lagoon; bluff	Barrier beach; sand beach; mud flat; delta
Relief	0 to 20 Percentile	21 to 40 Percentile	41 to 60 Percentile	61 to 80 Percentile	81 to 100 Percentile
Natural Habitats	Coral reef; mangrove; coastal forest	High dune; marsh	Low dune	Seagrass; kelp	No habitat
Sea Level Change	0 to 20 Percentile	21 to 40 Percentile	41 to 60 Percentile	61 to 80 Percentile	81 to 100 Percentile
Wave Exposure	0 to 20 Percentile	21 to 40 Percentile	41 to 60 Percentile	61 to 80 Percentile	81 to 100 Percentile
Surge Potential	0 to 20 Percentile	21 to 40 Percentile	41 to 60 Percentile	61 to 80 Percentile	81 to 100 Percentile
Population	0 to 20 Percentile	21 to 40 Percentile	41 to 60 Percentile	61 to 80 Percentile	81 to 100 Percentile

Appendix B. Wind and Wave Exposure Calculations

Sharp et al., 2016 chooses the maximum of the swell (E_w^0) or wind generated (E_w^1) relative wave exposure of shoreline segment. The wave exposure, E_w

$$E_w = \max(E_w^0, E_w^1), \quad \text{(B.1)}$$

The swell based wave exposure, $\mathbf{E_w^0}$, is calculated from

$$E_w^0 = \sum_{k=1}^{16} H[F_k] P_k^0 O_k^0 \quad \text{(B.2)}$$

$$E_w^1 = \sum_{k=1}^{16} P_k^1 O_k^1 \quad \text{(B.3)}$$

In Eq. B.2, $H[F_k]$ is the Heaviside step function for 16 equiangular wind sectors of **k** for fetch distances F_k. Since the fetch distance threshold for this research is chosen to be 60 km, $H[F_k] = 0$ for fetch distance, F_k, is smaller than 60 km and , $H[F_k] = 1$ for otherwise. In Eqs. B.2 and B.3, the highest 10% of the average wave power values, P_w, in the direction of **k** angular sector is weighted by the percentage of time, O_w. The power is calculated by,

$$P_k = 0.5\, H^2 T \quad \text{(B.4)}$$

where, H is observed wave height and T is wave period and unit is m^2s.

The wind exposure, E_{wind}, on the other hand is based on Keddy, 1982, includes the highest 10% average of the wind speed, U_n , percentage of the wind speed, P_n, and fetch distance, F_n, in the n^{th} equiangular sector (Eq. B.5)

$$E_{wind} = \sum_{n=1}^{16} U_n P_n F_n \quad \text{(B.5)}$$

The detailed information can be found in Sharp et al., 2016.

Appendix C. Probability Density Function of Distributions

Weibull Distribution

The Weibull probability density function with shape parameter, $\beta > 0$, and scale parameter, $\alpha > 0$,

$$f(t) = \alpha\beta x^{\beta-1} - e^{-\alpha x^{\beta}}, x \geq 0, \quad \text{(C.1)}$$

Elsewhere is zero for x random variable.

Generalized Extreme Value Distribution

The generalized extreme value distribution probability density function with shape parameter, $k \neq 0$, scale parameter, σ, and location parameter μ,

$$f(t) = \left(\frac{1}{\sigma}\right) \exp\left(-\left(1 + k\frac{x-\mu}{\sigma}\right)^{-\frac{1}{k}}\right)\left(1 + k\frac{x-\mu}{\sigma}\right)^{-1-\frac{1}{k}}, \quad \text{(C.2)}$$

For $1 + k\frac{x-\mu}{\sigma} > 0$

Extreme Value Distribution

The extreme value distribution probability density function with scale parameter, σ, and location parameter μ,

$$f(t) = \left(\frac{1}{\sigma}\right) \exp\left(\frac{x-\mu}{\sigma}\right) \exp\left(-\exp\frac{x-\mu}{\sigma}\right), \quad \text{(C.3)}$$

Generalized Pareto Distribution

The generalized Pareto distribution probability density function with shape parameter, $k \neq 0$, scale parameter, σ, and threshold parameter θ,

$$f(t) = \left(\frac{1}{\sigma}\right)\left(1 + k\frac{x-\theta}{\sigma}\right)^{-1-\frac{1}{k}} \quad \text{(C.4)}$$

For $\theta < x$, when $k > 0$, or for $\theta < x < \theta - {}^{\sigma}/_{k}$ when $k < 0$.

Gamma Distribution

The gamma probability density function with scale parameter, $\beta > 0$, and shape parameter, $\alpha > 0$,

$$f(t) = \frac{1}{\beta^{\alpha}\Gamma(\alpha)} x^{\alpha-1} e^{\frac{-x}{\beta}},\ x \geq 0 \qquad \text{(C.5)}$$

Where $\Gamma()$ is the gamma function.

Inverse Gaussian Distribution

The inverse Gaussian distribution probability density function with scale parameter, λ, and shape parameter μ,

$$f(t) = \sqrt{\frac{\lambda}{2\pi x^3}} \exp\left(\frac{-\lambda}{2\mu^2 x}(x-\mu)^2\right) \qquad \text{(C.6)}$$

Appendix D. Island Exposure Maps

These images demonstrate the input variable, erosion and exposure index distributions of the each Hawaiian Islands.

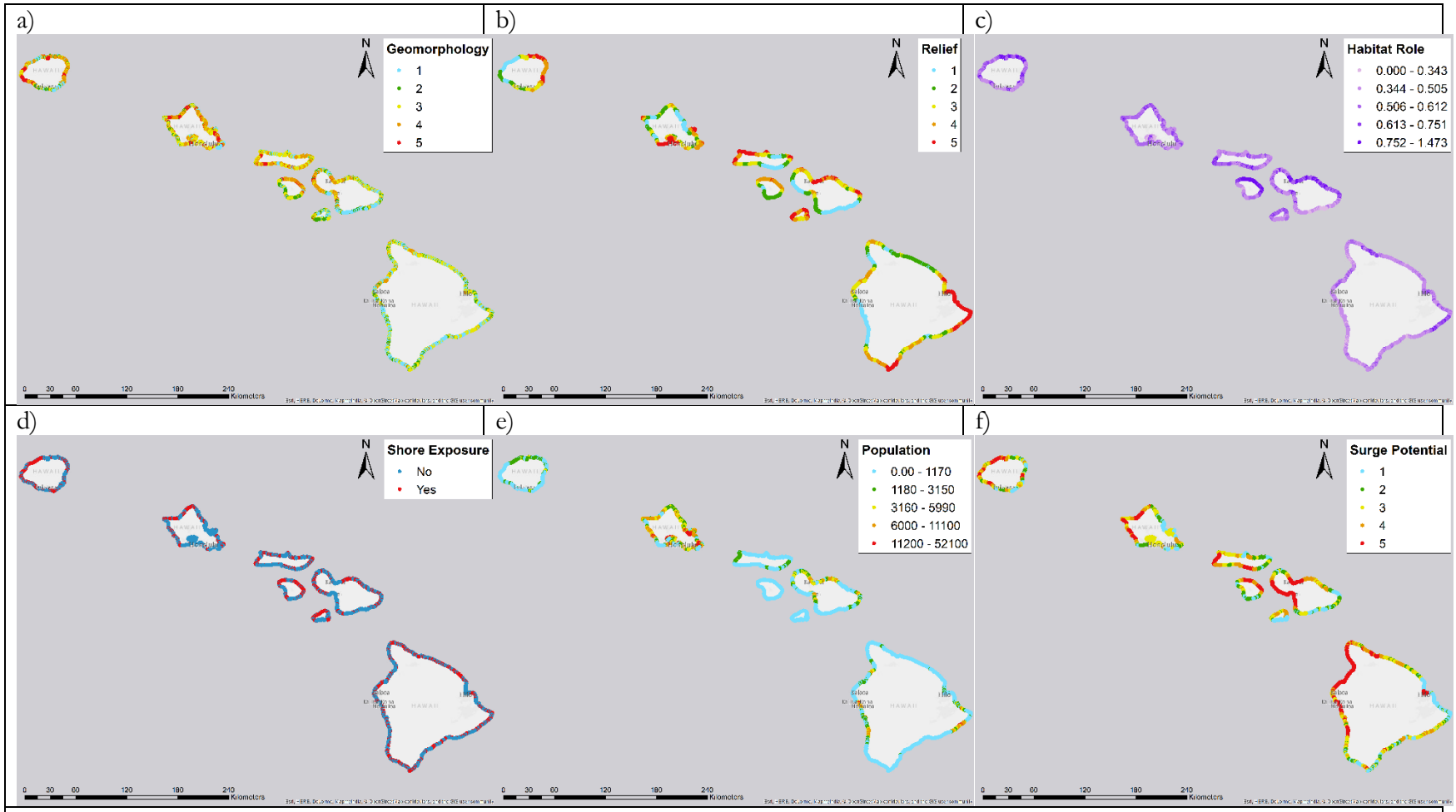

Figure A.1 continues

Figure A.1 continues

g)

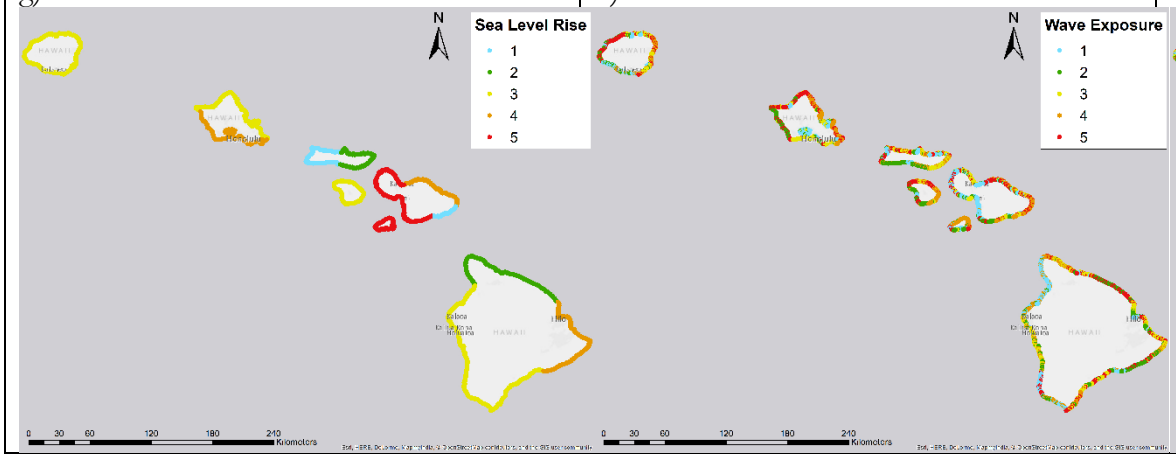

h)

i)

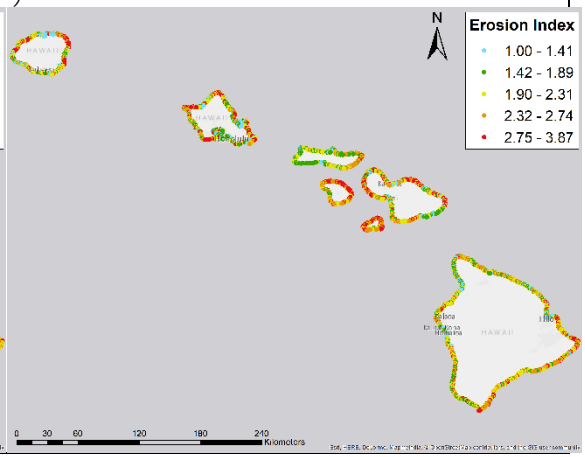

Figure A. 1: Input vulnerability metric distribution of the map of the islands (1: very low vulnerability–5: very high (extreme) vulnerability. Geomorphology (a), relief (b), natural habitat role (c), shore exposure (d), population (e), surge exposure (f), sea level rise (g), wave exposure (h), erosion index (i).

Bibliography

Aarnes, O.J., Abdalla, S., Bidlot, J.R., Breivik, Ø., 2015. Marine wind and wave height trends at different ERA-interim forecast ranges. J. Clim. 28, 819–837. doi:10.1175/JCLI-D-14-00470.1

Abuodha, P.A.O., Woodroffe, C.D., 2010. Assessing vulnerability to sea-level rise using a coastal sensitivity index: A case study from southeast Australia. J. Coast. Conserv. 14, 189–205. doi:10.1007/s11852-010-0097-0

Adger, N., Huq, S., Brown, K., Conway, D., Hulme, M., Adger, W.N., Huq, S., Brown, K., Conway, D., Hulme, M., 2003. Adaptation to climate change in the developing world. Prog. Dev. Stud. 3, 179–195. doi:10.1191/1464993403ps060oa

Adger, W.N., Arnell, N.W., Tompkins, E.L., 2005. Successful adaptation to climate change across scales. Glob. Environ. Chang. 15, 77–86. doi:10.1016/j.gloenvcha.2004.12.005

Allan, J., Komar, P., 2000. Are ocean wave heights increasing in the eastern North Pacific? Eos, Trans. Am. Geophys. Union 81, 561. doi:10.1029/EO081i047p00561-01

Alves, J.H.G.M., 2006. Numerical modeling of ocean swell contributions to the global wind-wave climate. Ocean Model. 11, 98–122. doi:10.1016/j.ocemod.2004.11.007

Amante, C., Eakins, B.W., 2009. ETOPO1 1 Arc-Minute Global Relief Model: Procedures, Data Sources and Analysis. [WWW Document]. NOAA Tech. Memo. NESDIS NGDC-24. Natl. Geophys. Data Center, NOAA. doi:10.7289/V5C8276M

Anderson, T.R., Fletcher, C.H., Barbee, M.M., Frazer, L.N., Romine, B.M., 2015. Doubling of coastal erosion under rising sea level by mid-century in Hawaii. Nat. Hazards 78, 75–103. doi:10.1007/s11069-015-1698-6

Ardhuin, F., Chapron, B., Collard, F., 2009. Observation of swell dissipation across oceans. Geophys. Res. Lett. 36, 1–5. doi:10.1029/2008GL037030

Ardhuin, F., Jenkins, A.D., 2006. On the Interaction of Surface Waves and Upper Ocean Turbulence. J. Phys. Ocean. 36, 551–557. doi:10.1175/JPO2862.1

Ardhuin, F., Rogers, E., Babanin, A. V., Filipot, J.-F., Magne, R., Roland, A., van der Westhuysen, A., Queffeulou, P., Lefevre, J.-M., Aouf, L., Collard, F., 2010. Semiempirical Dissipation Source Functions for Ocean Waves. Part I: Definition, Calibration, and Validation. J. Phys. Oceanogr. 40, 1917–1941. doi:10.1175/2010JPO4324.1

Arinaga, R.A., Cheung, K.F., 2012. Atlas of global wave energy from 10 years of reanalysis and hindcast data. Renew. Energy 39, 49–64. doi:10.1016/j.renene.2011.06.039

Arkema, K.K., Griffin, R., Maldonado, S., Silver, J., Suckale, J., Guerry, A.D., 2017. Linking social, ecological, and physical science to advance natural and nature-based protection for coastal communities. Ann. N. Y. Acad. Sci. 1399, 5–26. doi:10.1111/nyas.13322

Arkema, K.K., Guannel, G., Verutes, G., Wood, S.A., Guerry, A., Ruckelshaus, M., Kareiva, P., Lacayo, M., Silver, J.M., 2013a. Coastal habitats shield people and property from sea-level rise and storms. Nat. Clim. Chang. 3, 913–918. doi:10.1038/nclimate1944

Arkema, K.K., Guannel, G., Verutes, G., Wood, S.A., Guerry, A., Ruckelshaus, M., Kareiva, P., Lacayo, M., Silver, J.M., 2013b. Coastal habitats shield people and property from sea-level rise and storms- Supplementary Material. Nat. Clim. Chang. 3, 913–918. doi:10.1038/nclimate1944

Arkema, K.K., Verutes, G., Bernhardt, J.R., Clarke, C., Rosado, S., Canto, M., Wood, S.A., 2014. Assessing habitat risk from human activities to inform coastal and marine spatial planning : a demonstration in Belize. Environ. Res. Lett. 9, 11. doi:10.1088/1748-9326/9/11/114016

Aucan, J., 2006. Directional wave climatology for the Hawaiian Islands from Buoy Data and the influence of ENSO on extreme wave events from Model Hindcast: 9th International Workshop on Wave Hindcasting and Forecasting, v. Bochicchio.

Babanin, A. V., 2006. On a wave-induced turbulence and a wave-mixed upper ocean layer. Geophys. Res. Lett. 33, 1–6. doi:10.1029/2006GL027308

Baker, R.G.V., McGowan, S.A., 2015. Periodicities in mean sea-level fluctuations and climate change proxies: Lessons from the modelling for coastal management. Ocean Coast. Manag. 98, 187–201. doi:10.1016/j.ocecoaman.2014.05.027

Balica, S., 2012. Approaches of understanding developments of vulnerability indices for natural disasters. Environ. Eng. Manag. J. 11, 963–974.

Battjes, J.A., Janssen, J.P.F.M., 1978. Energy Loss and Set-Up Due to Breaking of Random Waves. Coast. Eng. 1978 569–587. doi:10.1061/9780872621909.034

Bengtsson, L., Hodges, K.I., Keenlyside, N., 2009. Will extratropical storms intensify in a warmer climate? J. Clim. 22, 2276–2301. doi:10.1175/2008JCLI2678.1

Bengtsson, L., Hodges, K.I., Roeckner, E., 2006. Storm tracks and climate change. J. Clim. 19, 3518–3543. doi:10.1175/JCLI3815.1

Berry, G., Jakob, C., Reeder, M., 2011. Recent global trends in atmospheric fronts. Geophys. Res. Lett. 38, 1–6. doi:10.1029/2011GL049481

Bi, F., Song, J., Wu, K., Xu, Y., 2015. Evaluation of the simulation capability of the Wavewatch III model for Pacific Ocean wave. Acta Oceanol. Sin. 34, 43–57. doi:10.1007/s13131-015-0737-1

Bijlsma, L., Ehler, C.N., Kulshrestha, S.M., Mclean, R.F., Mimura, N., Nicholls, R.J., Nurse, L.A., Stakhiv, E.Z., Turner, R.K., Warrick, R.A., 1995. Coastal Zones and Small Islands, Climate Change 1995: Impacts, Adaptations and Mitigation of Climate Change: Scientific-Technical Analyses. Cambridge University Press, Cambridge,UK.

Blender, R., Schubert, M., 2000. Cyclone Tracking in Different Spatial and Temporal Resolutions. Mon. Weather Rev. 128, 377. doi:10.1175/1520-0493(2000)128<0377:CTIDSA>2.0.CO;2

Bodge, K.R., Sullivan, S., 1999. Hawaii pilot beach restoration project: coastal engineering investigation. State of Hawaii Department of Land and Natural Resources, Honolulu, pp. 38–40.

Bolter, K., 2013. Communicating Sea Level Rise Risk with a Coastal Vulnerability Index, in: Association of Collegiate Schools of Architecture: Subtropical Cities: DESIGN INTERVENTIONS FOR CHANGING CLIMATES. Fort Lauderdale, FL.

Boruff, B., Emrich, C., Cutter, S., 2005. Erosion Hazard Vulnerability of US Coastal Counties. J.

Coast. Res. 215, 932–942. doi:10.2112/04-0172.1

Bowler, D.E., Buyung-Ali, L.M., Knight, T.M., Pullin, A.S., 2010. A systematic review of evidence for the added benefits to health of exposure to natural environments. BMC Public Health 10, 456. doi:10.1186/1471-2458-10-456

Brancome, L.E., Gutowski, W.J., 1992. The impact of doubled CO2 on the energetics and hydrologic processes of mid-lattitude transient eddies. Clim. Dyn. 8, 29–37.

Bromirski, P.D., Cayan, D.R., Flick, R.E., 2005. Wave spectral energy variability in the northeast Pacific. J. Geophys. Res. C Ocean. 110, 1–15. doi:10.1029/2004JC002398

Brown, E.K., Cox, E.F., Tissot, B., Jokiel, P.L., Rodgers, K.S., Smith, W.R., Coles, S.L., 2004. Development of benthic sampling methods for the Coral Reef Assessment and Monitoring Program (CRAMP) in Hawai'i. Pacific Sci. 7, 145–158.

Businger, S., Yildiz, S., Robinson, T.E., 2015. The Impact of Hurricane Force Wind Fields on the North Pacific Ocean Environment. Weather Forecast. 30, 742–753. doi:10.1175/WAF-D-14-00107.1

Cabral, P., Augusto, G., Akande, A., Costa, A., Amade, N., Niquisse, S., Atumane, A., Cuna, A., Kazemi, K., Mlucasse, R., Santha, R., 2017. Assessing Mozambique's exposure to coastal climate hazards and erosion. Int. J. Disaster Risk Reduct. 23, 45–52. doi:10.1016/j.ijdrr.2017.04.002

Caccamise, D.J., 2003. Sea and Land Level Changes in Hawai'i. University of Hawai'i at Manoa, HI.

Caires, S., Sterl., A., Bidlot, J.-R., Graham, N., Swail, V., 2004. Intercomparison of Different Wind – Wave Reanalyses. J. Clim. 17, 1893–1913. doi:10.1175/1520-0442(2004)017<1893:IODWR>2.0.CO;2

Caldwell, P., 2005. Validity of north shore, Oahu, Hawaiian Islands surf observations. J. Coast. Res. 216, 1127–1138. doi:10.2112/03-0092.1

Caldwell, P.C., Vitousek, S., Aucan, J.P., 2009. Frequency and Duration of Coinciding High Surf and

Tides along the North Shore of Oahu, Hawaii, 1981–2007. J. Coast. Res. 25(3), 734–743. doi:10.2112/08-1004.1

Carter, A.R.W.G., Orford, J.D., Lauderdale, F., Carter, R.W.G., 1993. The Morphodynamics of Coarse Clastic Beaches and Barriers : A Short- and Long-term Perspective. J. Coast. Res. Special Is, 158–179.

Chambers, D.P., Merrifield, M.A., Nerem, R.S., 2012. Is there a 60-year oscillation in global mean sea level? Geophys. Res. Lett. 39, 1–6. doi:10.1029/2012GL052885

Chang, E.K.M., Fu, Y., 2002. Interdecadal variations in Northern Hemisphere winter storm track intensity. J. Clim. 15, 642–658. doi:10.1175/1520-0442(2002)015<0642:IVINHW>2.0.CO;2

Chang, E.K.M., Lee, S., Swanson, K.L., 2002. Storm track dynamics. J. Clim. 15, 2163–2183. doi:10.1175/1520-0442(2002)015<02163:STD>2.0.CO;2

Chang, E.K.M., Yau, A.M.W., 2016. Northern Hemisphere winter storm track trends since 1959 derived from multiple reanalysis datasets. Clim. Dyn. 47, 1435–1454. doi:10.1007/s00382-015-2911-8

Chawla, A., Spindler, D.M., Tolman, H.L., 2013. Validation of a thirty year wave hindcast using the Climate Forecast System Reanalysis winds. Ocean Model. 70, 189–206. doi:10.1016/j.ocemod.2012.07.005

Chen, S., Sanfod, L.P., Koch, E.W., Shi, F., North, E.W., 2007. A Nearshore Model to Investigate the Effects of Seagrass Bed Geometry on Wave Attenuation and Suspended Sediment Transport. Coast. Estuar. Res. Fed. 30, 296–310.

Chen, S.J., Kuo, Y.H., 1994. Cyclones and northern hemispheric temperature. Theor. Appl. Climatol. 49, 85–89.

Christensen, J.H., Krishna, K.K., Aldrian, E., An, S.., Cavalcanti, I.F.A., de Castro, M., Dong, W., Goswami, P., Hall, A., Kanyanga, J.K., Kitoh, A., Kossin, J., Lau, N.C., Renwick, J., Stephenson, D.B., Xie, S.P., Zhou, T., 2013. Climate phenomena and their relevance for future regional climate change., in: Climate Change 2013: The Physical Science Basis. Working Group

I Contribution to the Fifth Assessment Report of the Intergovernmental Panel on Climate Change, Technical Report. Geneva, Switzerland.

Chu, J.-H., Sampson, C.R., Levine, A.S., Fukada, E., 2002. The Joint Typhoon Warning Center Tropical Cyclone Best-Tracks (JTWC), 1945-2000 [WWW Document]. U. S. Nav. Oceanogr. Portal. URL http://www.usno.navy.mil/NOOC/nmfc-ph/RSS/jtwc/best_tracks/wpindex.php (accessed 6.12.17).

Church, J.A., White, N.J., Coleman, R., Lambeck, K., Mitrovica, J.X., 2004. Estimates of the Regional Distribution of Sea Level Rise over the 1950–2000 Period. Am. Meteorol. Soc. 17, 2609–2625. doi:10.1175/1520-0442(2004)017<2609:EOTRDO>2.0.CO;2

Clark, J.R.K., 2005. Beaches of O'ahu. University of Hawaii Press, Honolulu.

Cocke, S., 2014. Hawaii's Eroding Coastline Puts Homeowners and Government at Odds [WWW Document]. URL http://www.huffingtonpost.com/2014/01/03/hawaii-eroding-coastline_n_4537537.html (accessed 8.16.16).

Cogswell, A., Greenan, B.J.W., Greyson, P., 2018. Evaluation of two common vulnerability index calculation methods. Ocean Coast. Manag. 160, 46–51. doi:10.1016/j.ocecoaman.2018.03.041

Collard, F., Ardhuin, F., Chapron, B., 2009. Monitoring and analysis of ocean swell fields from space: New methods for routine observations. J. Geophys. Res. Ocean. 114, 1–15. doi:10.1029/2008JC005215

Cooper, J.A.G., McLaughlin, S., 1998. Contemporary multidisciplinary approaches to coastal classification and environmental risk analysis. J. Coast. Res. 14, 512–524. doi:10.2112/JCOASTRES-D-12-00

Core Writing Team, Pachauri, R.K., Reisinger, A. (eds. ., 2007. IPCC AR4: Climate Change Synthesis Report. Contribution of Working Groups I, II and III to the Fourth Assessment Report of the Intergovernmental Panel on Climate Change. Geneva, Switzerland.

Costanza, R., Pérez-Maqueo, O., Martinez, M.L., Sutton, P., Anderson, S.J., Mulder, K., 2008. The Value of Coastal Wetlands for Hurricane Protection. AMBIO A J. Hum. Environ. 37, 241–248.

doi:10.1579/0044-7447(2008)37[241:TVOCWF]2.0.CO;2

Coyne, A.M.A., Fletcher, C.H., Richmond, B.M., 2012. Mapping Coastal Erosion Hazard Areas in Hawaii: Observations and Errors. J. Coast. Res. SI, 171–184.

D'angelo, C., 2016. Giant Waves Lash Hawaii Oceanfront Homes In Historic Surf Event [WWW Document]. Huffpost.

Dail, H.J., Merrifield, M.A., Bevis, M., 2000. Steep beach morphology changes due to energetic wave forcing. Mar. Geol. 162, 443–458. doi:10.1016/S0025-3227(99)00072-9

Delpey, M.T., Ardhuin, F., Collard, F., Chapron, B., 2010. Space-time structure of long ocean swell fields. J. Geophys. Res. Ocean. 115, N/A.

Denner, K., Phillips, M.R., Jenkins, R.E., Thomas, T., 2015. A coastal vulnerability and environmental risk assessment of Loughor Estuary, South Wales. Ocean Coast. Manag. 116, 478–490. doi:10.1016/j.ocecoaman.2015.09.002

Dollar, S., 1982. Coral Reefs, in: Wave Stress and Coral Community Structure in Hawaii. Springer, pp. 71–81.

Domingues, C.M., Church, J. a, White, N.J., Gleckler, P.J., Wijffels, S.E., Barker, P.M., Dunn, J.R., 2008. Improved estimates of upper-ocean warming and multi-decadal sea-level rise. Nature 453, 1090–3. doi:10.1038/nature07080

Doukakis, E., 2005. Identifying Coastal Vulnerability Due to Climate Changes. J. Mar. Environ. Eng. 8, 155–160.

Duriyapong, F., Nakhapakorn, K., 2011. Coastal vulnerability assessment: a case study of Samut Sakhon coastal zone. Sonklanakarin J. Sci. … 33, 469–476.

Eastern Research Group, 2013. What Will Adaptation Cost? An Economic Framework for Coastal Community Infrastructure, National Oceanic and Atmospheric Administration.

Eichler, T., Higgins, W., 2006. Climatology and ENSO-related variability of North American extratropical cyclone activity. J. Clim. 19, 2076–2093. doi:10.1175/JCLI3725.1

Elliff, C.I., Kikuchi, R.K.P., 2015. The ecosystem service approach and its application as a tool for integrated coastal management. Nat. e Conserv. 13, 105–111. doi:10.1016/j.ncon.2015.10.001

Eversole, D., Andrews, A., 2014. Climate Change Impacts in Hawaii: A summary of climate change and its impacts to Hawai'i's ecosystems and communities. A Publ. Univ. Hawai'i Manoa Sea Grant Coll. Program. UNHI-SEAGR, 36pp.

Fan, Y., Lin, S.J., Griffies, S.M., Hemer, M.A., 2014. Simulated global swell and wind-sea climate and their responses to anthropogenic climate change at the end of the twenty-first century. J. Clim. 27, 3516–3536. doi:10.1175/JCLI-D-13-00198.1

Fatorić, S., Chelleri, L., 2012. Vulnerability to the effects of climate change and adaptation: The case of the Spanish Ebro Delta. Ocean Coast. Manag. 60, 1–10. doi:10.1016/j.ocecoaman.2011.12.015

FEMA, 2011. FEMA Flood Map Service. [WWW Document] https://msc.fema.gov/portal/search Last Accesed:05/18/17

Ferrario, F., Beck, M.W., Storlazzi, C.D., Micheli, F., Shepard, C.C., Airoldi, L., 2014. The effectiveness of coral reefs for coastal hazard risk reduction and adaptation. Nat. Commun. 5, 1–9. doi:10.1038/ncomms4794

Findley, D.F., Monsell, B.C., Bell, W.R., Otto, M.C., Chen, B.C., 1998. New Capabilities and Methods of the X-12-ARIMA Seasonal-Adjustment Program. J. Bus. Econ. Stat. 16, 127–152.

Firing, Y.L., Merrifield, M.A., 2004. Extreme sea level events at Hawaii: Influence of mesoscale eddies. Geophys. Res. Lett. 31, 1–4. doi:10.1029/2004GL021539

Fischer-Bruns, I., Storch, H. von, González-Rouco, J.F., Zorita, E., 2005. Modelling the variability of midlatitude storm activity on decadal to century time scales. Clim. Dyn. 25, 461–476. doi:10.1007/s00382-005-0036-1

Fletcher, B.C.H., Romine, B.M., Genz, A.S., Barbee, M.M., Dyer, M., Anderson, T.R., Lim, S.C., Vitousek, S., Bochicchio, C., Richmond, B.M., 2011. National Assessment of Shoreline Change : Historical Shoreline Changes in the Hawaiian Islands.

Fletcher, C.H., 2000. Coastal Erosion Management Plan (COEMAP) of the State of Hawaii. Department of Land and Natural Resources, Coastal Lands Program. Honolulu, Hawaii.

Fletcher, C.H., Boyd, R., Neal, W.J., Tice, V., 2010. Living on the shores of Hawaii: Natural hazards, the environment, and our communities. University of Hawaii Press, Honolulu.

Fletcher, C.H., Grossman, E.E., Richmond, B.M., Gibbs, A.E., 2002. Atlas of Natural Hazards in the Hawaiian Coastal Zone, U.S. Geological Survey Geologic Investigations Series I-2761.

Fletcher, C.H., Mullane, R.A., Richmond, B.M., 1997. Beach Loss Along Armored Shorelines on Oahu, Hawaiian Islands. J. Coast. Res. 13, 209–215.

Fletcher, C.H., Romine, B.M., Genz, A.S., Barbee, M.M., Dyer, M., Anderson, T.R., Lim, S.C., Vitousek, S., Bochicchio, C., Richmond, B.M., 2012. National assessment of shoreline change; historical shoreline change in the Hawaiian Islands, U.S. Geological Survey Open-File Report 2011-1051.

Francis, O.P., Atkinson, D.E., 2012a. Synoptic forcing of wave states in the southeast Chukchi Sea, Alaska, at offshore locations. Nat. Hazards 62, 1273–1300. doi:10.1007/s11069-012-0148-y

Francis, O.P., Atkinson, D.E., 2012b. Synoptic forcing of wave states in the southeast Chukchi Sea, Alaska, at nearshore locations. Nat. Hazards 62, 1273–1300. doi:10.1007/s11069-012-0148-y

Francis, O.P., Panteleev, G.G., Atkinson, D.E., 2011. Ocean wave conditions in the Chukchi Sea from satellite and in situ observations. Geophys. Res. Lett. 38, 1–5. doi:10.1029/2011GL049839

Fussel, H.-M., Klein, R.J.T., 2006. Climate change vulnerability assessments: An evolution of conceptual thinking. Clim. Change 75, 301–329. doi:10.1007/s10584-006-0329-3

Fyfe, J.C., 2003. Extratropical Southern Hemisphere cyclones: Harbingers of climate change? J. Clim. 16, 2802–2805. doi:10.1175/1520-0442(2003)016<2802:ESHCHO>2.0.CO;2

Gallina, V., Torresan, S., Critto, A., Sperotto, A., Glade, T., Marcomini, A., 2016. A review of multi-risk methodologies for natural hazards: Consequences and challenges for a climate change

impact assessment. J. Environ. Manage. 168, 123–132. doi:10.1016/j.jenvman.2015.11.011

Gemmrich, J., Thomas, B., Bouchard, R., 2011. Observational changes and trends in northeast Pacific wave records. Geophys. Res. Lett. 38, 1–5. doi:10.1029/2011GL049518

Geng, Q., Sugi, M., 2003. Possible change of extratropical cyclone activity due to enhanced greenhouse gases and sulfate aerosols - Study with a high-resolution AGCM. J. Clim. 16, 2262–2274. doi:10.1175/1520-0442(2003)16<2262:PCOECA>2.0.CO;2

Geng, Q., Sugi, M., 2001. Variability of the North Atlantic Cyclone activity in winter analyzed from NCEP-NCAR reanalysis data. J. Clim. 14, 3863–3873. doi:10.1175/1520-0442(2001)014<3863:VOTNAC>2.0.CO;2

Giambelluca, T.W., Schroeder, T.A., 1998. Climate in Atlas of Hawai'i, 3rd ed. University of Hawai'i Press, Honolulu, Hawai'i.

Gilbert, R.O., 1987. Statistical methods for environmental pollution monitoring. John Wiley & Sons.

Gitelman, A.I., Risbey, J.S., Kass, R.E., Roswen, R.D., 1997. Trends in the surface meridional temperature gradient. Geophys. Res. Lett. 24, 1243–1246.

Gornitz, V., 1991. Global coastal hazards from future sea level rise. Palaeogeogr. Palaeoclimatol. Palaeoecol. 89, 379–398. doi:10.1016/0031-0182(91)90173-O

Gornitz, V.M., 1990. Vulnerability of the East Coast, USA to future sea level rise. J. Coast. Res. 9, 201–237.

Grachev, A.A., Fairall, C.W., 2001. Upward Momentum Transfer in the Marine Boundary Layer. J. Phys. Oceanogr. 31, 1698–1711. doi:10.1175/1520-0485(2001)031<1698:UMTITM>2.0.CO;2

Graham, N.E., Cayan, D.R., Bromirski, P.D., Flick, R.E., 2013. Multi-model projections of twenty-first century North Pacific winter wave climate under the IPCC A2 scenario. Clim. Dyn. 40, 1335–1360. doi:10.1007/s00382-012-1435-8

Graham, N.E., Diaz, H.F., 2001. Evidence for intensification of North Pacific winter cyclones since 1948. Bull. Am. Meteorol. Soc. 82, 1869–1893. doi:10.1175/1520-

0477(2001)082<1869:EFIONP>2.3.CO;2

Graham, N.E., Strange, R.R., Diaz, H.F., 2001. Intensification of North Pacific Winter Cyclones 1948-98 : Impacts on California Wave Climate, Scripps Instiurion of Oceanography Reference. La Jolla.

Grigg, R.W., 1983. Community structure, succession and development of coral reefs in Hawaii: Marine Ecology, in: Marine Ecology Progress Series. JSTOR, pp. 1–14.

Griggs, G.B., Trenhaile, A.S., 1994. Coastal cliffs and platforms, in: Carter, R.W.G., Woodroffe, C.D. (Eds.), Coastal Evolution: Late Quaternary Shoreline Morphodynamics. Cambridge University Press, Cambridge, UK, pp. 425–450.

Guannel, G., Arkema, K., Ruggiero, P., Verutes, G., 2016. The power of three: Coral reefs, seagrasses and mangroves protect coastal regions and increase their resilience. PLoS One 11, 1–22. doi:10.1371/journal.pone.0158094

Guannel, G., Guerry, A., Brenner, J., Faries, J., Thompson, M., Silver, J., Griffin, R., Proft, J., Carey, M., Toft, J., Verutes, G., 2014. Changes in the Delivery of Ecosystem Services in Galveston Bay, TX, under a Sea-Level Rise Scenario.

Guannel, G., Ruggiero, P., Faries, J., Arkema, K., Pinsky, M., Gelfenbaum, G., Guerry, A., Kim, C.K., 2015. Integrated modeling framework to quantify the coastal protection services supplied by vegetation. J. Geophys. Res. Ocean. 120, 1–22. doi:10.1002/2014JC009821

Guerry, A.D., Ruckelshaus, M.H., Arkema, K.K., Bernhardt, J.R., Guannel, G., Kim, C.-K., Marsik, M., Papenfus, M., Toft, J.E., Verutes, G., Wood, S.A., Beck, M., Chan, F., Chan, K.M.A., Gelfenbaum, G., Gold, B.D., Halpern, B.S., Labiosa, W.B., Lester, S.E., Levin, P.S., McField, M., Pinsky, M.L., Plummer, M., Polasky, S., Ruggiero, P., Sutherland, D.A., Tallis, H., Day, A., Spencer, J., 2012. Modeling benefits from nature: using ecosystem services to inform coastal and marine spatial planning. Int. J. Biodivers. Sci. Ecosyst. Serv. Manag. 8, 107–121. doi:10.1080/21513732.2011.647835

Gulev, S.K., Grigorieva, V., 2006. Variability of the winter wind waves and swell in the North

Atlantic and North Pacific as revealed by the voluntary observing ship data. J. Clim. 19, 5667–5685. doi:10.1175/JCLI3936.1

Gulev, S.K., Zolina, O., Grigoriev, S., 2001. Extratropical cyclone variability in the Northern Hemisphere winter from the NCEP/NCAR reanalysis data. Clim. Dyn. 17, 795–809. doi:10.1007/s003820000145

Hall, N.M.J., Hoskins, B.J., Valdes, P.J., Senior, C.A., 1994. Storm tracks in a high resolution GCM with doubled carbon dioxide. Q. J. R. Met. Soc. 120, 1209–1230.

Hanafin, J.A., Quilfen, Y., Ardhuin, F., Sienkiewicz, J., Queffeulou, P., Obrebski, M., Chapron, B., Reul, N., Collard, F., Corman, D., De Azevedo, E.B., Vandemark, D., Stutzmann, E., 2012. Phenomenal sea states and swell from a north atlantic storm in february 2011: A comprehensive analysis. Bull. Am. Meteorol. Soc. 93, 1825–1832. doi:10.1175/BAMS-D-11-00128.1

Handmer, J.W., Dovers, S., Downing, T.E., 1999. Societal vulnerability to climate change and variability. Mitig. Adapt. Strateg. Glob. Chang. 4, 267–281.

Hanson, J.L., Phillips, O.M., 2001. Automated Analysis of Ocean Surface Directional Wave Spectra. J. Atmos. Ocean. Technol. 18, 277–293. doi:10.1175/1520-0426(2001)018<0277:AAOOSD>2.0.CO;2

Harnik, N., Chang, E.K.M., 2004. The Effects of Variations in Jet Width on the Growth of Baroclinic Waves: Implications for Midwinter Pacific Storm Track Variability. J. Atmos. Sci. 61, 23–40. doi:10.1175/1520-0469(2004)061<0023:TEOVIJ>2.0.CO;2

Hasselmann, S., Hasselmann, K., Allender, J.H., Barnett, T.P., 1985. Computations and parameterizations of the nonlin- ear energy transfer in a gravity-wave spectrum. Part II: Parameterizations of the nonlinear energy transfer for applications in wave models. J. Phys. Oceanogr. 15, 1378–1391.

Hawai'i Mapping Research Group, 2014. Main Hawaiian Islands Multibeam Bathymetry and Backscatter Synthesis [WWW Document]. SOEST, Univ. Hawai'i Manoa. URL

http://www.soest.hawaii.edu/HMRG/Multibeam/bathymetry.php (accessed 10.10.17).

Hemer, M.A., Church, J.A., Hunter, J.R., 2010. Variability and trends in the directional wave climate of the Southern Hemisphere. Int. J. Climatol. 30, 475–491. doi:10.1002/joc.1900

Hemer, M., Katzfey, J., Hotan, C., 2011. The wind-wave climate of the Pacific, Final report for the Pacific Adaptation Strategy Assistance Program,Department of Climate Change and Energy Efficien.

Hirsch, R.M., Slack, J.R., Smith, R.A., 1982. Techniques of trend analysis for monthly water quality data. Water Resour. Res. 18, 107–121. doi:10.1029/WR018i001p00107

HNL C&C., 2016. GIS Hawaii Flood Maps [WWW Document]. URL http://gis.hicentral.com/pubwebsite (accessed 11.18.16).

Hodges, K.I., Hoskins, B.J., Boyle, J., Thorncroft, C., 2003. A Comparison of Recent Reanalysis Datasets Using Objective Feature Tracking: Storm Tracks and Tropical Easterly Waves. Mon. Weather Rev. 131, 2012–2037. doi:10.1175/1520-0493(2003)131<2012:ACORRD>2.0.CO;2

Hoskins, B.J., Hodges, K.I., 2002. New Perspectives on the Northern Hemisphere Winter Storm Tracks. J. Atmos. Sci. 59, 1041–1061. doi:10.1175/1520-0469(2002)059<1041:NPOTNH>2.0.CO;2

Hwang, D., 1981. Beach changes on Oahu as revealed by aerial photographs. Honolulu, Hawaii.

Inatsu, M., Mukougawa, H., Xie, S.P., 2003. Atmospheric response to zonal variations in midlatitude SST: Transient and stationary eddies and their feedback. J. Clim. 16, 3314–3329. doi:10.1175/1520-0442(2003)016<3314:ARTZVI>2.0.CO;2

InVEST Coastal Vulnerability Model, 2016.[WWW Document] URL https://www.naturalcapitalproject.org/invest/ (accessed 05.11.18).

IPCC Climate Change 2014: Synthesis Report. Contribution of Working Groups I, II and III to the Fifth Assessment Report of the Intergovernmental Panel on Climate Change, 2014. , IPCC. [Core Writing Team, R.K. Pachauri and L.A. Meyer (eds.)], Geneva, Switzerland.

doi:10.1017/CBO9781107415324

Iwao, K., Inatsu, M., Kimoto, M., 2012. Recent changes in explosively developing extratropical cyclones over the winter northwestern Pacific. J. Clim. 25, 7282–7296. doi:10.1175/JCLI-D-11-00373.1

Janssen, P.A.E.M., 1991. Quasi-linear Theory of Wind-Wave Generation Applied to Wave Forecasting. J. Phys. Oceanogr. doi:10.1175/1520-0485(1991)021<1631:QLTOWW>2.0.CO;2

Jelenak, Z., Ahmad, K., Sienkiewicz, J., Chang, P.S., Nws, N., Opc, N., 2009. A statistical study of wind field distribution within extra-tropical cyclones in North Pacific ocean from 7-years of QuikSCAT wind data, in: IEEE International Geoscience and Remote Sensing Symposium. p. I-104-I-107.

Jiang, H., Stopa, J.E., Wang, H., Husson, R., Mouche, A., Chapron, B., Chen, G., 2016. Tracking the attenuation and nonbreaking dissipation of swells using altimeters. Geophys. Res. Ocean. 121, 1446–1458. doi:10.1002/2015JC011536.Received

Jokiel, P.L., Rodgers, K.S., Brown, E., 2004. Assessment, Mapping and Monitoring of Selected "Most Impaired" Coral Reef Areas in the State of Hawai'i. Honolulu.

Kane, H.H., Fletcher, C.H., Frazer, L.N., Barbee, M.M., 2014. Critical elevation levels for flooding due to sea-level rise in Hawai'i. Reg. Environ. Chang. 15, 1679–1687. doi:10.1007/s10113-014-0725-6

Kane, H.H., Fletcher, C.H., Romine, B.M., Anderson, T.R., Frazer, N.L., Barbee, M.M., 2012. Vulnerability Assessment of Hawai'i " s Cultural Assets Attributable to Erosion Using Shoreline Trend Analysis Techniques. J. Coast. Res. 28, 533–539. doi:10.2112/JCOASTRES-D-11-00114.1

Karl, T.R., Melillo, J.M., Peterson, T.C., 2009. Global Climate Change Impacts in the United States, Society.

Kelly, P.M., Adger, W.N., 2000. Theory and practice in assessing vulnerability to climate change and facilitating adaptation. Clim. Change 47, 325–352. doi:10.1023/A:1005627828199

Kelly, P.M., Granich, S.L. V, Secrett, C.M., 1994. Global Warming : Responding to an Uncertain Future. Asia Pacific J. Environ. Dev. 1, 28–45.

Kendall, M.G., 1975. Rank Correlation Methods,. Charles Griffin, London.

Kim, K., Pant, P., Yamashita, E., 2017. Integrating travel demand modeling and flood hazard risk analysis for evacuation and sheltering. Int. J. Disaster Risk Reduct. 0–1. doi:10.1016/j.ijdrr.2017.10.025

Kim, K., Pant, P., Yamashita, E., 2015. Evacuation Planning for Plausible Worst Case Innundation Scenarios in Honolulu, Hawaii. J. Emerg. Manag. 13, 93–108.

Klein, R.J.T., Nicholls, R.J., Mimura, N., 1999. Coastal adaptation to Climate Change. Can the IPCC technical guidelines be applied? Mitig. Adapt. Strateg. Glob. Chang. 4, 239–252. doi:10.1023/A:1009681207419

Kobayashi, N., Raichle, A.W., Asano, T., 1993. Wave Attenuation by Vegetation. J. Water 119, 30–48.

Komen, G.J., Cavaleri, L., Donelan, M., 1996. Dynamics and modelling of ocean waves. Cambridge university press.

Komen, G.J., Cavaleri, L., Donelan, M., Hasselmann, K., Hasselmann, S., Janssen, P.A.E.M., 1994. Dynamics and modelling of ocean waves. Cambridge University Press.

Kopp, R.E., Hay, C.C., Little, C.M., Mitrovica, J.X., 2015. Geographic variability of sea-level change. Curr. Clim. Chang. Reports 1, 192–204.

Kopp, R.E., Kemp, A.C., Bittermann, K., Horton, B.P., Donnelly, J.P., Gehrels, W.R., Rahmstorf, S., 2016. Temperature-driven global sea-level variability in the Common Era, in: Proceedings of the National Academy of Sciences of the United States of America.

Lambert, S.J., 1996. Intense extratropical northern hemisphere winter cyclone events: 1899–1991. J. Geophys. Res. 101, 21319–21325. doi:10.1029/96JD01653

Lambert, S.J., Fyfe, J.C., 2006. Changes in winter cyclone frequencies and strengths simulated in

enhanced greenhouse warming experiments: Results from the models participating in the IPCC diagnostic exercise. Clim. Dyn. 26, 713–728. doi:10.1007/s00382-006-0110-3

Landsea, C., Franklin, J., Blake, E., Tanabe, R., 2016. Northeast and North Central Pacific hurricane database (HURDAT2) 1949-2016 [WWW Document]. Natl. Hurric. Cent. Data Arch. URL http://www.nhc.noaa.gov/data/hurdat/hurdat2-nepac-1949-2016-041317.txt (accessed 6.12.17).

Langridge, S.M., Hartge, E.H., Clark, R., Arkema, K., Verutes, G.M., Prahler, E.E., Stoner-Duncan, S., Revell, D.L., Caldwell, M.R., Guerry, A.D., Ruckelshaus, M., Abeles, A., Coburn, C., O'Connor, K., 2014. Key lessons for incorporating natural infrastructure into regional climate adaptation planning. Ocean Coast. Manag. 95, 189–197. doi:10.1016/j.ocecoaman.2014.03.019

Lawal, D.U., Matori, A.-N., Hashim, A.M., Chandio, I.A., Sabri, S., Balogun, A.-L., Abba, H.A., 2011. Geographic Information System and Remote Sensing Applications in Flood Hazards Management: A Review. Res. J. Appl. Sci. Eng. Technol. 3, 933–947.

Le Cozannet, G., Garcin, M., Bulteau, T., Mirgon, C., Yates, M.L., Méndez, M., Baills, A., Idier, D., Oliveros, C., 2013. An AHP-derived method for mapping the physical vulnerability of coastal areas at regional scales. Nat. Hazards Earth Syst. Sci. 13, 1209–1227. doi:10.5194/nhess-13-1209-2013

Li, N., Cheung, K.F., Stopa, J.E., Hsiao, F., Chen, Y.-L., Vega, L., Cross, P., 2016. Thirty-four years of Hawaii wave hindcast from downscaling of climate forecast system reanalysis. Ocean Model. 100, 78–95. doi:10.1016/j.ocemod.2016.02.001

Li, N., Stopa, J., Cheung, K.F., 2012. Wave Power Analysis for Representative Hawaiian Island Sites.

Lindberg, W.J., Seaman, W., 2011. Guidelines and Management Practices for Artificial Reef Siting, Use, Construction, and Anchoring in Southeast Florida.

Löptien, U., Zolina, O., Gulev, S., Latif, M., Soloviov, V., 2008. Cyclone life cycle characteristics over the Northern Hemisphere in coupled GCMs. Clim. Dyn. 31, 507–532. doi:10.1007/s00382-007-0355-5

Maanan, M., Maanan, M., Rueff, H., Adouk, N., Zourarah, B., Rhinane, H., 2018. Assess the human and environmental vulnerability for coastal hazard by using a multi-criteria decision analysis. Hum. Ecol. Risk Assess. An Int. J. 1–17. doi:10.1080/10807039.2017.1421452

Makai Engineering, Inc. and Sea Engineering, I., 1991. Aerial photograph analysis of coastal erosion on the islands of Kauai, Molokai, Lanai, Maui and Hawaii.

Mangubhai, S., Wilson, J.R., Rumetna, L., Maturbongs, Y., Purwanto, 2015. Explicitly incorporating socioeconomic criteria and data into marine protected area zoning. Ocean Coast. Manag. 116, 523–529. doi:10.1016/j.ocecoaman.2015.08.018

Mani Murali, R., Ankita, M., Amrita, S., Vethamony, P., 2013. Coastal vulnerability assessment of Puducherry coast, India, using the analytical hierarchical process. Nat. Hazards Earth Syst. Sci. 13, 3291–3311. doi:10.5194/nhess-13-3291-2013

Mann, H.B., 1945. Non-parametric tests against trend. Econometrica 13, 245–259.

Marchant, M., 2017. Application of Coastal Vulnerability Index (CVI) on the Island of Oahu. University of Hawai'i at Manoa.

Mazzarella, A., Scafetta, N., 2012. Evidences for a quasi 60-year North Atlantic Oscillation since 1700 and its meaning for global climate change. Theor. Appl. Climatol. 107, 599–609. doi:10.1007/s00704-011-0499-4

McCabe, G.J., Clark, M.P., Serreze, M.C., 2001. Trends in Northern Hemisphere surface cyclone frequency and intensity. J. Clim. 14, 2763–2768. doi:10.1175/1520-0442(2001)014<2763:TINHSC>2.0.CO;2

Mcivor, A., Möller, I., Spencer, T., Spalding, M., 2012. Reduction of Wind and Swell Waves by Mangroves. Nat. Coast. Prot. Ser. 1–27. doi:ISSN 2050-7941.

Mclaughlin, S., Cooper, J.A.G., 2010. A multi-scale coastal vulnerability index: A tool for coastal managers? Environ. Hazards 9, 233–248. doi:10.3763/ehaz.2010.0052

Meehl, G. a, Washington, W.M., Collins, W.D., Arblastar, J.M., Hu, A., Buja, L.E., Strand, W.G.,

Teng, H., 2005. How Much More Global Warming and Sea Level How Much More Global Warming and Sea Level Rise ? Science (80-.). 1769, 1769–1773. doi:10.1126/science.1106663

Mendez, F.J., Izaguirre, C., Menendez, M., Reguero, B.G., Losada, I.J., 2010. Is the extreme wave climate in the NE Pacific increasing?, in: OCEANS 2010 MTS/IEEE. Seattle, pp. 1–7.

Menéndez, M., Méndez, F.J., Losada, I.J., Graham, N.E., 2008. Variability of extreme wave heights in the northeast Pacific Ocean based on buoy measurements. Geophys. Res. Lett. 35, 1–6. doi:10.1029/2008GL035394

Mengel, M., Levermann, A., Frieler, K., Robinson, A., Marzeion, B., Winkelmann, R., 2015. Future sea level rise constrained by observations and long-term commitment. Proc. Natl. Acad. Sci. 113, 2597–2602.

Mesquita, M.D.S., Atkinson, D.E., Hodges, K.I., 2010. Characteristics and variability of storm tracks in the North Pacific, Bering Sea, and Alaska. J. Clim. 23, 294–311. doi:10.1175/2009JCLI3019.1

Moberly, R., 1968. Loss of Hawaiian littoral sand. J. Sediment. Petrol. 38.

Moberly, R.M., Chamberlain, T., 1964. Hawaiian beach systems : Final report. Honolulu.

Musekiwa, C., Cawthra, H., Unterner, M., van Zyl, F., 2015. An assessment of coastal vulnerability for the South African coast. South African J. Geomatics 4, 123–137. doi:sajg.v4i2.5

National Oceanic and Atmospheric Administration, 2011. Coastal sea-level change societal challenge needs assessment report, NOAA Coastal Services Center.

Natural Capital Project, 2016. InVEST ver. 3.3.2 Sample Datasets [WWW Document]. URL http://data.naturalcapitalproject.org/invest-data/3.3.2/ (accessed 10.6.17).

Natural Capital Project, 2008. InVEST-Integrated valuation of ecosystem services and tradeoffs [WWW Document]. URL https://www.naturalcapitalproject.org/invest/#what-is-invest (accessed 3.5.18).

Neu, U., Akperov, M.G., Bellenbaum, N., Benestad, R., Blender, R., Caballero, R., Cocozza, A.,

Dacre, H.F., Feng, Y., Fraedrich, K., Grieger, J., Gulev, S., Hanley, J., Hewson, T., Inatsu, M., Keay, K., Kew, S.F., Kindem, I., Leckebusch, G.C., Liberato, M.L.R., Lionello, P., Mokhov, I.I., Pinto, J.G., Raible, C.C., Reale, M., Rudeva, I., Schuster, M., Simmonds, I., Sinclair, M., Sprenger, M., Tilinina, N.D., Trigo, I.F., Ulbrich, S., Ulbrich, U., Wang, X.L., Wernli, H., 2013. Imilast: A community effort to intercompare extratropical cyclone detection and tracking algorithms. Bull. Am. Meteorol. Soc. 94, 529–547. doi:10.1175/BAMS-D-11-00154.1

Nguyen, T.T.X., Bonetti, J., Rogers, K., Woodroffe, C.D., 2016. Indicator-based assessment of climate-change impacts on coasts: A review of concepts, methodological approaches and vulnerability indices. Ocean Coast. Manag. 123, 18–43. doi:10.1016/j.ocecoaman.2015.11.022

Nicholls, R.J., Cazenave, A., 2010. Sea-level rise and its impact on coastal zones. Science 328, 1517–1520. doi:10.1126/science.1185782

Nicholls, R.J., Hoozemans, F.M.J., Marchand, M., 1999. Increasing flood risk and wetland losses due to global sea-level rise: Regional and global analyses. Glob. Environ. Chang. 9. doi:10.1016/S0959-3780(99)00019-9

Nielsen, P., 1990. Tidal dynamics of the water table in beaches. Water Resour. Res. 26, 2127–2134. doi:10.1029/WR026i009p02127

NOAA National Center for Environmental Information, 2018. Pacific Decadal Oscillation (PDO) [WWW Document]. Dataset.

NOAA Needs Assessment Guide [WWW Document], 2016. . NOAA Off. Coast. Manag. URL https://coast.noaa.gov/digitalcoast/training/needs-assessment-guide (accessed 11.18.16).

NOAA Tides and Currents, 2013. Sea Levels Online: Sea Level Variations of the United States Derived from National Water Level Observation Network Stations [WWW Document]. URL http://tidesandcurrents.noaa.gov/sltrends/sltrends.html (accessed 5.23.17).

Now, H.N., 2016. Massive North Shore waves slam beach front properties [WWW Document]. URL http://www.hawaiinewsnow.com/story/31087011/massive-north-shore-swell-slams-beach-front-properties (accessed 6.20.17).

Onat, Y., Francis, O.P., Kim, K., 2018a. Vulnerability assessment and adaptation to sea level rise in high-wave environments: A case study on O'ahu, Hawai'i. Ocean Coast. Manag. 157, 147–159. doi:10.1016/j.ocecoaman.2018.02.021

Onat, Y., Marchant, M., Francis, O., Department of Civil and Environmental Engineering, University of Hawai'i at Manoa, C.H.E.R. (CHER) L., 2018b. Coastal vulnerability index GIS modeling of the Hawaiian Islands [WWW Document]. Mendeley Data, v1, 1. doi:10.17632/73jvpbs8tv.1

Özyurt, G., Ergin, A., 2010. Improving Coastal Vulnerability Assessments to Sea-Level Rise: A New Indicator-Based Methodology for Decision Makers. J. Coast. Res. 262, 265–273. doi:10.2112/08-1055.1

Paciorek, C.J., Risbey, J.S., Ventura, V., Rosen, R.D., 2002. Multiple indices of Northern Hemisphere cyclone activity, winters 1949-99. J. Clim. 15, 1573–1590. doi:10.1175/1520-0442(2002)015<1573:MIONHC>2.0.CO;2

Parise, C.K., Farina, L., 2014. Wave spectra generated by an extratropical cyclone in the South Atlantic Ocean. Tellus A 0, 1–11.

Parker, A., 2017. Honolulu sea level forecast based on local and global tide gauge measurements. New Concepts Glob. Tectonics 5, 268–276.

Parker, A., 2016a. Rates of subsidence and relative sea level rise in the Hawaii Islands. Nonlinear Eng. 5, 255–268. doi:10.1515/nleng-2016-0004

Parker, A., Ollier, C.D., 2016b. Coastal planning should be based on proven sea level data. Ocean Coast. Manag. 124, 1–9. doi:10.1016/j.ocecoaman.2016.02.005

Parker, A., Saad Saleem, M., Lawson, M., 2013. Sea-level trend analysis for coastal management. Ocean Coast. Manag. 73, 63–81. doi:10.1016/j.ocecoaman.2012.12.005

Pfeffer, W.T., Harper, J. T., O'Neel, S., 2008. Kinematic Constraints on Glacier Contributions to 21st-Century Sea-Level Rise 312, 1340–1343. doi:10.1126/science.1159099

Pickart, R.S., Macdonald, A.M., Moore, G.W.K., Renfrew, I.A., Walsh, J.E., Kessler, W.S., 2009. Seasonal Evolution of Aleutian Low Pressure Systems: Implications for the North Pacific Subpolar Circulation*. J. Phys. Oceanogr. 39, 1317–1339. doi:10.1175/2008JPO3891.1

Poulose, J., Rao, A.D., Bhaskaran, P.K., 2017. Role of continental shelf on non-linear interaction of storm surges, tides and wind waves: An idealized study representing the west coast of India. Estuar. Coast. Shelf Sci. 1–14. doi:10.1016/j.ecss.2017.06.007

Rahmstorf, S., 2007. Projecting Future Sea-Level Rise 368–370.

Rangel-Buitrago, N., Anfuso, G., 2015. Risk assessment of storms in coastal zones: case studies from Cartagena (Colombia) and Cadiz (Spain). Springer. doi:10.1007/978-3-319-15844-0

Rascle, N., Ardhuin, F., Queffeulou, P., Croizé-Fillon, D., 2008. A global wave parameter database for geophysical applications. Part 1: Wave-current-turbulence interaction parameters for the open ocean based on traditional parameterizations. Ocean Model. 25, 154–171. doi:10.1016/j.ocemod.2008.07.006

Richmond, B.M., Fletcher, C.H., Grossman, E.E., Gibbs, A.E., 2001. Islands at Risk : Coastal Hazard Assessment and Mapping in The Hawaiian Islands. Environ. Geosci. 8, 21–37.

Rizzo, A., Aucelli, P.P.C., Gracia, F.J., Anfuso, G., 2017. A novelty coastal susceptibility assessment method: application to Valdelagrana area (SW Spain). J. Coast. Conserv. doi:10.1007/s11852-017-0552-2

Romine, B.M., Fletcher, C.H., 2012. A Summary of Historical Shoreline Changes on Beaches of Kauai, Oahu, and Maui, Hawaii. J. Coast. Res. 29, 1–10. doi:10.2112/JCOASTRES-D-11-00202.1

Romine, B.M., Fletcher, C.H., Barbee, M.M., Anderson, T.R., Frazer, L.N., 2013. Are beach erosion rates and sea-level rise related in Hawaii? Glob. Planet. Change 108, 149–157. doi:10.1016/j.gloplacha.2013.06.009

Ruggiero, P., Komar, P.D., Allan, J.C., 2010. Increasing wave heights and extreme value projections: The wave climate of the U.S. Pacific Northwest. Coast. Eng. 57, 539–552.

doi:10.1016/j.coastaleng.2009.12.005

Ruth, M., Coelho, D., Karetnikov, D., 2007. The US Economic Impacts of Climate Change and the Costs of Inaction. Environ. Res. 2, 48.

Saha, S., Moorthi, S., Pan, H., Wu, X., Wang, J., Nadiga, S., Tripp, P., Kistler, R., Woollen, J., Behringer, D., Liu, H., Stokes, D., Grumbine, R., Gayno, G., Wang, J., Hou, Y., Chuang, H., Juang, H.H., Sela, J., Iredell, M., Treadon, R., Kleist, D., Van Delst, P., Keyser, D., Derber, J., Ek, M., Meng, J., Wei, H., Yang, R., Lord, S., van den Dool, H., Kumar, A., Wang, W., Long, C., Chelliah, M., Xue, Y., Huang, B., Schemm, J., Ebisuzaki, W., Lin, R., Xie, P., Chen, M., Zhou, S., Higgins, W., Zou, C., Liu, Q., Chen, Y., Han, Y., Cucurull, L., Reynolds, R.W., Rutledge, G., Goldberg, M., 2010a. NCEP Climate Forecast System Reanalysis (CFSR) Selected 6-Hourly Time-Series Products, January 1979 to December 2010. [WWW Document]. Res. Data Arch. Natl. Cent. Atmos. Res. Comput. Inf. Syst. Lab. Dataset. URL https://doi.org/10.5065/D69K487J. (accessed 8.4.17).

Saha, S., Moorthi, S., Pan, H.L., Wu, X., Wang, J., Nadiga, S., Tripp, P., Kistler, R., Woollen, J., Behringer, D., Liu, H., Stokes, D., Grumbine, R., Gayno, G., Wang, J., Hou, Y.T., Chuang, H.Y., Juang, H.M.H., Sela, J., Iredell, M., Treadon, R., Kleist, D., Van Delst, P., Keyser, D., Derber, J., Ek, M., Meng, J., Wei, H., Yang, R., Lord, S., Van Den Dool, H., Kumar, A., Wang, W., Long, C., Chelliah, M., Xue, Y., Huang, B., Schemm, J.K., Ebisuzaki, W., Lin, R., Xie, P., Chen, M., Zhou, S., Higgins, W., Zou, C.Z., Liu, Q., Chen, Y., Han, Y., Cucurull, L., Reynolds, R.W., Rutledge, G., Goldberg, M., 2010b. The NCEP climate forecast system reanalysis. Bull. Am. Meteorol. Soc. 91, 1015–1057. doi:10.1175/2010BAMS3001.1

Saha, S., Moorthi, S., Wu, X., Wang, J., Nadiga, S., Tripp, P., Behringer, D., Hou, Y., Chuang, H., Iredell, M., Ek, M., Meng, J., Yang, R., Mendez, M.P., van den Dool, H., Zhang, Q., Wang, W., Chen, M., Becker, E., 2011. NCEP Climate Forecast System Version 2 (CFSv2) Selected 6-Hourly Products. [WWW Document]. Res. Data Arch. Natl. Cent. Atmos. Res. Comput. Inf. Syst. Lab. Dataset. URL https://doi.org/10.5065/D61C1TXF (accessed 1.2.18).

Saha, S., Moorthi, S., Wu, X., Wang, J., Nadiga, S., Tripp, P., Behringer, D., Hou, Y.T., Chuang, H.Y., Iredell, M., Ek, M., Meng, J., Yang, R., Mendez, M.P., Van Den Dool, H., Zhang, Q.,

Wang, W., Chen, M., Becker, E., 2014. The NCEP climate forecast system version 2. J. Clim. 27, 2185–2208. doi:10.1175/JCLI-D-12-00823.1

Sasaki, W., 2014. Changes in the North Pacific wave climate since the mid-1990s. Geophys. Res. Lett. 7854–7860. doi:10.1002/2014GL061590.Received

Scafetta, N., 2014. Multi-scale dynamical analysis (MSDA) of sea level records versus PDO, AMO, and NAO indexes. Clim. Dyn. 43, 175–192. doi:10.1007/s00382-013-1771-3

Scripps Institution of Oceanography (SIO), 2013. Historic and ongoing buoy wave measurements, time series, spectral analysis, and other parameters (sea surface temperature, air temperature and pressure, wind speed and direction), worldwide, mostly US coastal, from November 1975 through present, from the [WWW Document]. Dataset. URL https://data.nodc.noaa.gov/cgi-bin/iso?id=gov.noaa.nodc:SIO-CDIP (accessed 7.4.18).

Sea Engineering Inc., 1988. Oahu Shoreline Study, Part 1, Data on Beach Changes. Honolulu, Hawaii.

Seiler, C., Zwiers, F.W., 2016. How will climate change affect explosive cyclones in the extratropics of the Northern Hemisphere? Clim. Dyn. 46, 3633–3644. doi:10.1007/s00382-015-2791-y

Semedo, A., Sušelj, K., Rutgersson, A., Sterl, A., 2011. A global view on the wind sea and swell climate and variability from ERA-40. J. Clim. 24, 1461–1479. doi:10.1175/2010JCLI3718.1

Semedo, A., Weisse, R., Behrens, A., Sterl, A., Bengtsson, L., Günther, H., 2013. Projection of global wave climate change toward the end of the twenty-first century. J. Clim. 26, 8269–8288. doi:10.1175/JCLI-D-12-00658.1

Sen, P.K., 1968. Estimates of the regression coefficient based on Kendall's tau. J. Am. Stat. Assoc. 63, 1379–1389.

Sharp, R., Tallis, H., Ricketts, T., Guerry, A., Wood, S., Chaplin-Kramer, R., Al., E., 2016. InVEST User's Guide. User Guide. Stanford, CA.

Shaw, J., Taylor, R.B., Forbes, D.L., Ruz, M.H., Solomon, S., 1998. Sensitivity of the coasts of

Canada to sea-level rise. Bull. Geol. Surv. Canada 1–79. doi:10.4095/210075

Shimura, T., Mori, N., Mase, H., 2015. Future projections of extreme ocean wave climates and the relation to tropical cyclones: Ensemble experiments of MRI-AGCM3.2H. J. Clim. 28, 9838–9856. doi:10.1175/JCLI-D-14-00711.1

Simmonds, I., Keay, K., 2002. Surface fluxes of momentum and mechanical energy over the North Pacific and North Atlantic Oceans. Meteorol. Atmos. Phys. 80, 1–18. doi:10.1007/s007030200009

Sinclair, M., Revell, M., 2000. Classification and Composite Diagnosis of Extratropical Cyclogenesis Events in the Southwest Pacific. Am. Meteorol. Soc. 128, 1089–1105. doi:10.1175/1520-0493(2000)128<1089:CACDOE>2.0.CO;2

Sinclair, M.R., 1994. An Objective Cyclone Climatology for the Southern Hemisphere. Mon. Weather Rev. doi:10.1175/1520-0493(1994)122<2239:AOCCFT>2.0.CO;2

Sinclair, M.R., Watterson, I.G., 1999. Objective assessment of extratropical weather systems in simulated climates. J. Clim. 12, 3467–3485. doi:10.1175/1520-0442(1999)012<3467:OAOEWS>2.0.CO;2

Slangen, A.B.A., Carson, M., Katsman, C.A., van de Wal, R.S.W., Köhl, A., Vermeersen, L.L.A., Stammer, D., 2014. Projecting twenty-first century regional sea-level changes. Clim. Change 124, 317–332.

Smit, B., Burton, I., Klein, R.J.T., Street, R., 1999. The science of adaptation: a framework for assessment. Mitig. Adapt. Strateg. Glob. Chang. 4, 199–213. doi:10.1023/A:1009652531101

Smit, B., Pilifosova, O., 2003. From adaptation to adaptive capacity and vulnerability reduction., in: Climate Change, Adaptive Capacity and Development. pp. 9–28.

Smit, B., Wandel, J., 2006. Adaptation, adaptive capacity and vulnerability. Glob. Environ. Chang. 16, 282–292. doi:10.1016/j.gloenvcha.2006.03.008

Smith, R.B., Grubišić, V., 1993. Aerial Observations of Hawaii's Wake. J. Atmos. Sci.

doi:10.1175/1520-0469(1993)050<3728:AOOHW>2.0.CO;2

Snodgrass, A.F.E., Groves, G.W., Hasselmann, K.F., Miller, G.R., Munk, W.H., Powers, W.H., 1966. Propagation of Ocean Swell across the Pacific Source : Philosophical Transactions of the Royal Society of London . Series A , Mathematical Published by : Royal Society Stable URL : http://www.jstor.org/stable/73313 (b) The great-circle event of 1 9 Augu. Philos. Trans. R. Soc. A Math. Phys. Eng. Sci. 259, 431–497.

Solomon, S., Plattner, G.-K., Knutti, R., Friedlingstein, P., 2009. Irreversible climate change due to carbon dioxide emissions. Proc. Natl. Acad. Sci. U. S. A. 106, 1704–9. doi:10.1073/pnas.0812721106

Sorteberg, A., Walsh, J.E., 2008. Seasonal cyclone variability at 70°N and its impact on moisture transport into the Arctic. Tellus, Ser. A Dyn. Meteorol. Oceanogr. 60 A, 570–586. doi:10.1111/j.1600-0870.2008.00314.x

State of Hawaii Office of Planning, 2015. Roads GIS files [WWW Document]. URL http://planning.hawaii.gov/gis/download-gis-data-expanded/ (accessed 10.6.17).

Stearns, H.T., Vaksvik, K.N., 1935. Geology and Ground-Water Resources of the Island of Oahu, Hawaii.

Stopa, J.E., 2013. Periodicity and patterns of the global wind and wave climate. University of Hawaii.

Stopa, J.E., Ardhuin, F., Babanin, A., Zieger, S., 2016. Comparison and validation of physical wave parameterizations in spectral wave models. Ocean Model. 103, 2–17. doi:10.1016/j.ocemod.2015.09.003

Stopa, J.E., Cheung, K.F., 2014. Intercomparison of wind and wave data from the ECMWF Reanalysis Interim and the NCEP Climate Forecast System Reanalysis. Ocean Model. 75, 65–83. doi:10.1016/j.ocemod.2013.12.006

Stopa, J.E., Cheung, K.F., Tolman, H.L., Chawla, A., 2013a. Patterns and cycles in the Climate Forecast System Reanalysis wind and wave data. Ocean Model. 70, 207–220. doi:10.1016/j.ocemod.2012.10.005

Stopa, J.E., Filipot, J.F., Li, N., Cheung, K.F., Chen, Y.L., Vega, L., 2013b. Wave energy resources along the Hawaiian Island chain. Renew. Energy 55, 305–321. doi:10.1016/j.renene.2012.12.030

Sweet, W. V, Kopp, R.E., Weaver, C.P., Obeysekera, J., Horton, R.M., Thieler, E.R., Zervas, C.E., 2017. Global and Regional Sea Level Rise Scenarios for the United States. Silver Spring, Maryland.

Szlafsztein, C., Sterr, H., 2007. A GIS-based vulnerability assessment of coastal natural hazards, state of Para, Brazil. J. Coast. Conserv. 11, 53–66. doi:10.1007/s11852-007-0003-6

Tahri, M., Maanan, M., Maanan, M., Bouksim, H., Hakdaoui, M., 2017. Using Fuzzy Analytic Hierarchy Process multi-criteria and automatic computation to analyse coastal vulnerability. Prog. Phys. Geogr. 41, 268–285. doi:10.1177/0309133317695158

The WAVEWATCH III Development Group, 2016. User manual and system documentation of WAVEWATCH III version 5.16 Tech. Note 329. NOAA/NWS/NCEP/MMAB, College Park, MD, USA. doi:10.3390/ijerph2006030011

Thieler, E.R., Hammar-Klose, E., 1999. National assessment of coastal vulnerability to sea-level rise. Preliminary results for U.S. Atlantic Coast. Reston, VA.

Tolman, H.L., 2009. User Manual and System Documentation of WAVEWATCH III version 3.14.

Tolman, H.L., 1991. A third generation model for wind waves on slowly varying, unsteady and inhomogeneous depths and currents. J. Phys. Oceanogr. 21.

Torresan, S., Critto, A., Dalla Valle, M., Harvey, N., Marcomini, A., 2008. Assessing coastal vulnerability to climate change: Comparing segmentation at global and regional scales. Sustain. Sci. 3, 45–65. doi:10.1007/s11625-008-0045-1

Trenberth, K.E., 1990. Recent Observed Interdecadal Climate Changes in the Northern Hemisphere. Bull. Am. Meteorol. Soc. doi:10.1175/1520-0477(1990)071<0988:ROICCI>2.0.CO;2

Trenberth, K.E., Hurrell, J.W., 1994. Decadal atmosphere-ocean variations in the Pacific. Clim. Dyn. 9, 303–319.

Twitchell, P.F., Rasmussen, E.A., Davidson, K.L., 1989. Polar and Arctic Lows, International Conference on Polar/Arctic Lows. A Deepak Pub.

Tysban, A.., Everett, J.., Titus, J.., 1990. World Oceans and Coastal Zones, in: Tegart, W., Sheldon, G.W., Griffiths, D.C. (Eds.), Climate Change: The IPCC Impacts Assessment. Australian Government Publishing Service, Canberra, Australia, pp. 1–28.

U.S. Census Bureau, G.D., 2010. TIGER/Line Shapefile, 2010 Census Hawaii State [WWW Document]. URL https://www.census.gov/geo/maps-data/data/tiger-line.html (accessed 10.3.17).

Ulbrich, U., Leckebusch, G.C., Pinto, J.G., 2009. Extra-tropical cyclones in the present and future climate: A review. Theor. Appl. Climatol. 96, 117–131. doi:10.1007/s00704-008-0083-8

UNISDR, 2015. Sendai Framework for Disaster Risk Reduction 2015 - 2030, Third World Conference on Disaster Risk Reduction, Sendai, Japan, 14-18 March 2015. doi:A/CONF.224/CRP.1

Vitousek, S., Fletcher, C.H., 2008. Maximum Annually Recurring Wave Heights in Hawai'i. Pacific Sci. 62, 541–553. doi:10.2984/1534-6188(2008)62[541:MARWHI]2.0.CO;2

Vogl, A.L., Hamel, P., Silver, J., Griffin, R., Wood, S.A., Rogers, L., Chaplin-kramer, B., Arkema, K.K., 2016. Incorporating Climate Change Scenarios.

Vose, R.S., Applequist, S., Bourassa, M.A., Pryor, S.C., Barthelmie, R.J., Blanton, B., Bromirski, P.D., Brooks, H.E., Degaetano, A.T., Dole, R.M., Easterling, D.R., Jensen, R.E., Karl, T.R., Katz, R.W., Klink, K., Kruk, M.C., Kunkel, K.E., Maccracken, M.C., Peterson, T.C., Shein, K., Thomas, B.R., Walsh, J.E., Wang, X.L., Wehner, M.F., Wuebbles, D.J., Young, R.S., 2014. Monitoring and understanding changes in extremes: Extratropical storms, winds, and waves. Bull. Am. Meteorol. Soc. 95, 377–386. doi:10.1175/BAMS-D-12-00162.1

Wallace, J.M., Lim, G.-H., Blackmon, M.L., 1988. Relationship between Cyclone Tracks,

Anticyclone Tracks and Baroclinic Waveguides. J. Atmos. Sci. 45, 439–462. doi:10.1175/1520-0469(1988)045<0439:RBCTAT>2.0.CO;2

Wang, C.-H., Baynes, T., McFallan, S., West, J., Khoo, Y.B., Wang, X., Quezada, G., Mazouz, S., Herr, A., Beaty, R.M., Langston, A., Li, Y., Wai Lau, K., Hatfield-Dodds, S., Stafford-Smith, M., Waring, A., 2015. Rising tides: adaptation policy alternatives for coastal residential buildings in Australia. Struct. Infrastruct. Eng. 2479, 1–14. doi:10.1080/15732479.2015.1020500

Wang, C.H., Khoo, Y.B., Wang, X., 2015. Adaptation benefits and costs of raising coastal buildings under storm-tide inundation in South East Queensland, Australia. Clim. Change 132, 545–558. doi:10.1007/s10584-015-1454-7

Wang, X.L., Feng, Y., Chan, R., Isaac, V., 2016. Inter-comparison of extra-tropical cyclone activity in nine reanalysis datasets. Atmos. Res. 181, 133–153. doi:10.1016/j.atmosres.2016.06.010

Wang, X.L., Feng, Y., Compo, G.P., Swail, V.R., Zwiers, F.W., Allan, R.J., Sardeshmukh, P.D., 2013. Trends and low frequency variability of extra-tropical cyclone activity in the ensemble of twentieth century reanalysis. Clim. Dyn. 40, 2775–2800. doi:10.1007/s00382-012-1450-9

Wang, X.L., Swail, V.R., 2001. Changes of extreme Wave Heights in northern Hemisphere Oceans and related atmospheric circulation regimes. J. Clim. 14, 2204–2221. doi:10.1175/1520-0442(2001)014<2204:COEWHI>2.0.CO;2

Wang, X.L., Swail, V.R., Zwiers, F.W., 2006. Climatology and changes of extratropical cyclone activity: Comparison of ERA-40 with NCEP-NCAR reanalysis for 1958-2001. J. Clim. 19, 3145–3166. doi:10.1175/JCLI3781.1

Widley, T.M.L., 2005. The Climate Change Commitment. Science (80-.). 307, 1766–1769. doi:10.1126/science.1225053

Wolter, K., 2018. Multivariate ENSO Index [WWW Document]. NOAA Earth Syst. Res. Lab.

Wu, L., Qin, J., Wu, T., Li, X., 2017. Trends in global ocean surface wave characteristics as represented in the ERA-Interim wave reanalysis for 1979–2010. J. Mar. Sci. Technol. doi:10.1007/s00773-017-0450-1

Wu, S.-Y., Yarnal, B., Fisher, A., 2002. Vulnerability of coastal communities to sea level rise: a case study of Cape May County, New Jersey, USA. Clim. Res. 22, 255–270.

Yamanaka, T., Raffaelli, D., White, P.C.L., 2013. Non-Linear Interactions Determine the Impact of Sea-Level Rise on Estuarine Benthic Biodiversity and Ecosystem Processes. PLoS One 8. doi:10.1371/journal.pone.0068160

Yang, L. and Francis, O. P., 2018. Sea level rise rate deriving from tide gauge and satellite altimeter in Hawaii [WWW Document]. Coast. Hydraul. Eng. Resil. Lab, Univ. Hawaii Manoa, Mendeley Data, v1. doi:10.17632/3w3mf49gxp.1

Yang, Y., Chen, Y.-L., 2003. Circulations and Rainfall on the Lee Side of the Island of Hawaii during HaRP. Mon. Weather Rev. 131, 2525–2542. doi:10.1175/1520-0493(2003)131<2525:CAROTL>2.0.CO;2

Yin, J.H., 2005. A consistent poleward shift of the storm tracks in simulations of 21st century climate. Geophys. Res. Lett. 32, 1–4. doi:10.1029/2005GL023684

Yoo, G., Kim, A.R., Hadi, S., 2014. A methodology to assess environmental vulnerability in a coastal city: Application to Jakarta, Indonesia. Ocean Coast. Manag. 102, 169–177. doi:10.1016/j.ocecoaman.2014.09.018

Young, I.R., Zieger, S., Babanin, A. V., 2011. Global Trends in Wind Speed and Wave Height. Science (80-.). 332, 451–455.

Zhang, H., Cheng, W., Qiu, X., Feng, X., Gong, W., 2017. Tide-surge interaction along the east coast of the Leizhou Peninsula, South China Sea. Cont. Shelf Res. 142, 32–49. doi:10.1016/j.csr.2017.05.015

Zhang, K.Q., Douglas, B.C., Leatherman, S.P., 2004. Global warming and coastal erosion. Clim. Change 64, 41–58. doi:10.1023/b:clim.0000024690.32682.48

Zhang, Y., Wang, W.C., 1997. Model-simulated northern winter cyclone and anticyclone activity under a greenhouse warming scenario. J. Clim. 10, 1616–1634. doi:10.1175/1520-0442(1997)010<1616:MSNWCA>2.0.CO;2

Zheng, K., Sun, J., Guan, C., Shao, W., 2016. Analysis of the global swell and wind sea energy distribution using WAVEWATCH III. Adv. Meteorol. 2016. doi:10.1155/2016/8419580

Zieger, S., Babanin, A. V., Erick Rogers, W., Young, I.R., 2015. Observation-based source terms in the third-generation wave model WAVEWATCH. Ocean Model. 96, 2–25. doi:10.1016/j.ocemod.2015.07.014